Department of Laboratory Medicine
Karolinska Institutet, Stockholm, Sweden

NOVEL INJECTABLE CALCIUM SULFATE DEPOT FORMULATIONS FOR LOCAL CANCER TREATMENT

Stefan Grudén

Karolinska Institutet

Stockholm 2021

Front cover shows painting named “Cancer battle” by Tyra Grudén.
Published by Karolinska Institutet.
Printed by Universitetsservice US-AB, 2021.

ISBN 978-91-8016-164-0

Novel injectable calcium sulfate depot formulations for local cancer treatment

AKADEMISK AVHANDLING

som för avläggande av medicine doktorsexamen vid Karolinska Institutet offentligen försvaras på engelska språket i Birkeaulan, F51, Karolinska Universitetssjukhuset, Huddinge, Karolinska Institutet

Fredagen den 28 maj, 2021, kl. 13.00

av

Stefan Grudén

Huvudhandledare:
Professor Moustapha Hassan
Karolinska Institutet
Department of Laboratory Medicine
Division of Clinical Research Center

Bihandledare:
Assoc. Prof. Niklas Axén
LIDDS AB
Department of Materials and Devices
Division of Research and Development

Dr. Martin Sandelin
AstraZeneca AB
Department of Oncology and Hematology, Nordics
Division of Lung Cancer, Medical Affairs

Dr. Ying Zhao
Karolinska Institutet
Department of Laboratory Medicine
Division of Clinical Research Center

Opponent:
Professor Lars Hovgaard
University of Copenhagen
Department of Pharmacy
Division of Drug Design and Pharmacology

Betygsnämnd:
Professor Ken Welch
Uppsala University
Department of Materials Science and Engineering
Division of Nanotechnology and Functional Materials

Professor Katalin Dobra
Karolinska Institutet
Department of Laboratory Medicine
Division of Pathology

Assoc. Prof. Jaan Hong
Uppsala University
Department of Immunology, Genetics and Pathology
Division of Clinical Immunology

To my beloved family

"If I would have to choose between eating candy and being with my family,
...hmmmm... I think that I would choose both."

Hedvig Grudén

POPULAR SCIENCE SUMMARY OF THE THESIS

In the present doctoral thesis, we focused on a technology named NanoZolid®. We showed that this technology can successfully be used to produce novel drug formulations for cancer treatment. The advantage of drugs produced using NanoZolid technology is that we can use it for local cancer treatment. By this strategy, the drug will only affect the tumor progression locally, since the drug is released at the site of administration. The new strategy will improve the treatment efficacy and reduce the general side-effects, which occur when using drugs that are administrated and distributed to the entire body.

The NanoZolid technology is based on principles developed in the materials industry utilizing high pressures. In pressure chambers, the materials are subjected to high pressures where they gain different characteristics. Under high pressure, the materials are transformed to very dense microstructures having unique properties, e.g. strong steels or diamond. In the present thesis we utilized the pressure technique to develop drug carriers that can remain a long period in the area of administration and release the active substance slowly over long time. The material that has been used in the thesis is calcium sulfate which is biocompatible, or in other words that during the treatment while the drug is released, the drug carrier will be absorbed, degraded and eliminated from the body in a slow manner.

At the present, cancer treatment using chemotherapy is mainly carried out by administrating the drugs orally or intravenously, by which the drugs are distributed to all organs which will cause severe adverse effects. Despite the recent success in cancer treatment, still the results are far from satisfactory due the toxic effect on liver, kidneys, urine bladder, lungs, CNS, and disturbance of the hormonal balance. Several of these side effects may lead to increase morbidity, mortality, decrease in life quality and most of all, in less success in clinical outcome.

Recently, targeted drug therapy, monoclonal antibodies, cellular therapy, stem cell transplantation and local treatment have been introduced in order to increase the cancer treatment efficacy and to minimize the adverse side effects. In the present thesis, we have investigated a novel drug formulation using biocompatible drug carrier system to deliver the active substance into the tumor site. Preclinical studies and clinical trials indicated that chemotherapeutic agents administered using the NanoZolid formulations have good anti-cancer effect with lower toxicity. Using imaging guided injection, the administration of NanoZolid depot can be performed with a high precision and safety. After the optimization of the manufacture and preparation procedure, the release of the active substance from the implanted depot can be achieved over weeks or months. As described in the thesis, this strategy has been evaluated both for hormone treatment of patients with prostate cancer, and for treatment with cytotoxic substances in animal cancer models.

The present results in animals and in humans have shown a good tolerability to the NanoZolid formulation containing drug, as well as a good anticancer effect with reduced adverse effects. We concluded that the NanoZolid technology is a promising approach to develop new drug formulations for cancer treatment that may enhance treatment efficacy and reduce the side effects, which benefit the patients and the society by better life quality and less economic burden in treating the adverse effect, respectively.

POPULÄRVETENSKAPLIG SAMMANFATTNING

I denna doktorsavhandling fokuserar vi på en teknologi som kallas NanoZolid®. Vi har lyckats visa att denna teknologi kan användas för att tillverka nya läkemedel för cancerbehandling. Fördelen med läkemedel som tillverkas med NanoZolid-teknologin är att de enbart behandlar den del i kroppen som har cancer, och låter de friska delarna förbli obehandlade. Denna princip förbättrar cancerbehandlingen och minskar risken för biverkningar som annars är vanliga vid behandling av hela kroppen med t.ex. cellgifter.

NanoZolid-teknologin baseras på tillverkningsmetoder som utvecklats i materialindustrin och inkluderar mycket höga kompressionstryck. Material formas i en tryckkammare med mycket högt tryck. Trycket används för att tillverka material som får väldigt hög densitet med unika egenskaper. Exempelvis, så kan man tillverka hårt stål eller omvandla grafit till diamant i en sådan tryckkammare. I denna avhandling använder vi denna tryckteknik för att utveckla nya läkemedelsformuleringar baserade på kalciumsulfatbärare som kan stanna länge i kroppen och frisätta aktiv substans långsamt till ett specifikt område i kroppen. När behandlingen är färdig, vilket är ett långsamt förlopp, har både den aktiva substansen frisatts samt den nedbrytbara läkemedelsbäraren tagits upp av kroppen.

Idag ges de flesta läkemedel oralt eller via intravenös injektion. Sådan behandling ger ofta biverkningar eftersom den aktiva substansen distribueras över hela kroppen. Trots nya framsteg inom cancerforskningen är resultaten fortfarande långt ifrån tillfredsställande pga. biverkningar på lever, njurar, urinblåsa, lungor, CNS, och hormonbalansen. Många av dessa biverkningar kan leda till ökad sjuklighet, dödlighet, minskad livskvalitet och därigenom avsaknad av lyckade kliniska resultat.

På senare tid har riktad läkemedelsbehandling, monoklonala antikroppar, cellterapi, stamcells-transplantation samt lokal behandling introducerats för att öka den lokala anti-cancer effekten och minska risken för biverkningar. I denna avhandling har vi undersökt en ny läkemedelsteknologi med en biokompatibel bärare som kan frisätta den aktiva substansen i tumörområdet. Prekliniska studier och kliniska prövningar indikerar att cancerläkemedel som ges med NanoZolid uppvisar lovande anti-cancer effekt och låg toxicitet. Med moderna avbildningstekniker går det att följa injektionsförfarandet med hög precision och säkerhet. Efter optimering av tillverkningsprocessen har vi lyckats utforma nya formuleringar av läkemedel som frisläpper den aktiva substansen långsamt under flera veckor eller månader. Som beskrivs i avhandlingen, så har denna strategi utvärderats för både hormonbehandling av patienter med prostatacancer samt för behandling med cellgifter av djur med cancertumörer.

Resultaten från studierna i djur och patienter uppvisar en hög vävnadstolerans av NanoZolid-läkemedel samt en lovande anti-cancer effekt med få biverkningar. Sammanfattningsvis visar arbetena i denna avhandling att den kalciumsulfatbaserade läkemedels-teknologin NanoZolid är en lovande möjlighet för att utveckla nya läkemedel för cancerbehandling vilka kan förbättra behandlingseffektiviteten och minska biverkningarna, vilket ger patienterna en bättre livskvalitet och även samhället en ekonomisk fördel genom möjligheten att undvika kostnader för att behandla biverkningarna.

ABSTRACT

In the present thesis, a novel drug delivery technology named NanoZolid® based on hydrating inorganic calcium sulfate, is investigated. NanoZolid is injected as a liquid suspension of calcium sulfate, which solidifies *in vivo* by hydration forming a biocompatible and bioresorbable depot that slowly dissolves and releases the active substance.

In order to optimize the formulation and preparation procedure of NanoZolid, we have characterized the material properties of calcium sulfate and its influence on drug release. In **paper I**, the *in vitro* release of the antiandrogen, 2-hydroxyflutamide (2-HOF) was investigated using formulations containing porous and densified drug-loaded powder fractions. The formulations were produced for the local long-term treatment of prostate cancer. The densified powder fractions were prepared utilizing cold isostatic pressing (CIP), a new process introduced into the pharmaceutical industry. Reproducible *in vitro* release profiles were achieved from solidified depots with a drug release time of at least five months.

Calcium sulfate-based drug product candidates were evaluated in both preclinical and clinical settings. A xenograft mouse model of Lewis lung carcinoma (LLC) was used in **paper II** for evaluating intratumorally injected depots loaded with docetaxel. The study showed similar antitumor effects from the local depots, as from the systemic administration of docetaxel. Adverse effects including decreased levels of blood cells and weight loss were observed in mice treated with intraperitoneal administration, while not in mice that received intratumor depots. In addition, no adverse tissue reactions were observed from the depot.

In **Paper III,** we evaluated the possibility of encapsulating a biomolecule in the NanoZolid as a drug delivery system. Both *in vivo* solidification process to a depot and *in vivo* slow release of the biomolecule, epidermal growth factor (EGF), were studied using a mouse xenograft model inoculated subcutaneously with A549 human lung cancer cells. A fluorescence-labelled EGF was encapsulated into the NanoZolid depot that was injected subcutaneously in the neck. Results showed that the EGF released *in vivo* targeted the corresponding tumor receptors on the hind leg with a slow-release pattern and maintained its bioactivity.

To better understand the potential of intraprostatic depot injections with the antiandrogen 2-HOF, the effects of the new formulations on prostate specific antigen (PSA), prostate volume, testosterone levels and local tissue reactions, were investigated in a multicenter clinical trial (**paper IV**). The study included sixty-one men with localized prostate cancer who received intraprostatic depot injections (Liproca® Depot). The treatment was well tolerated and showed potential for long-term suppression of the tumor – as indicated by a decrease in PSA value, lower prostate volume and unchanged or improved MRI results in the majority of the patients.

In conclusion, the present results show that the calcium sulfate-based drug delivery system, NanoZolid, is a promising approach for local cancer treatment, and may benefit both individual patients and society as a whole.

LIST OF SCIENTIFIC PAPERS

I. **Stefan Grudén**, Moustapha Hassan, Niklas Axén. Cold isostatic pressing of hydrating calcium sulfate as a means to produce parenteral slow-release drug formulations. *Journal of Drug Delivery Science and Technology*. 2018, 46: 482-489. doi:10.1016/j.jddst.2018.06.013

II. **Stefan Grudén**, Martin Sandelin, Veera Räsänen, Patrick Micke, Mikael Hedeland, Niklas Axén, Marie Jeansson. Antitumoral effect and reduced systemic toxicity in mice after intratumoral injection of an in vivo solidifying calcium sulfate formulation. *European Journal of Pharmaceutics and Biopharmaceutics*. 2017, 114: 186-193. doi:10.1016/j.ejpb.2017.01.018

III. **Stefan Grudén,** Charlott Brunmark, Bo Holmqvist, Erwin D. Brenndörfer, Martin Johansson, Jian Liu, Ying Zhao, Niklas Axén, Moustapha Hassan. Biodistribution of fluorescence-labelled EGF protein from slow release NanoZolid depots in mouse. *International Journal of Pharmaceutics* (accepted). doi:10.1016/j.ijpharm.2021.120588

IV. Laurence Klotz, **Stefan Grudén***, Niklas Axén, Charlotta Gauffin, Cecilia Wassberg, Anders Bjartell, Jonathan Giddens, Peter Incze, Kenneth Jansz, Mindaugas Jievaltas, Ricardo Rendon, Patrick O. Richard, Albertas Ulys, Teuvo L. Tammela. Liproca Depot: A new antiandrogen treatment for active surveillance patients. *European Urology Focus* (accepted). doi:10.1016/j.euf.2021.02.003

*: Corresponding author

PUBLICATIONS NOT INCLUDED IN THIS THESIS

PAPERS

I. Hans Sjöberg, **Stefan Persson**#, Ninus Caram-Lelham. How interactions between drugs and agarose-carrageenan hydrogels influence the simultaneous transport of drugs. *Journal of Controlled Release*. 1999, 59(3): 391-400.

#: Birth name

II. Ulf Holmbäck, Anders Forslund, **Stefan Grudén**, Göran Alderborn, Arvid Söderhäll, Per M. Hellström, Hans Lennernäs. Effects of a novel combination of orlistat and acarbose on tolerability, appetite and glucose metabolism in persons with obesity. *Obesity Science and Practice*. 2020, 6: 313-323.

III. **Stefan Grudén**, Anders Forslund, Göran Alderborn, Arvid Söderhäll, Per M. Hellström, Ulf Holmbäck. Safety of a novel weight loss combination product containing orlistat and acarbose. *Clinical Pharmacology in Drug Development* (accepted).

PATENTS

I. *Nicotine-containing pharmaceutical compositions giving a rapid transmucosal absorption*
Sven Börje Andersson, Tomas Landh, Stefan Jonn, **Stefan Persson**#, Nils-Olof Lindberg.
Patent number WO0030641 (A1), Publication date 2000-06-02.

#: Birth name

II. *A modified release composition of orlistat and acarbose for the treatment of obesity and related metabolic disorders*
Göran Alderborn, Anders Forslund, Ulf Holmbäck, Hans Lennernäs, **Stefan Grudén**.
Patent number WO2016097170A1, Publication date 2016-06-23.

III. *A new method for producing calcium sulphate hemihydrate with unique properties*
Niklas Axén, **Stefan Grudén**.
Patent number WO2018073165A1, Publication date 2018-04-26.

IV. *Bioresorbable controlled-release compositions with STING modulating molecules*
Stefan Grudén, Niklas Axén, Martin Johansson.
Patent number WO2019170912A1, Publication date 2019-09-12.

CONTENTS

LIST OF ABBREVIATIONS

2-HOF	2-hydroxyflutamide
ADC	Apparent diffusion coefficient
ADT	Androgen deprivation therapy
AhR	Aryl hydrocarbon receptor
ANOVA	Analysis of variance
Bcl-2	B-cell lymphoma 2
CIP	Cold isostatic press
CW	Continuous wave
CTLA-4	Cytotoxic T-lymphocyte-associated protein 4
DNA	Deoxyribonucleic acid
DTX	Docetaxel
DWI	Diffusion-weighted image
EDS	Energy-dispersive X-ray spectroscopy
EGF	Epidermal growth factor
EGFR	Epidermal growth factor receptor
f_2	Similarity factor, expressed in percent between two dissolution curves
FDA	Food and Drug Administration
FOXO1	Forkhead box protein O1
G2/M	Cell life cycle point between the second growth phase and the mitosis phase
GDP	Guanosine di-phosphate
GMP	Good manufacturing practice
GTP	Guanosine tri-phosphate
HDPE	High-density polyethylene
HPLC	High performance liquid chromatography

i.p.	Intraperitoneal
IRDye	Infrared dye
kGy	Kilogray, absorbed radiation dose (1 Gy = 1 Joule/kg)
LLC	Lewis lung carcinoma
MNCs	Mononuclear cells
MRI	Magnetic resonance imaging
MS	Mass spectrometry
NSCLC	Non-small cell lung cancer
NIR	Near-infrared
NMRI	Naval medical research institute
NZ	NanoZolid®
PBS	Phosphate buffer solution
PD-1	Programmed cell death protein 1
PD-L1	Programmed death-ligand 1
PI-RADS	Prostate imaging-reporting and data system
PLGA	Polylactic-co-glycolic acid
PSA	Prostate specific antigen
PV	Prostate volume
s.c.	Subcutaneous
SEM	Scanning electron microscopy
STING	Stimulator of interferon genes
T2WI	T2-weighted image
TLR	Toll-like receptor
XRPD	X-ray powder diffraction

1 INTRODUCTION

Cancer is the second most common cause of death in the developed world. However, the treatment of cancer is still dependent on surgery, chemotherapy, radiotherapy, immunotherapy and recently cell therapy. In the clinical setting, surgery in combination with chemotherapy, with or without radiotherapy, are the most used cancer treatment regimens. Among chemotherapies, cytostatic drugs which target fast-dividing cells are used frequently.

Patients treated with chemotherapy experience severe side effects due to non-specific cytotoxicity, including tiredness, vomiting, hair loss, infections, anemia, skin bruising and loss of appetite as the chemotherapy also effects normal dividing cells such as epithelial cells, hair follicle cells, neurons and vascular endothelial cells. Heart, liver and kidney toxicity can be long term and life-threatening. One strategy for overcoming chemotherapy-induced side effects, is tumor-targeted drug delivery and local treatment to avoid drug distribution to non-target organs.

Also hormonal therapy is one of the major modalities for cancer. It involves the manipulation of the endocrine system through administration of specific hormones or drugs which inhibit the production or activity of such hormones. Hormonal therapy is used for several types of cancers derived from hormonally responsive tissues, including prostate and breast cancer.

In this thesis, we investigated drug formulations based on the excipient calcium sulfate for local parenteral drug delivery. The investigated formulations consist of a calcium sulfate powder loaded with an active substance and an aqueous diluent. Prior to administration, the powder and diluent are mixed to form an injectable suspension, which is then injected locally and solidifies *in vivo* to form an implant-like depot. The biocompatible and bioresorbable drug depot dissolves *in vivo* and releases the active substance to the surrounding tissues in a controlled manner.

The drug-loaded powder is prepared in such a way as to have a controlled granule size and porosity. The aqueous diluent is a sodium carboxymethyl cellulose solution that defines the viscosity of the suspension before injection and the solidification time of the depot after injection. The system used to produce such depots is known as NanoZolid®. The working principle of NanoZolid is to utilize the ability of calcium sulfate hemihydrate powder to solidify by hydration to calcium sulfate dihydrate when exposed to water. In addition, we used cold isostatic pressing (CIP) in NanoZolid formulations to generate extremely dense bodies to achieve slow drug release over several months.

NanoZolid formulations designed for local cancer treatment are investigated in this thesis, with the aim of improving local anti-cancer effects and reducing systemic side effects.

1.1 BIOCERAMICS FOR MEDICAL USE

1.1.1 Ceramics and bioceramics

Ceramics can be described as inorganic materials with a combination of covalent and ionic chemical bonds. The development of novel ceramic materials is an integral part of the historical progress of mankind. Several thousand years ago, the possibility of storing grains in ceramic pots made it possible for humans to evolve from nomad hunters to settlers.

The ability to handle ceramic materials has been a part of human civilization for at least 25 000 years, since the Upper Paleolithic period of the Stone Age, as demonstrated by a fired ceramic figurine of a nude female "Venus" uncovered during archaeological excavations in Moravia (present day Czech republic).[1] Quality of life improved when it became possible to make structural ceramics such as clay bricks and tiles. Almost all large cities in the Indus valley were built with a combination of sun-dried and baked bricks, around 9 000 years ago.[2]

One of the first breakthroughs in the fabrication of ceramics was the invention of the wheel, at least 5 500 years ago – initially not for transportation, but for the formation of round pottery.[2]

In the 1950s, the development of functional ceramics including dielectrics, piezoelectrics, magnets, and semiconductors created a revolution in modern industry. Ceramic semiconductors may be the most well-known items today, and these include microchips in computers and cell phones and form the basis of the industry in Silicon Valley.[3] Today, solar photovoltaic cells are also made from ceramic materials, generally doped crystalline silicon.

Ceramics can also be used in medical applications. Ceramics that are biocompatible are called *bioceramics*, and have been widely used in medical applications since the 1970s when Hench *et al*. discovered that various types of ceramics and glass could bond to human bones.[4,5]

1.1.2 Bioceramics for medical applications

With an increasingly aging population, the need to develop new materials for the manufacture of medical implants has increased. The function of implants is to repair and regenerate tissues that have been damaged by disease or trauma. Bioceramics have been typically used as implants in orthopedics and dentistry.

The most commonly used bioceramic material is hydroxyapatite, which was approved for medical use in the 1970s. Another widely-used bioceramic is calcium sulfate ($CaSO_4 \cdot XH_2O$), which is used as a bone implant in dental and orthopedic applications, and was first reported in 1892 by the German doctor, H. Dreesmann.[6] Calcium sulfate hemihydrate ($CaSO_4 \cdot 0.5H_2O$), also sometimes called plaster of Paris, is named after the gypsum quarries of Montmartre in Paris. When mixed with water, calcium sulfate hemihydrate recrystallizes to a viscous suspension and eventually solidifies.

Bioceramics for medical applications can be divided into three subcategories: 1) inert, 2) bioactive, and 3) biodegradable according to their degree of biological activity (Figure 1). The biodegradable sulfates are of special interest as they can potentially act as drug delivery carriers for active substances.

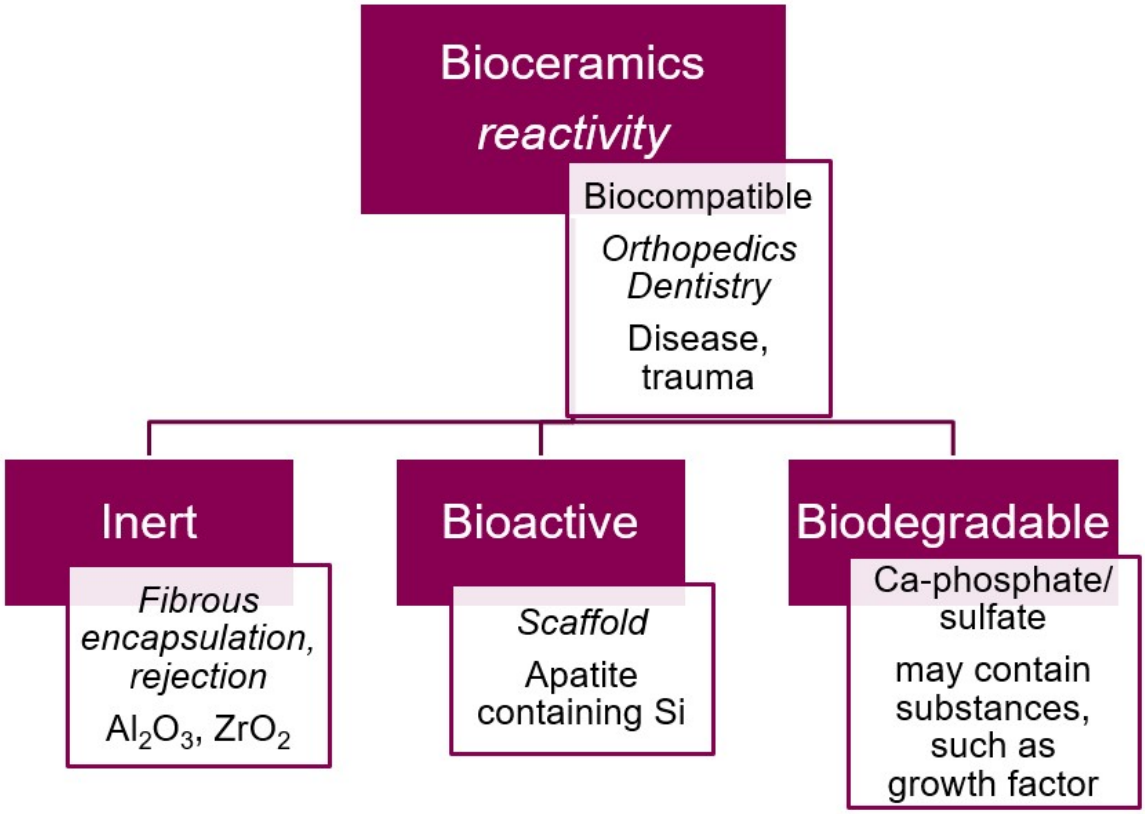

Figure 1. Types of bioceramics for medical application.

1.1.3 Hydrating calcium sulfate for parenteral drug administration

Calcium sulfate is a rapidly resorbing material and is considered safe as a drug carrier for parenteral administration. Its medical application as bone implants has shown that it is highly biocompatible without causing a substantial inflammatory response. Furthermore, calcium sulfate is a well-established pharmaceutical excipient used primarily for oral formulations. Calcium sulfate has a pharmacopoeial monograph that enable verification for eventual clinical use.[7] Some parenteral products based on calcium sulfate have been approved for clinical use, for example, implantable beads containing antibiotics.[8]

When calcium sulfate dihydrate is heated over 100°C under controlled conditions, it transforms to calcium sulfate hemihydrate, with a half-unit of crystal water per calcium sulfate molecule. Calcium sulfate hemihydrate can be reversed to calcium sulfate dihydrate if water is added to the hemihydrate according to the following formula:[9]

$$(CaSO_4)_2 \cdot H_2O\ (s) + 3H_2O\ (l) \leftrightarrow 2CaSO_4 \cdot 2H_2O\ (s) \qquad [1]$$

Calcium sulfate dihydrate and hemihydrate have different crystal structures and the transformation process from hemihydrate to dihydrate involves a recrystallization process.

If water is mixed with a fine-grained powder of calcium sulfate hemihydrate, with or without a drug, an injectable suspension is formed. After injection, this suspension solidifies *in vivo*

and forms a local slow-release depot with an open porosity of approximately 30%.[10–12] The depot releases the loaded drug content relatively fast (typically within weeks).

Another advantage of using calcium sulfate as a drug carrier is that the location and degradation of the depots can be followed in real-time by non-invasive imaging techniques such as ultrasound.[13,14]

1.1.4 Cold isostatic pressing of hydrating ceramics

Ceramics are traditionally created by heating minerals at very high temperatures, a process called sintering, which generates highly crystalline structures.

When conventionally sintering powders which are unable to recrystallize by hydration, decreasing the porosity usually requires both high temperature and pressure to create the necessary atomic mobility in a process known as hot isostatic pressing (HIP).[15–17]

Generally, ceramic sintering is performed at a temperature, T_s which is generally 50%–75% of the melting temperature, T_m of the material – according to the formula:[18,19]

$$T_s = \sim 0.5\text{-}0.75 \cdot T_m \qquad [2]$$

A normal T_s for calcium sulfate anhydrite is approximately 1100 °C.[20]

One way of decreasing the sintering temperature is to add a sintering aid, such as a small amount of cobalt, to the calcium sulfate (or other ceramic powder). This has recently been applied to the 3D manufacture of bioceramic medicinal implants.[21]

Depending on the intended use of a bioceramic, poor or low crystalline bioceramics may also be considered, as well as various alternative manufacturing methods.[22]

The solidification of calcium sulfate hemihydrate–water suspensions generates porous solid bodies of calcium sulfate dihydrate. Their porosity varies depending on the powder grain size and water content. The open porosity for solidified gypsum is typically 30%.[10–12] The porosity of solid calcium sulfate dihydrate bodies can be reduced by performing the hydration under an external isostatic pressure, utilizing a cold isostatic press (CIP).[23] CIP compaction is normally performed at room temperature (Figure 2).

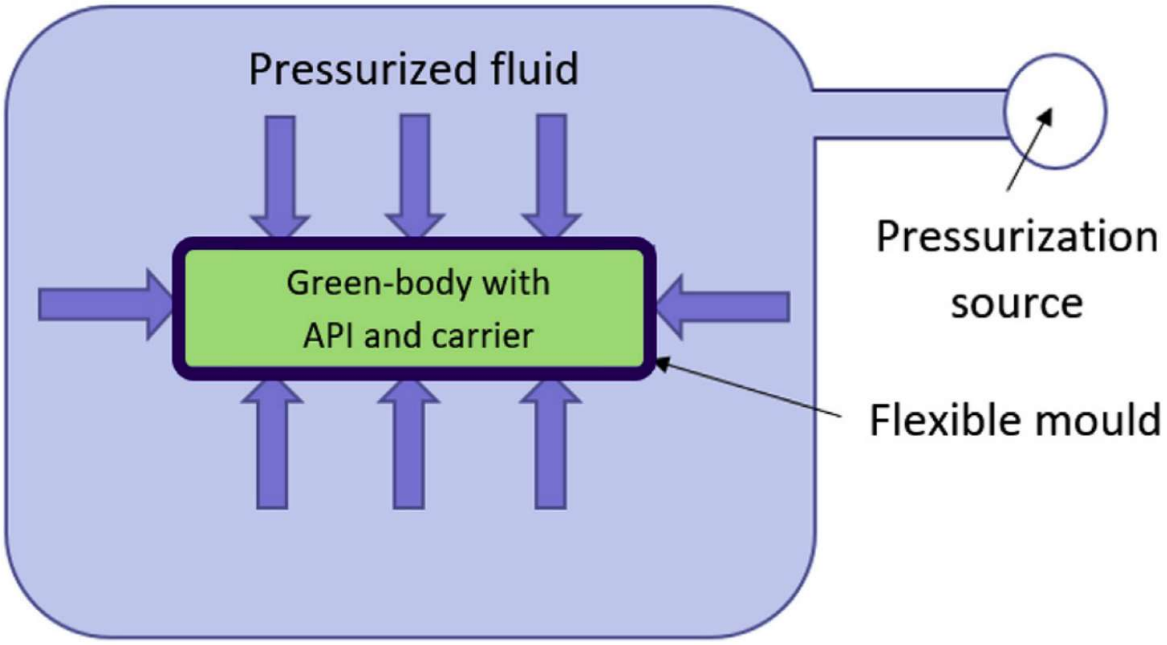

Figure 2. Schematic illustration of a Cold Isostatic Press (CIP).
The CIP is loaded with a green-body of calcium sulfate and active substance encased in a non-permeable flexible mold (e.g. rubber) and exposed to pressurized fluid (e.g. water).

To achieve a completely dense structure, the CIP process is applied to a calcium sulfate hemihydrate powder wetted with a fixed amount of water corresponding to 1.5 stoichiometric units of water of crystallization. The increased atomic mobility resulting from the recrystallization from hemihydrate to dihydrate leads to a strong reduction in porosity. This densification procedure performed at room temperature is analogous to sintering.

Conventionally, roller compaction and tablet compression are used for powder compression in the pharmaceutical industry.[24] In the materials industry, the CIP process has been used for decades; however, CIP equipment has not been commercially available for pharmaceutical manufacturing in a clean room environment. In this thesis, CIP is utilized and optimized for application in the pharmaceutical industry for the first time.

1.2 PARENTERAL IMPLANT DRUG RELEASE

1.2.1 Polymeric micro- and nanoparticulate systems

Depot drug delivery systems for parenteral use are generally designed to have a long-term therapeutic effect with the following potential advantages: less frequent administration, better efficacy versus dose, fewer systemic adverse effects, and better patient compliance.[25]

Parenteral implant products are often microparticulate polymer formulations delivered as subcutaneous or intramuscular injections for a systemic effect or local treatment.[26–28] For example, poly-lactic-co-glycolic acid (PLGA) high density microspheres carrying a high drug load (up to 40%) using hot-melt extrusion followed by wet-milling has been reported.[29]

Polymeric nanoparticles have been widely investigated as carriers for drug delivery. Nanoparticles can be designed to have controlled release properties and to be

biocompatible. Typical examples of synthetic polymers for nanoparticle formulations are polyesters, polyanhydrides and poly-alkyl-cyanoacrylates.[30–34] Natural polymers can also be used, for example, polysaccharides such as chitosan, alginate, hyaluronan, dextran, starch, or proteins such as albumin, collagen or gelatin.[35-37] Several FDA-approved products including polymeric delivery systems, e.g. Abraxane® (albumin bound paclitaxel) and Genexol-PM® (polymeric micelle formulation of paclitaxel), are primarily for intravenous administration.[38,39] The polymers may be combined with other materials such as degradable polymer coatings on titanium oxide (titania) nanotubes to achieve a controlled drug release. This combination has recently been reported to be useful as orthopedic drug-eluting implants.[40,41]

The manufacture of polymeric drug delivery systems is associated with certain practical limitations. The elimination of organic solvents from the product in order to meet pharmaceutical requirements and to comply with environmental regulations can be potentially costly. Furthermore, aseptic processing may be the only possibility as terminal sterilization is often not feasible for polymer drug delivery systems, because of their sensitivity to heat, moisture and radiation. Taken together, these issues can make the cost of the final product a challenging hurdle to overcome.

1.2.2 Hydrogel implants

Injectable and *in situ*-forming hydrogels, such as polyethylene glycol (PEG) and poly-isopropyl-acrylamide-based thermosensitive gels, are being used in products for numerous biomedical applications.[42–44] A typical application concerns the local treatment of retinoblastoma in children using a hydrogel containing antitumor drugs (topotecan and vincristine). The standard treatment for children involves systemic chemotherapy, which carries side effects including losing their vision, or a need to enucleate their eye, as described by Cocarta *et al*.[45] Recent research in dentistry reported by Li *et al*. describes the successful combination of several gelling components including chitosan, glycerophosphate and gelatin in the same formulation to produce an injectable thermosensitive hydrogel for erythropoietin delivery to enhance new bone formation.[46] Injectable hydrogel implants for extended drug release have been designed for both small molecules and proteins.[47–49] The hydrogel systems have been widely used because of their chemical simplicity as water-based systems. These systems are used as liquid or semi-solid injectables, which transform to gel-implants after injection. However, it has been shown that several peptide and protein drugs are not stable upon exposure to organic solvents used in the manufacturing process, which has limited the application of hydrogel implants.

1.2.3 Hydrating ionic salt implants

A hydrate is a compound with a specific number of water molecules in its crystalline molecular structure. An anhydrate is formed when all the water is removed from a hydrate. This reduction in crystal water content is often achieved by heating – a process that removes the water as steam. There are several inorganic ionic salts that have the ability to hydrate, i.e. to take up water and re-crystallize forming a new crystal with a higher molecular water content.[50]

Two of these ionic salts, calcium phosphate and calcium sulfate, are of particular interest for medical implant applications as they are both biocompatible and biodegradable.

Calcium phosphate is a hydrating inorganic ionic salt that contains calcium ions (cations) together with various anions including orthophosphate, metaphosphate, or pyrophosphate, and on occasion also hydrogen or hydroxide ions. The main calcium form present in milk and blood is calcium phosphate. It is also the principal component of bone (~60 wt%), and of tooth enamel (~90 wt%). Calcium phosphates are known as apatites, e.g. hydroxyapatite, when they have a calcium/phosphate ratio in the range between 1.5 (3/2) and 1.67 (5/3). The word apatite was first coined in 1786 by the German geologist, A.G. Werner, from the Greek word *apatao,* "to mislead or deceive".[51] Biomaterials based on calcium phosphate can hydrate and are sparingly water-soluble (2.5 mg/100 ml water at 25°C)[52] and biodegradable. They are used both as bone substitutes and as drug delivery carriers, especially in dentistry, bone regeneration and orthopaedics.[53] Melville *et al*. reported on the use of drug-loaded hydroxyapatite powders modified by heat treatment to generate a tailored drug release.[54]

Calcium sulfate is slightly water-soluble (205 mg/100 ml water at 25°C)[55], but is still much more soluble than calcium phosphate. Calcium sulfate is insoluble in organic solvents. When a drug is mixed with calcium sulfate in an organic solvent, it can be distributed homogeneously on the calcium sulfate particles. Thereafter the solvent can be gently evaporated using heat or a vacuum. The active substance may also be added as a dry powder to the calcium sulfate. Such a powder mix can be sterilized by a γ- or β-radiation dose in the range 25–50 kGy for parenteral injection; however, the effect of irradiation on drug degradation and drug release properties needs to be thoroughly considered.[56] By mixing the drug-loaded calcium sulfate hemihydrate with water, a viscous suspension is formed that can be injected and will solidify to an implant *in vivo*.

1.2.4 Implant drug release modelling

The release of the drug 2-HOF from a modified-release calcium sulfate depot formulation has been modelled by Sjögren *et al*.[57] The powder formulation itself consists of three different components before solidification: a) pure calcium sulfate hemihydrate (no drug included), b) calcium sulfate hemihydrate loaded with drug, and c) densified calcium sulfate dihydrate granules containing drug. After solidification, the drug content of the depot is divided into three different fractions: 1) unbound drug, 2) drug bound to the porous component or matrix, and 3) drug bound to the dense component (granules), see also section 3.1.1. Hence, the included powder components and the positioning of the drug after reconstitution in the depot are not the same (both the unbound fraction and the porous fraction arise predominantly from the porous part).

Assuming that the formulation forms a sphere that shrinks symmetrically during the dissolution process and that the depot volume has a constant relative drug load, the surface area can be considered as proportional to the amount or weight of released drug (W), expressed as $W^{2/3}$ (from the Noyes−Whitney equation: $\mathrm{d}W/\mathrm{d}t = DA\Delta C/L$, i.e. the dissolution rate ($\mathrm{d}W/\mathrm{d}t$) equals the diffusion coefficient (D) times the surface area (A) times the concentration gradient (ΔC) divided by the thickness of the diffusion layer (L)). If it is further assumed that drug release from the depot occurs simultaneously with the dissolution of the formulation, the drug release rate can be considered as a constant (k) over time. Under these circumstances, the Noyes−Whitney equation can be expanded to Equation 3 by including three separate fractions describing the amount of released drug (weight – W) over time (t). See Figure 3:[57]

$$\frac{dW_{tot}}{dt} = \frac{dW_{p-ub}}{dt} + \frac{dW_{p-b}}{dt} + \frac{dW_{np}}{dt} = k_{p-ub}W_{p-ub}^{2/3} + k_{p-b}W_{p-b}^{2/3} + k_{np}W_{np}^{2/3} \quad [3]$$

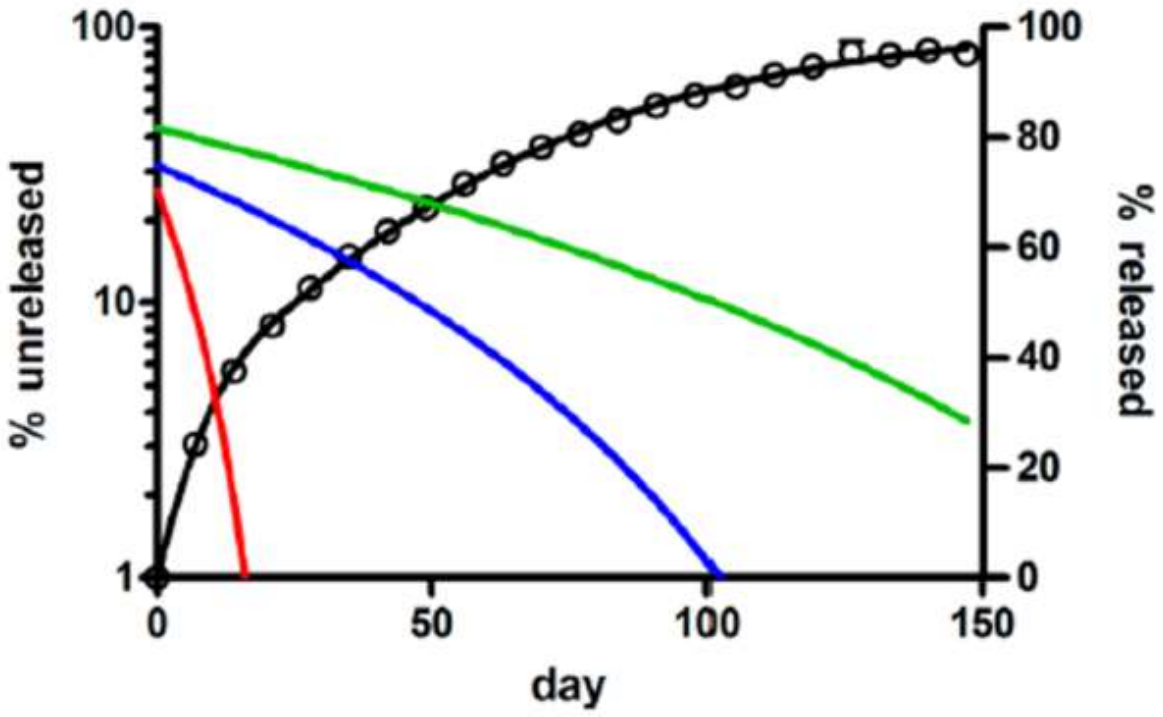

Figure 3. *In vitro* drug release (2-hydroxyflutamide) from calcium sulfate depots, and theoretical prediction of release from the three drug fractions. Drug fraction abbreviations: p-ub (porous and unbound) – red line, p-b (porous and bound) – blue line, and np (non-porous) – green line.

The circles are the measurements of cumulative *in vitro* drug release.

As illustrated in Figure 3, a good correlation between theoretical and *in vitro* drug release was achieved when combining different densities of calcium sulfate loaded with 2-HOF. However, one limitation of this model is that drug release from the individual fractions is affected by the change over time of the depot surface structure. A further limitation is that the initial burst release of the drug is not only from the porous and unbound fraction, but also from all components positioned at the depot surface due to the concentration difference with the surrounding aqueous media.[57]

A simplified explanation of drug release from a depot that releases drug in parallel with its dissolution, was given by Mönkäre *et al*., who described the drug release as the result of an erosion-like dissolution, see Equation 4:[58]

$$\text{Erosion (\%)} = 100 - 100 \cdot [\, m_{imp}(t) - m_{drug}(t) \,/\, m_{imp}(0) - m_{drug}(0)] \quad [4]$$

where $m_{imp}(0)$ and $m_{drug}(0)$ represent the mass of the implant and the drug in the implant, respectively, at the start of the test, while $m_{imp}(t)$ and $m_{drug}(t)$ represent the measured mass of the implant and the drug in the implant, respectively, at the time of sampling.

This model does not take into account:

1) the decrease in diffusive driving force following the time-dependent decline in drug concentration at the depot surface,
2) the relatively static layer of surrounding medium which reduces the release rate,
3) the possible saturation of the depot and drug leakage, which accelerates drug release.

Also, the model is not adapted for depots containing a combination of porous and dense fractions with different drug loads, for which the relative drug loads may vary over time.

Attempts to describe an initial hydration/wetting/swelling phase followed by erosion-based release have been performed with chitosan-based implants, for which the swelling (water uptake) and erosion evaluations were studied using equilibrium weight methods.[59–61] However, such evaluations are primarily relevant for implants that are associated with a swelling phase.

Despite the current large number of marketed parenteral controlled release products, there is still a shortage of adequate *in vitro* dissolution test methods for implants offering biorelevant test conditions.[62] However, the wide variation in release times and patterns for the different parenteral products make it very challenging to use standardized *in vitro* methods for release characterization.

1.2.5 *In vitro* drug release test method criteria

Certain key criteria should be carefully considered for an *in vitro* release test method. These include: (i) Relevance to physiological conditions, (ii) Reproducibility, (iii) Robustness, (iv) User friendly, (v) Easy readout, (vi) Controlled agitation, (vii) Cost effectiveness.[63,64]

Unfortunately, it is difficult to standardize all the above mentioned criteria for all parenteral products, due to the complexity and diversity of individual release patterns. On the other hand, the *in vitro* test method may consequently be designed more freely to be suited for the aimed release profile and specific application.

1.3 CANCER TREATMENT

Cancer treatment strategies include surgery, chemotherapy, radiotherapy, immunotherapy and cell therapy. In clinical practice, surgery and/or radiotherapy in combination with chemotherapy are the most widely used cancer treatment strategies. Among available chemotherapies, cytostatic drugs which target rapidly dividing cells are the most common. Chemotherapy can be used either before surgery/radiotherapy to reduce the cancer burden (neoadjuvant therapy), or after surgery to eliminate the residual tumor and/or metastasis (adjuvant therapy).

Patients that receive high-dose chemotherapy suffer from severe adverse effects due to the non-specific toxicity of the treatment. Typical side effects include tiredness, vomiting, hair loss, infections, anemia, skin bruising and loss of appetite as the chemotherapy also effects normal cells (for example, gastrointestinal tract epithelial cells, hair follicle cells, neurons and blood endothelial cells). Severe toxicity of the heart, liver and kidneys can be long-term and even life threatening. One strategy used to overcome chemotherapy-induced side effects is tumor-targeted drug delivery, by which we can avoid drug distribution to non-target organs. Targeted cancer therapies include treatment with small molecule drugs, e.g. check

point inhibitors, signal transduction inhibitors, gene expression modulators, apoptosis inducers, angiogenesis inhibitors, and/or large molecules such as hormone therapies monoclonal antibodies.[65-67]

Targeting mechanisms can be divided into: 1) passive targeting via enhanced tumor permeability and increased retention time in the tumor, and 2) active targeting, which involves binding specific receptors/mediators on the cell surface.[68,69] Unfortunately, targeted therapy is not suitable for all patients, for example, the monoclonal antibody, trastuzumab, used for the treatment of breast cancer is only effective for HER2-positive breast cancer patients.[70]

Recently, drug delivery systems based on nanoparticles have been used in the targeted treatment of cancer. These systems have been used mostly for systemic administration with moderate results, probably due to rapid clearance of the nanoparticles by phagocytes.[71]

This thesis focuses on local cancer treatment with depot implants that have been evaluated for local intraprostatic treatment of prostate cancer, local intratumoral treatment of lung cancer and targeted protein drug delivery from subcutaneously injected implants.

1.3.1 Local cancer treatment

Local cancer treatment can potentially be a way of overcoming some of the limitations associated with systemic administration. These include whole body distribution of cytostatic drugs, limited drug distribution to the tumor, and adverse effects due to the general distribution. For successful local tumor treatment, a sufficient local concentration of the drug is needed. Advantages of local treatment include a reduction in systemic toxicity, and higher treatment efficacy and hence a better quality of life for the patient.

One method of reaching the tumor would be to inject the drug in a suitable depot formulation directly into or close to the tumor. The prolonged residence time at the tumor for cytotoxic drugs such as docetaxel may enhance tumor cell death and increase the concentration of tumor antigens, thereby decreasing the number of immuno-suppressive tumor cells.[72]

1.3.2 Antiandrogens for prostate cancer treatment

Prostate cancer is the most frequently diagnosed cancer in men worldwide, with approximately 1.3 million cases and 359 thousand deaths annually.[73] Using current treatment protocols, the deaths associated with prostate cancer have been significantly reduced. Minor invasive therapies are available for early-stage prostate cancer, and include high-intensity focused ultrasound, cryotherapy, and brachytherapy. Despite such progress, there are still several challenges in prostate cancer treatment: 1) a high degree of recurrence,[74,75] 2) inadequate therapies, 3) overtreatment of benign disease,[76] and 4) significant side effects, including high rates of impotence and incontinence. Consequently, alternative therapy strategies are needed to improve treatment outcomes.

Androgens play an important role in the development of the prostate gland and regulation of its functions. The androgen receptor is a steroid hormone receptor with multiple phosphorylation sites and ligand binding domains. After ligand binding, the receptor first dimerizes, followed by phosphorylation and translocation from the cytoplasm to the cell

nucleus. In the nucleus, the androgen receptor mediates numerous downstream pathways involved in cell division, cell differentiation and apoptosis.[77]

Antiandrogens play a key role in prostate cancer treatment as they compete with circulating or locally derived androgens for binding to the androgen receptor. Antiandrogens are classified as either steroidal or non-steroidal. Steroidal antiandrogens can decrease the levels of testosterone but also bind to other hormone receptors, which can have undesirable side effects for the patient, such as loss of libido and impotence and also certain androgenic effects, i.e. blocking the negative feedback mechanism from the hypothalamic and pituitary pathway eventually resulting in an increased testosterone level.[78] This has led to the development of non-steroidal antiandrogens, which target the androgen receptor with greater specificity.

First generation non-steroidal antiandrogens developed for the androgen receptor were flutamide and nilutamide followed by bicalutamide and topilutamide. Flutamide and nilutamide were mainly designed to provide a combined androgen blockade when used in combination with castration. This combination therapy displayed moderate clinical advantages compared to castration alone. With a growing knowledge of the structure and biological functions of the androgen receptor, a second generation of non-steroidal antiandrogen drugs without agonist activity was developed to deliver higher efficacy. In 2012, enzalutamide was the first member of the second generation to be approved (Figure 4).[79]

1st Generation

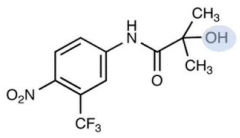

(2-Hydroxyflutamide)

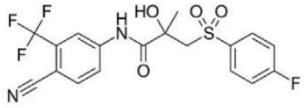

Bicalutamide

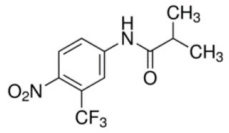

Flutamide

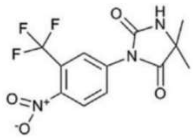

Nilutamide

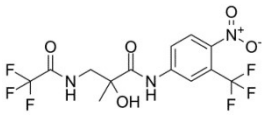

Topilutamide

2nd Generation

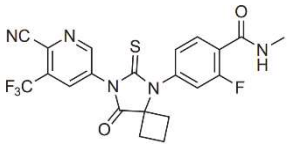

Apalutamide

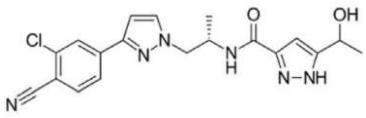

Darolutamide

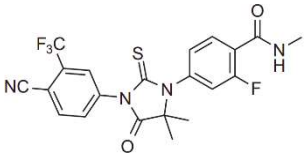

Enzalutamide

Figure 4. Molecular structures of non-steroidal antiandrogens, androgen receptor antagonists.

Flutamide's active metabolite 2-hydroxyflutamide (in parentheses) is not yet included as a marketed product, but is relevant for this thesis. The hydroxyl group at position 2 is highlighted in blue.

Low to intermediate risk prostate cancer is a disease that is often detected in older men and is associated with at least 15 years of metastasis-free survival, meaning that patients are unlikely to die from their cancer.[80] However, once the disease has metastasized, the median survival time is only approximately 3.5 years.[81] Therefore, treating prostate cancer at localized stages is warranted, which in turn requires development of new effective treatment alternatives. For patients diagnosed with low- and/or intermediate risk localized prostate cancer, there is an option to treat these patients with a local antiandrogen instead of following them without treatment, so called 'active surveillance'. A possible alternative treatment is an intraprostatic slow-release implant loaded with an antiandrogen, in order to delay cancer progression. This treatment strategy may cause fewer adverse effects compared to systemic antiandrogen treatment.[14]

1.3.3 Mechanism of action of 2-hydroxyflutamide

2-Hydroxyflutamide (2-HOF) is a non-steroidal antiandrogen and the major active metabolite of flutamide (see Figure 4), which is considered as a prodrug of 2-HOF.[82,83] Flutamide is metabolized by CYP1A2 to 2-HOF in the liver, therefore, the metabolite 2-HOF should be used for intraprostatic administration to achieve the intended local therapeutic effect.[14,84] 2-HOF works by preventing testosterone from triggering cancer cell division and inhibits the growth of, and sometimes even shrinks, the tumor.

2-Hydroxyflutamide acts by binding to the intracellular androgen receptor (AR) thereby inhibiting ligand-dependent transcription. 2-HOF is therefore categorized as an AR antagonist.[85] The 3D structure of the AR consists of a bundle of 12 helices (H1–H12) arranged in three layers. The binding of the antagonist to the AR induces an inactive ligand binding domain conformation where helix 12 (H12) – acting as a lid for the ligand binding pocket – is removed from its hormone-bound position.[86,87] This modification prevents the coactivators from binding and/or facilitates the recruitment of transcriptional corepressors (Figure 5).[88–90]

The anti-cancer effect of 2-HOF can also act through other pathways. In prostate cancer cells that are androgen receptor negative, 2-HOF induces a rapid activation of two protein kinase signaling pathways; the Ras-mitogen-activated (MAPK) pathway and the protein kinase B (AKT) pathway, resulting in modulation of genes transcription.[91,92] Furthermore, 2-HOF has been reported to bind as a ligand to the aryl hydrocarbon receptor (AhR). A decrease in expression of AhR has been shown to reverse the anti-proliferative effects of 2-HOF on several cancer cell lines. AhR-dependent effects of 2-HOF in human hepatocellular carcinoma cells are facilitated by the stimulation of transforming growth factor-β1 (TGF-β1), see Figure 5.[93,94]

2-HOF treatment suppresses prostate cancer by inducing apoptosis, or by inhibiting cell growth through cell cycle arrest. Both mechanisms may result in the long term suppression of cancer.[95,96] Therefore, the administration of intraprostatic 2-HOF for low- to intermediate risk (localized) prostate cancer patients may delay cancer progression and enhance their quality of life by improving erectile function and urination.[97]

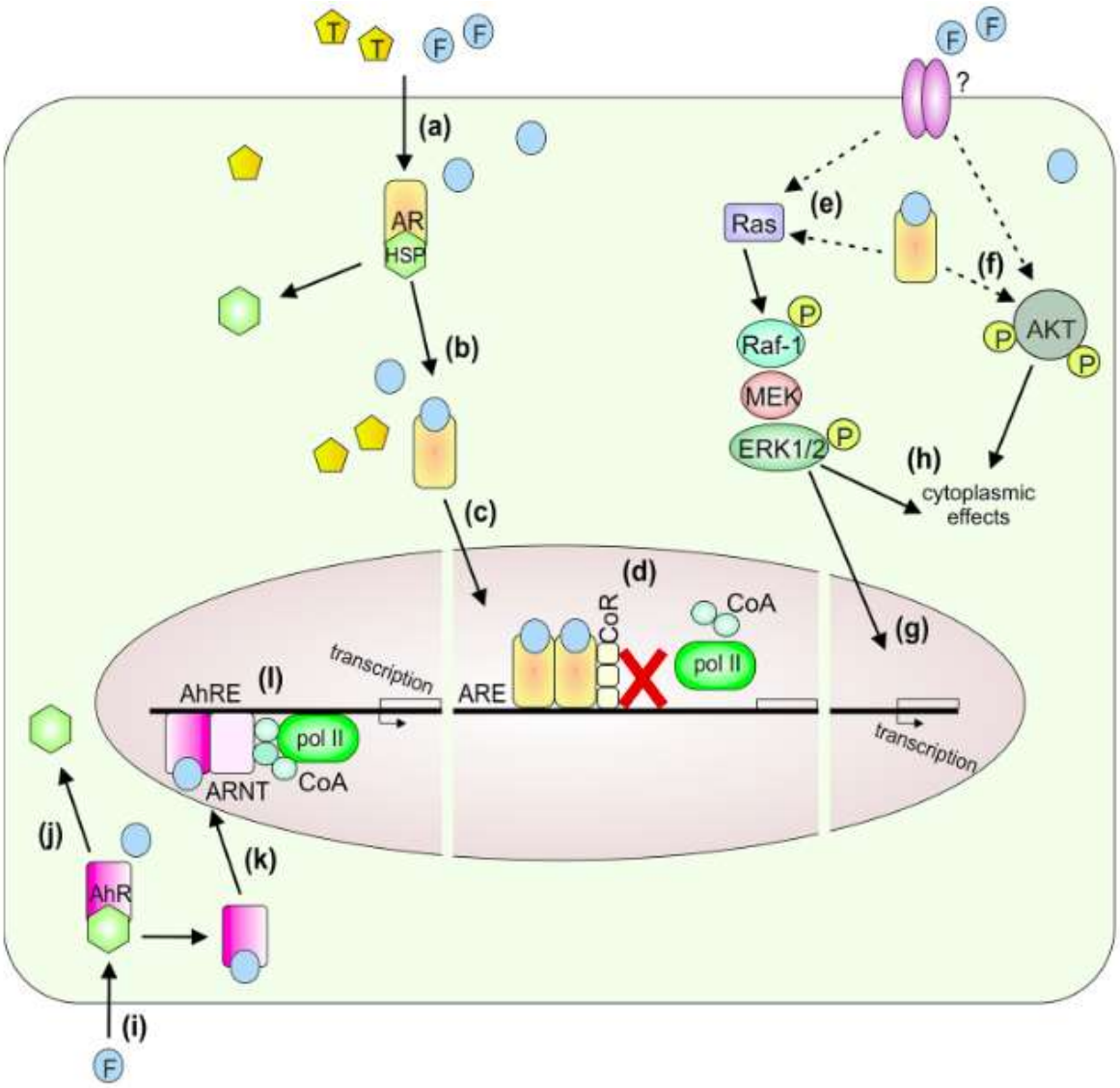

Figure 5. 2-HOF actions on the target cancer cell level.

(a) 2-HOF (F) competes with testosterone (T) and binds preferentially to the androgen receptor (AR), displacing bound heat shock proteins (HSP). (b) 2-HOF/AR complex enters the nucleus, (c) Blocking the AR decreases its association with coactivators (e.g. STAT3, GRIP1, and TIF2), inhibits polymerase II binding to the promoter, and consequently inhibits transcriptional activity (d) 2-HOF may also trigger MAPK (e) or AKT (f) pathway activation (via an unknown mechanism – dotted line arrows), which modulates gene transcription (e.g. cyclin D1, leading to cell proliferation) (g) and/or cytoplasmic effects (e.g. junction protein phosphorylation, leading to altered cell-cell adhesion) (h). Alternatively, 2-HOF binds to AhR (i) resulting in dissociation from HSP (j) and nuclear translocation (k). AhR heterodimerizes with ARNT forming an active transcription factor complex, which binds to AhRE, recruits transcriptional machinery, and initiates target gene transcription (l). N.B. 2-HOF does not induce AhR transcriptional activity.

Abbreviations: AhR – aryl hydrocarbon receptor; AhRE – arylhydrocarbon receptor response element; AKT – protein kinase B; AR – androgen receptor; ARE– androgen response element; ARNT – AhR nuclear translocator; CoA – coactivators; CoR –corepressors; ERK1/2 – extracellular signal regulated kinase 1/2; F – 2-HOF; HSP – heat shock proteins; MAPK – mitogen-activated protein kinases; MEK – mitogen-activated protein kinase; pol II – RNA polymerase II; Ras – Ras protein; Raf-1 – proto-oncogene serine/threonine-protein kinase 1; P – ortho-phosphoric acid residue; T – testosterone; ? – hypothetical membrane receptor binding 2-HOF.

1.3.4 Chemotherapy for non-small cell lung cancer treatment

Lung cancer is the deadliest form of cancer worldwide. Non-small cell lung cancer (NSCLC) represents at least 80% of diagnosed lung cancer cases. More than 50% of patients diagnosed with lung cancer have less than one year survival, and the 5-year survival rate for NSCLC is approximately 26%.[98] The high death rate is explained by late detection of the cancer and by the fact that NSCLC is particularly resistant to cytostatic treatment.

Even if many lung cancer patients are elderly and often have a history of smoking, there are also many young non-smokers who suffer from lung cancer. Irrespective of age or personal habits, receiving a lung cancer diagnosis is devastating for all patient groups. In Sweden, committed individuals have initiated supportive podcasts on the internet, for example: ”Lungcancerpodden” (https://www.lungcancerpodden.se) and “En podd om cancer” (https://enpoddomcancer.se), where the public and medical experts can share experiences with lung cancer patients and their relatives. The podcasts allow people to support each other and learn how to enjoy normal daily life.

Systemic chemotherapy based on platinum compounds, such as cisplatin and carboplatin, is a corner stone in the treatment of advanced NSCLC. In phase III trials in patients with NSCLC, combining taxanes (see next section), such as docetaxel or paclitaxel, with a platinum-based drug has been successful in increasing time to progression and improving quality of life but does not increase survival time.[99,100]

Although commonly employed, chemotherapy has only modest effects in early-stage NSCLC, and produces severe systemic adverse effects.[101] Intratumoral treatment with cytostatic agents administered with a catheter through a flexible bronchoscope may be considered for local treatment to reduce systemic toxicity.[102] Studies have also been performed with transpleural administration of hypotonic cisplatin in distilled water in NSCLC patients, showing a possibility to administer drugs intratumorally through the pleura.[103]

1.3.5 Mechanisms of action of docetaxel

In 1979 Schiff *et al*. discovered the mechanism of action of taxanes.[104] Docetaxel is part of the taxane family and is a cytostatic agent acting via mitotic inhibition. The principal mechanism of action is disruption of microtubule function, which is essential in cell division.[105]

Docetaxel is structurally similar to paclitaxel. Paclitaxel is the first approved taxane drug that was isolated from the Pacific yew, *Taxus brevifolia.* Docetaxel is the second generation taxane isolated from European yew, *Taxus baccata*. Docetaxel is semi-synthetic and differs from paclitaxel at two positions (Figure 6), making docetaxel more water-soluble (3–25 µg/ml) compared to paclitaxel (0.4–0.7 µg/ml). This generates a 1.9-fold higher binding affinity to microtubules and potentially also results in a higher intracellular accumulation, which results in two times higher microtubule stabilization in relation to paclitaxel.[106–108] When administering docetaxel in a local depot, it needs to be released and dissolved for transport into cancer cells.[109] As docetaxel has a higher solubility compared to paclitaxel, it may be advantageous for local treatment formulations.

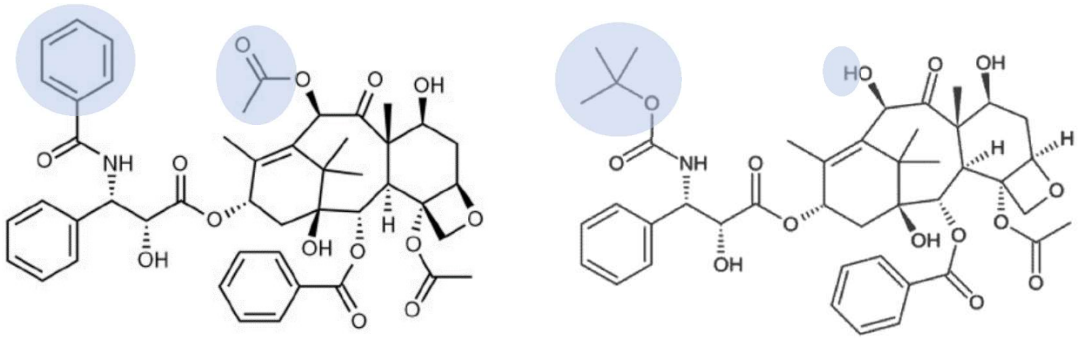

Figure 6. Molecular structures of paclitaxel and docetaxel (differences highlighted in blue).

Docetaxel reversibly binds to and stabilizes microtubules. During cell division, microtubules undergo constant polymerization and disassembly due to their dynamic instability, resulting in growing and shrinking phases. During polymerization, the tubulin αβ-heterodimers – the basic element of microtubules – are bound to a guanosine tri-phosphate (GTP) molecule, where the α-tubulin is stable but the GTP bound to β-tubulin is hydrolyzed to guanosine di-phosphate (GDP). The hydrolysis follows the addition of the next dimer to the positive end of the previous one. Docetaxel stabilizes GDP-bound tubulin, which prevents microtubule depolymerization and thus chromosome separation. The cell cycle is arrested at the G2/M phase and cellular apoptosis occurs.[110]

In addition to microtubule binding, docetaxel has two other ways of inducing apoptosis. One is to down-regulate the expression of the androgen receptor, including forkhead box protein O1 (FOXO1) mediated repression of androgen receptor transcriptional activity, and the other one is to induce phosphorylation of Bcl-2 in the endoplasmic reticulum, as described in Figure 7.[111,112]

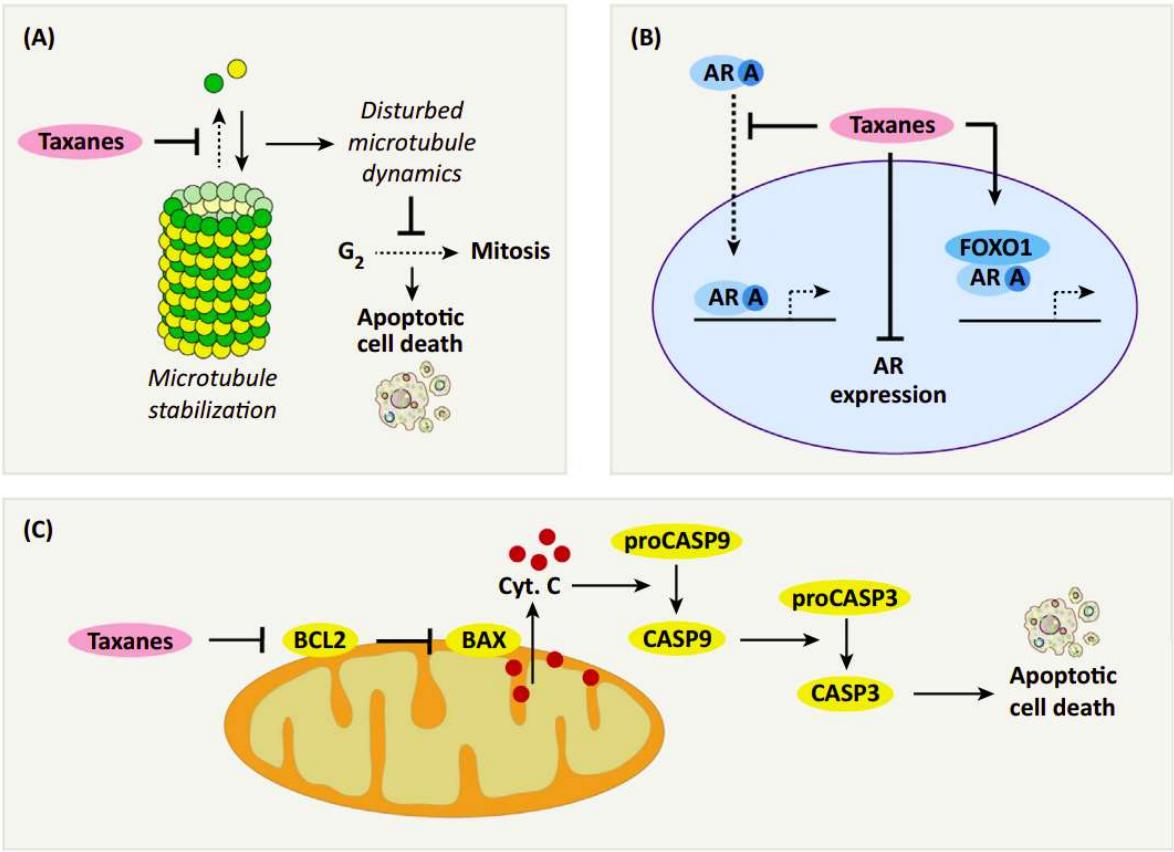

Figure 7. Mechanisms of action of the antitumor activity of taxanes.

(A) Taxanes bind to microtubules and thereby prevent their disassembly, resulting in G2/M cell cycle arrest and apoptosis. (B) Alternatively, taxanes are able to inhibit androgen receptor (AR) transcriptional activity (AR A) by constraining AR expression, blocking AR nuclear translocation, and facilitating FOXO1-mediated repression of AR transcriptional activity. (C) Finally, taxanes may inhibit the expression of antiapoptotic Bcl-2, favoring apoptotic cell death through the relief of BAX-mediated cytochrome c (Cyt. C) release.

Abbreviations: FOXO1 – Forkhead Box O1 protein coding gene, Bcl-2 – apoptosis regulator protein coding gene, BAX – Bcl-2 Associated X apoptosis regulator protein coding gene, CASP – caspase.

Taxanes display synergistic effects with other chemotherapeutic agents, and also an enhanced effect with radiotherapy.[113] Docetaxel has shown a favorable anti-cancer response by the activation of pro-inflammatory M1 ("killer") macrophages.[114] In addition, Millrud *et al.* reported that when mononuclear cells (MNCs) and macrophages from peripheral blood collected from healthy donors were incubated with docetaxel at a concentration of 0.1–10 µM, the MNCs and macrophages showed an activated phenotype with up-regulated expression of the surface receptor HLA-DR (human leukocyte antigen - DR isotype), and the membrane protein, CD86.[114] Furthermore, docetaxel studies in mice showed increased cytotoxic T cell activity as well as an increased infiltration of immune cells into the tumor microenvironment.[115] Chen *et al.* have reported that docetaxel has similar effects on B cells as on T cells.[116] In a preclinical study with triple negative breast cancer tumor-bearing mice, docetaxel has been shown to inhibit myeloid-derived suppressor cells.[117] Also, intratumoral injection treatment with docetaxel has shown promising results in a renal cancer mouse model.[118]

A beneficial feature of docetaxel for intratumoral delivery, compared to DNA-binding vesicant drugs such as doxorubicin, is that formulation leakage off target is less toxic to the healthy surrounding tissue. Therefore, the cytostatic drug depot does not necessarily need to be positioned within the tumor.[119]

1.3.6 Local drug delivery of biomolecules

Drug depot formulations may also be applicable for the delivery of biomolecules to a tumor.[120] In the preparation of biomolecule depot formulations, it is often a challenge to maintain the functionality of the molecule.[121–123]

In immunotherapy, a variety of bioactive proteins are used, such as monoclonal antibodies (mAbs), including inhibitors of CTLA-4 (ipilimumab, 149 kDa) and PD-1/PD-L1 (nivolumab, 144 kDa). Another protein that has been reported for local drug delivery is the granulocyte-macrophage colony-stimulating factor (GM-CSF, 14 kDa), also known as colony-stimulating factor 2 (CSF2).[124–127] In addition, there are several other synthetic and natural compounds used as immune adjuvants and agonists, including toll-like receptor (TLR) agonists, e.g. unmethylated cytosine-guanine (CpG) oligonucleotides. TLR agonists play a key role in the innate immune system and the development of cancer, and have been shown to have potential in the treatment of solid tumors as well as for hematologic malignancies like leukemia.[128-130]

Intratumoral injections with TLR agonists have shown good anti-tumor effect when combined with systemically injected cytostatic agents or checkpoint inhibitors.[131,132] These treatments activated TLR9 on B-cells and dendritic cells to a pro-inflammatory Th1-type cytokine (mainly interferon gamma) response both locally and systemically. The TLR agonists also affect the recruitment of immune cells such as macrophages, dendritic cells, B-cells and T-cells to the tumor.[133]

Local slow release from intratumoral depots are of particular interest for immunoactive biomolecules that risk provoking excessive systemic immunoreactions or rapid enzymatic degradation (e.g. STING agonists).[134] In addition, slow release depots of TLR9 agonists, for example, may help to reduce the number of injections from twice weekly to once every four to six weeks.[135,136]

1.3.7 Combination of local and systemic treatment

In order to obtain synergistic effect, local and systemic cancer treatment may be combined. Recently, promising results have been reported from combining systemic chemotherapy (5-fluorouracil) with local radioactive (^{125}I) seed implantation (brachytherapy) for the treatment of patients with advanced colorectal cancer.[137]

Similarly, positive results were observed in treating high-risk localized prostate cancer, using external beam radiotherapy (EBRT) in combination with systemic androgen deprivation therapy (ADT) and after prostatectomy when adding systemic docetaxel.[138]

1.3.8 Abscopal effect

The abscopal (from Latin *ab* "position away from", and ancient Greek *skopós* "target") effect has been observed in radiotherapy and is characterized by regression in tumors or lesions beyond the irradiated target. The phenomenon was first reported by R.H. Mole in 1953.[139]

Since then, the effect has been observed in radiotherapy of both the primary tumor and the metastases of various types of cancer. Abscopal effects (or anenestic "uninjected" effects) have also been more frequently reported in the field of immune oncology, as the use of locally injected immune oncology agents increases.[140,141] This is an additional potential benefit derived from the administration of intratumoral slow-release depots in cancer treatment.

1.3.9 Limitations of local tumor treatment

Local tumor treatment has several limitations:

1. Failure to reach circulating cancer cells and metastases.
2. Parenteral depot injections, especially polymers and hydrogels, tend to produce an uneven release profile with a high initial release followed by a decrease in concentration gradient over time.[142] Consequently, this requires frequent injections to maintain a therapeutic concentration, which may alter the treatment efficacy.
3. Intratumoral administration is often more complicated and invasive than oral or intravenous administrations.
4. The long-term release of active substances may lead to the development of tumor resistance.

1.4 IMAGING TO EVALUATE BIODISTRIBUTION

To achieve reliable preclinical results during the development of anti-cancer drugs, there is a need for tools to facilitate the evaluation of drug candidates in animals. For example, non-invasive imaging in combination with contrast agents/probes can be used for the evaluation of pharmacokinetics, biodistribution and to follow treatment efficacy. One of the commonly used methods in preclinical cancer research is optical imaging, including fluorescence and bioluminescence imaging.[143,144]

In optical imaging, a cooled charge-coupled device (CCD) camera is used to detect the light emitted from a fluorescent or bioluminescent light source in live animals. Several optical imaging systems are commercially available. One possible application of fluorescence imaging in drug depot characterization is to label the drug with a fluorescent marker and then to follow the drug release and biodistribution *in situ*. Fluorescence imaging in the near-infrared (NIR) range gives a high signal/background ratio in the body. In the visible wavelength range (350–700 nm), biological tissues commonly display a high degree of background due to light absorbance from pigments and hemoglobin. Such background noise can be reduced by performing optical imaging in the NIR range. Therefore, NIR fluorescent dyes with excitation/emission wavelengths in the range 700–900 nm are more suitable for *in vivo* applications compared to other fluorophores.[145-147]

In a longitudinal *in vivo* fluorescence imaging study, it is worth noting that the fluorescence signals detected from the surface of the animal are different from the original light sources inside the body, especially for deep tissue imaging. There are two different configurations available for fluorescence imaging: tomographic and reflectance. Tomographic imaging allows measurements of deep tissue, while reflectance imaging can only measure a few millimeters below the surface of the animal as it utilizes continuous wave (CW) excitation light.[148] To obtain an accurate evaluation of drug biodistribution, *ex vivo* fluorescence imaging and histological analysis are often performed to confirm the *in vivo* imaging.[149] For example, the release and clearance of the probe IRDye 800 CW can be followed by fluorescence imaging over time in the same mouse (Figure 8).

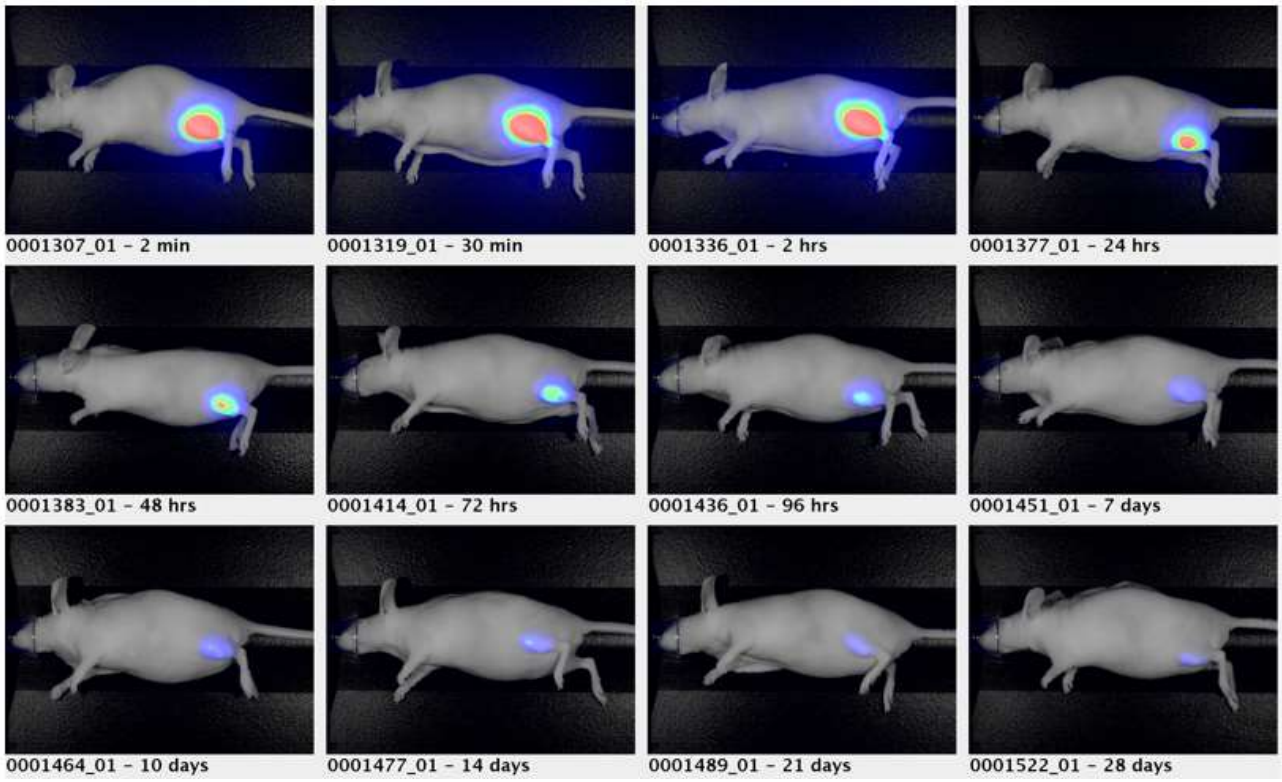

Figure 8. Fluorescence longitudinal images of the release and clearance of a probe from a calcium sulfate depot over 28 days.

Subcutaneous implant injection with 50 µl NanoZolid and 0.1 nM IRDye 800 CW (probe) in left thigh.

2 AIMS

The main aim of the present thesis was to evaluate calcium sulfate as a novel drug delivery system, using the NanoZolid technology. The evaluation was performed by using the newly developed injectable depots for local cancer treatment.

The main aim would be achieved via the following specific aims:

- To characterize the physical and chemical properties of the drug delivery system and explore its fields of application.

- To study the drug release of different NanoZolid formulations *in vitro* and *in vivo*.

- To investigate the treatment efficacy of intratumoral injections using NanoZolid containing docetaxel in a prelinical model.

- To study the NanoZolid formulation as a carrier for biomolecule that can be used for treatment.

- To evaluate the clinical effects of NanoZolid containing an antiandrogen in cancer patients.

3 MATERIALS AND METHODS

3.1 MANUFACTURING OF NANOZOLID FORMULATIONS

The NanoZolid depot formulations consist of a powder (calcium sulfate) containing drug which is mixed with an aqueous diluent prior to administration. The manufacturing processes of 2-hydroxyflutamide (2-HOF) loaded powder and the diluent are described below.

3.1.1 Manufacturing process of NanoZolid powder

Calcium sulfate dihydrate is transformed to calcium sulfate hemihydrate by heating at 200°C for 4 hours. For the heat treatment on laboratory scale, an even layer of 250 g of powder is transferred to a crystallization dish (190 x100 mm, w x h). Two such powder filled dishes are loaded simultaneously in an oven with a fan-controlled air flow. After heat treatment, the remaining approximately 200 g of powder per dish is cooled to RT and thereafter transferred to a 1 liter plastic (HDPE) container with screw lid, together with 500 g of milling balls (10 mm diameter of silicon nitride) and 165 g of water-free isopropanol. The filled and sealed plastic container is mounted in a tumbling mixer and shaken at 46 rpm for 24 hours. After milling, the milling balls are removed and the hence produced slurry of milled powder in isopropanol is poured into the vessel of a rotary evaporator and kept at 35°C with a water bath until the isopropanol is completely evaporated (approximately 4 hours). The dried powder is deagglomerated in a conical mill with a 1.2 mm sieve. The result is a fine-grained calcium sulfate hemihydrate powder of about 2-3 µm average grain size, as described in more detail in **paper I**. To produce the clinical material, the heat treatment was performed with 500 g of calcium sulfate dihydrate per crystallization dish and a total of 16 dishes per oven-load.

The drug (2-HOF) is added to the milled calcium sulfate hemi-hydrate powder. The 2-HOF powder is completely dissolved in isopropanol (1:2 w/w). The calcium sulfate hemihydrate powder is then added to the 2-HOF solution (1:1 w/w). The ratio of drug to calcium sulfate has been varied according to the desired drug load. The isopropanol is removed from the solution/suspension with a rotary evaporator at 35°C (for 200 g of calcium sulfate and 200 g of 2-HOF in 400 g of isopropanol the drying process takes approximately 6 hours). Also this powder is deagglomerated in a conical mill with a 1.2 mm sieve. The result is a fine-grained powder with 2-HOF well distributed in calcium sulfate.

The calcium sulfate-2-HOF powder mix is used as starting material for the production of densified cylinders using an isostatic press. The cylinders are produced using cylindrical silicon rubber molds, in two compression steps. First, a rubber mold is filled with 150 g of the powder mix and pre-compressed without water at a pressure of 100 MPa for 2 min. This leads to a cohesive but porous and dry cylindrical body. Secondly, the rubber mold is opened and 15 g of water for injection is added to the porous pre-compressed cylinder. The rubber mold containing the wetted cylinder is re-sealed and put under compression at 400 MPa for 60 min. During this time the calcium sulfate hemihydrate is recrystallized and transformed to di-hydrate absorbing the majority of the added water. The hydration under pressure leads to calcium sulfate dense cylinders (**paper I**).

The densified cylinders of calcium sulfate containing 2-HOF are crushed to coarse granules with a jaw crusher (coarse milling to mm-sized lumps) and with an ultracentrifuge mill (finer milling to granules < 500 µm). To achieve a specific granule size range, the granules are passed through two sieves corresponding to the desired size range. For the 2-HOF depot, the granule size range is 125-300 µm. The coarser material can be passed through the centrifuge mill again. The discarded material constitutes approximately 30 % of the total amount. This process achieves granules with a drug substance encapsulated in non-porous calcium sulfate dihydrate.

The process described above produce three powder types: the pure calcium sulfate hemihydrate, the powder mix of calcium sulfate hemihydrate and 2-HOF, and the densified granules with 2-HOF in calcium sulfate di-hydrate. By mixing these powders in different proportions, composite powder formulations of varied properties are obtained. A tumbling mixer is used to form homogeneous mixture.

For clinical and preclinical application, the selected powder mixture is dispensed in plastic syringe. The syringes are individually packed in hermetically sealed aluminium foil pouches and sterilized with a dose of above 25 kGy gamma radiation (standard dose for sterility, defined as <1 cfu/1 million product units).

To achieve a faster release, NanoZolid formulations may contain only non-densified powder, e.g. EGF and docetaxel formulations (see 3.2.6).

3.1.2 Manufacturing process of NanoZolid diluent

A medium viscosity sodium carboxymethyl cellulose (Ashland, The Netherlands, grade 9M31XF) with a substitution degree of 0.92 (average number of carboxymethyl groups per anhydroglucose unit of the cellulose backbone) is used to produce the NanoZolid diluent, a 0.25% sodium carboxymethyl cellulose aqueous solution. The sodium carboxymethyl cellulose is dissolved in water at 70°C, and left to swell for two hours while stirring. Thereafter, the solution is left to swell overnight without stirring or heat.

The swelled solution is filtered through a 30 µm filter and a 0.45 µm filter, then sterilized at a temperature of at least 121°C for at least 15 min.

The NanoZolid diluent slows down the solidification rate of calcium sulfate suspension, compared to pure water. The solidification time becomes 10 to 20 min using sodium carboxymethyl cellulose diluent. The ratio of diluent:powder also affects the viscosity of the suspension, see description in section 3.2.3.

3.2 PHYSICOCHEMICAL CHARACTERIZATION

3.2.1 Powder grain size

The particle size of calcium sulfate powders (both milled and un-milled) as well as compressed granules were characterized utilizing either laser light diffraction with a Malvern Mastersizer 2000 wet sample dispersion unit (Malvern Panalytical Ltd, UK) or X-ray absorption with a

SediGraph III 5120 wet sedimentation particle size analyzer (Micrometrics Instrument Corp., USA). The X-ray absorption method was mostly used and is suitable for measuring grains in the size range 0.1-300 µm, i.e. ideal for the calcium sulfate powders. Laser diffraction with the sample dispersed in liquid medium has a measuring range 0.02-2000 µm and could with a margin also include granule analysis. An error has been made in **paper I**, where the methods part describes laser light diffraction but the graphs shown were actually performed with X-ray absorption.

Specific surface area was evaluated with nitrogen gas adsorption using a Brunauer-Emmet-Teller (BET) Micrometrics Gemini II 2370 analyzer (Micrometrics Instrument Corp., USA).

To evaluate the crystal structure and to identify the calcium sulfate hydrates typical diffraction peaks, X-ray powder diffraction (XRPD) method was used,[150] utilizing a PANalytical X'Pert PRO XRPD diffractometer (Malvern Panalytical B.V., The Netherlands) with a radiation wavelength of $\lambda = 0.154$ nm **(paper I**).

3.2.2 Powder flowability and compressibility

To measure the ability of calcium sulfate-drug powders to be homogeneously filled in syringes and handled in general, flowability tests were performed. Carr's compressibility index was calculated from measured bulk and tapped densities from filled syringes. Visual measurements were also performed for static angle of repose by use of protractor for the symmetrical cone of powder.[151,152]

Low pressure pre-compression of dry powder bodies ("green bodies") and high pressure compression tests of wetted and hydrating powders were performed with an isostatic press, mostly in the scale of 150 g per green body. The isostatic pressure, the pressing time and amount of hydration water were optimized in pre-compression and main-compression processes, by evaluating porosity and density after different isostatic compression cycles as described in **paper I**.

3.2.3 Solidified depots for *in vitro* characterization

To prepare the NanoZolid depot, the drug-containing powder syringe was connected via a Luer-lok® screw-fit connection to the syringe containing the aqueous diluent. The two components were mixed/reconstituted to a suspension by pushing the plungers back and forth and hence forcing the formulation through the Luer node (Figure 9A). After the reconstitution, 0.3 g depots of the viscous suspension were dispensed on a small soft plastic polyethylene lid placed on a balance, where they solidified to pea-shaped depots. The softness of the plastic lid made it easy to detach the depot after solidification (Figure 9B).

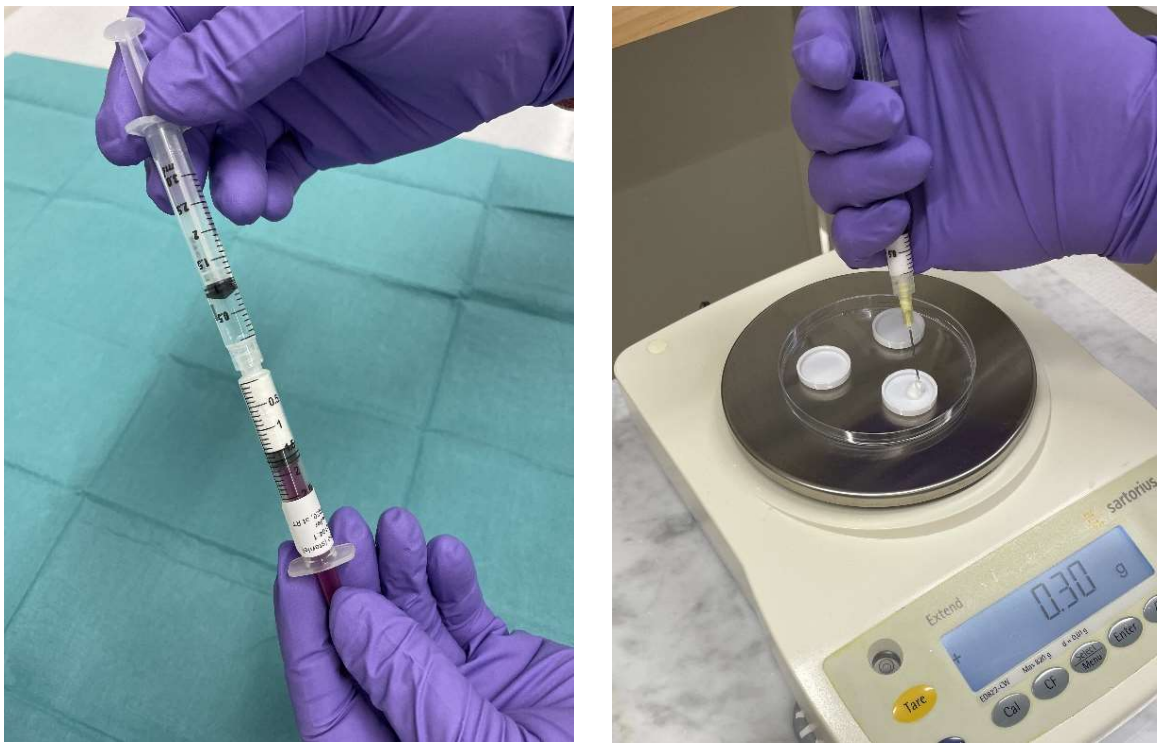

Figure 9. A) Reconstitution of powder and diluent, and B) Dispensing of 0.3 g depots.

3.2.4 Scanning electron microscopy (SEM) and energy dispersive spectroscopy (EDS)

Cross-sections of solidified depots were analyzed using a combination of field emission gun scanning electron microscopy (FEGSEM) and energy dispersive X-ray spectroscopy (EDS), Zeiss 1530 (Carl Zeiss Microscopy Deutschland GmbH, Germany), for topographical features and elemental mapping. The FEGSEM can deliver images with a higher resolution compared to conventional SEM as the electron source is field emission instead of thermionic heating. EDS identifies individual elements of an atomic number above 4 that are present at the sample surface, and at a depth down to approximately 5 µm (**paper I**).

3.2.5 *In vitro* drug release

Molded depots were used for *in vitro* evaluation of depot disintegration and of drug release.

Disintegration test was performed to evaluate the ability of the molded depot to maintain a physically stable 3D-structure (cohesion) in an aqueous milieu. This test was carried out at RT in a crystallization dish (190 mm) with two molded depots positioned in saline solution for 48 h (Figure 10).

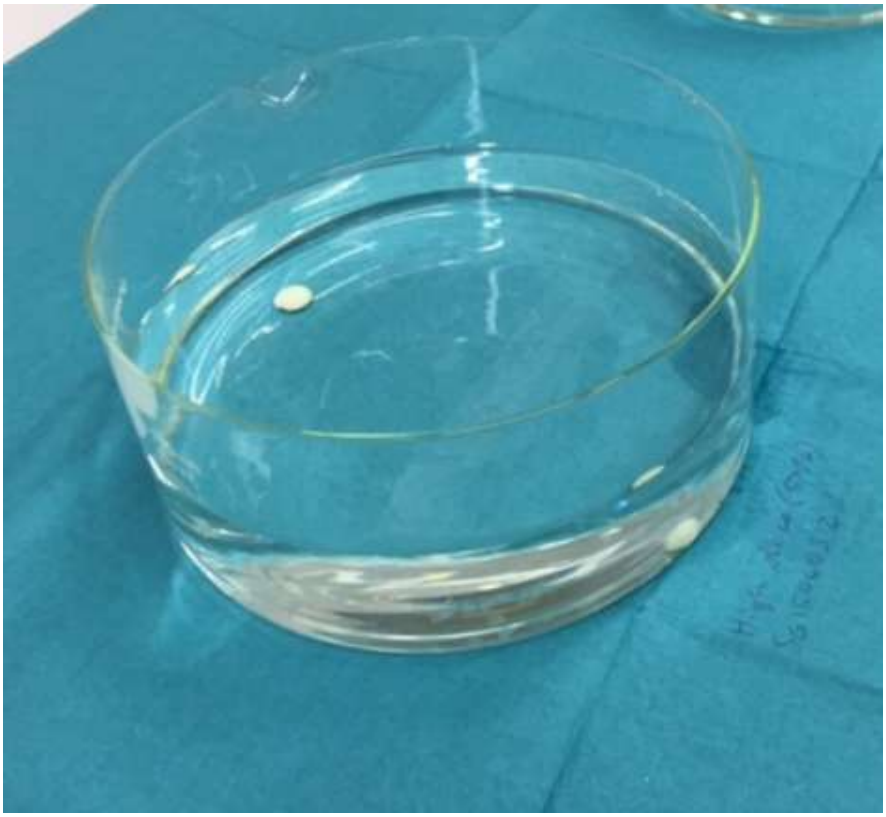

Figure 10. Physical disintegration test setup for solidified depots.

After passing this disintegration test, depots from the same batch were evaluated for drug release *in vitro* in an aqueous solution. Drug concentrations were analyzed using High Performance Liquid Chromatography (HPLC) and ultra-violet (UV) detector. The *in vitro* dissolution was performed by individually submerging 300 mg solid depots of the formulations in 300 ml saline at 37°C. The drug concentration in the saline was measured daily or weekly, depending on formulation. The evaluation was performed normally 2 or 3 weeks, up to 5 months. In order to evaluate the reproducibility in formulation release behavior, the dissolution method was chosen because it is sensitive enough to discriminate potentially critical differences between formulations.

The *in vitro* drug release of 2-HOF from calcium sulfate depots (Liproca Depot) during 3-week and 5-month were evaluated using different formulations containing different amount of 2-HOF. For mathematical comparison of dissolution profiles, the similarity factor f_2 was calculated according to the formula proposed by Moore and Flanner:

$$f_2 = 50 \cdot log\left\{(1 + (1/n)\ \sum_{t=1}^{n}(R_t - T_t)^2)^{-0.5} \cdot 100\right\} \qquad [5]$$

where n is the total number of drug release test points, and R_t and T_t are the average percentages of drug released from a reference formulation and from a test formulation, respectively, at test number t **(paper I)**.[153]

The drug release profiles for docetaxel formulations were followed for 2 weeks. This was primarily related to the estimated follow-up period in animal studies **(paper II)**.

3.2.6 NanoZolid depot formulations

Seven calcium sulfate formulations with various active substances have been evaluated:

Liproca® Depot 25% is a slow-release drug depot for local antiandrogen treatment of prostate cancer. The powder contains 25% 2-HOF (w/w) in both densified granules (which constitute 1/3 of the powder) and in a non-densified powder fraction (constituting 2/3). The formulation is described and evaluated in **paper I**.

Liproca® Depot 33% is a slow-release drug depot for treatment of prostate cancer with an increased drug load compared to Liproca Depot 25%. The drug loaded powder contains 33% 2-HOF (w/w) in both densified granules (36% of the powder) and in a non-densified powder fraction (64% of the powder). The formulation is described and evaluated in detail in **paper I** and **paper IV**.

NZ-DTX Low is an experimental formulation for intratumoral treatment of solid tumors with docetaxel. The powder formulation contains 6.25% of docetaxel (w/w) and is described and evaluated in **paper II.**

NZ-DTX High is an experimental formulation for intratumoral treatment of solid tumors with an increased drug load of docetaxel compared to NZ-DTX Low. The powder formulation contains 12.5% of docetaxel (w/w) and is described and evaluated in **paper II.**

NZ-EGF-NIR Low is a model formulation for the *in vivo* study of drug release and biodistribution in a preclinical cancer model with a fluorescent biomolecule. The powder formulation contains 0.37% of the fluorescence-labelled epithelial growth factor protein EGF-NIR (w/w), as described and evaluated in **paper III**.

NZ-EGF-NIR High is a model formulation for the *in vivo* study of drug release and biodistribution in a preclinical cancer model with an increased amount of fluorescent biomolecule. The powder formulation contains 1.47% of the fluorescence-labelled epithelial growth factor protein EGF-NIR (w/w), as described and evaluated in **paper III**.

NZ Placebo is a calcium sulfate powder formulation without drug, consisting of non-densified powder and was used as a control in **paper II**.

For reconstitution, the Liproca® powder formulations are mixed 1.00:0.98 (w/w) with diluent (0.25% sodium carboxymethyl cellulose aqueous solution), while all the other depot formulations are mixed with the diluent in proportion 1.00:1.00 (w/w).

An error has been made in **paper II**. On page 187, section 2.3, it is stated that the NZ-DTX formulations contained 5% (NZ-DTX Low) and 10% (NZ-DTX High) docetaxel in the powder. These numbers are the concentrations of the reconstituted suspensions when expressed as weight per volume (50 mg/ml and 100 mg/ml). The concentrations in the NZ-DTX Low and NZ-DTX High powders are 6.25% and 12.5% docetaxel, respectively.

3.3 ANIMAL EXPERIMENTS

3.3.1 Lewis lung cancer cell mouse model for intratumoral docetaxel

The lung cancer model with subcutaneous Lewis Lung Carcinoma (LLC) cells in mice is well-established and suitable for both systemic and local administration of cytostatic agents. This model was used to evaluate the formulations NZ-DTX Low, NZ-DTX High and NZ placebo (**paper II**).

Tumor dimensions were measured using digital calipers and the tumor volumes were calculated as 0.5 x Length x Width x Height.

Blood samples were collected from the tail vein and analyzed with Ultra High Performance Liquid Chromatography-Tandem Mass Spectrometry (UHPLC-MS/MS).

Tumors were dissected at endpoint and fixated in 4% formalin overnight followed by 70% alcohol. Tissues were paraffin embedded, sectioned at 3 µm, and stained with hematoxylin and eosin (HE). Morphology was evaluated for each tumor. The area of necrosis was estimated in relation to the total area (rounding up or down to the nearest 5% step), and mitotic index was evaluated by counting mitosis in 10 high power fields.

3.3.2 A549 lung cancer cell mouse model for biodistribution of EGF

The biodistribution of fluorescence-labeled epithelial growth factor (EGF) protein released *in vivo* from calcium sulfate intratumoral depots was investigated in a mouse model with subcutaneously implanted A549 lung cancer cells. This model was used to evaluate the formulations NZ-EGF-NIR Low and NZ-EGF-NIR High. The A549 cells were chosen as they express a high level of EGF receptors (**paper III**).

Tumor dimensions were measured using digital calipers and the tumor volumes were calculated as $v = a \cdot b^2/2$, where v is the tumor volume, a is the largest and b is the smallest diameter.

A Pearl® Trilogy small animal imaging system from LI-COR Biosciences (USA) was used for the *in vivo* analyses of NIR fluorescence. Images were taken in the 800 nm laser channel (excitation with solid-state laser diode at 785 nm) and with visible light (532 nm). Longitudinal analyses were performed, i.e. repeated measurements on each subject at multiple follow-up times.

For the *ex vivo* fluorescence analyses, a LSM800 confocal laser scanning microscope (Carl Zeiss Microscopy Deutschland GmbH, Germany) with a 20X magnification dry lens was used.

Digital imaging of whole EGFR staining sections bright-field slide scanning (Hamamatsu NanoZoomer S60, Hamamatsu, Japan) was performed for image comparison with the digital images of EGF-NIR fluorescence recorded in whole sections.

3.4 HUMAN CLINICAL TRIAL

To test the formulation with 33% drug load of 2-HOF (Liproca Depot) in humans, a clinical trial was designed with urologists in Europe and North America, and performed at ten urological centers in Finland, Canada and Lithuania (**paper IV**).

Patients included in the study had a mean age of 64, ranging between 52 and 79. The patients were diagnosed with localized prostate cancer assigned to active surveillance with a Gleason score 3+3 or 3+4 and a PSA not above 20 ng/ml. The primary endpoints were tolerability and PSA reduction at 5 months after injection. Efficacy of the formulation was assessed by changes in PSA, prostate volume (PV), Prostate Imaging-Reporting and Data System (PI-RADS) score and with prostate biopsy histology.

After local anesthesia, the patients received the suspension, using a trans-rectal ultrasound probe for guidance of the needle; end-fire needle guide in Canada, and bi-planar needle guide in Finland and Lithuania. The ultrasound guided injections were performed through a 200 mm long 17 gauge needle in dose volumes of 5-24 ml (1150-5520 mg 2-HOF) distributed in proximity to the lesions between the prostate lobes (both sides of the urethra) as specified by magnetic resonance imaging (MRI) taken pre-injection (Figure 11).

Blood samples for assay analysis of 2-HOF were collected. PSA and testosterone were measured. PSA responders were defined as patients showing a PSA reduction of more than 15%, thus exceeding the expected normal variations. Blood serum samples of PSA and testosterone were analyzed with chemiluminescence assay and of 2-HOF with liquid chromatography tandem mass spectrometry (LC-MS/MS).

Prostate volume and PI-RADS version 2.0 scores were measured and evaluated by MRI at screening or performed within 12 months prior to screening and at month 5 post injection. MRI was used for lesion identification and planning of volume distribution in the prostate lobes. Measurements were performed with 3T (3 Tesla) clinical scanners using whole-body coils as both excitation and receiver phase-array coil. MRI examinations using the standard clinical protocol according to European Society of Urogenital Radiology included axial T1-weighted image, axial, coronal and sagittal T2-weighted image (T2WI), diffusion-weighted image (DWI) sequences including apparent diffusion coefficient (ADC). MRI for PI-RADS score evaluation was performed.

Transrectal ultrasound-guided prostate biopsies were taken at screening in all patients. Pathology response was not the primary endpoint, and therefore post treatment biopsies were not performed routinely. Biopsies were performed at month 6 (end of the study) on a subset of patients.

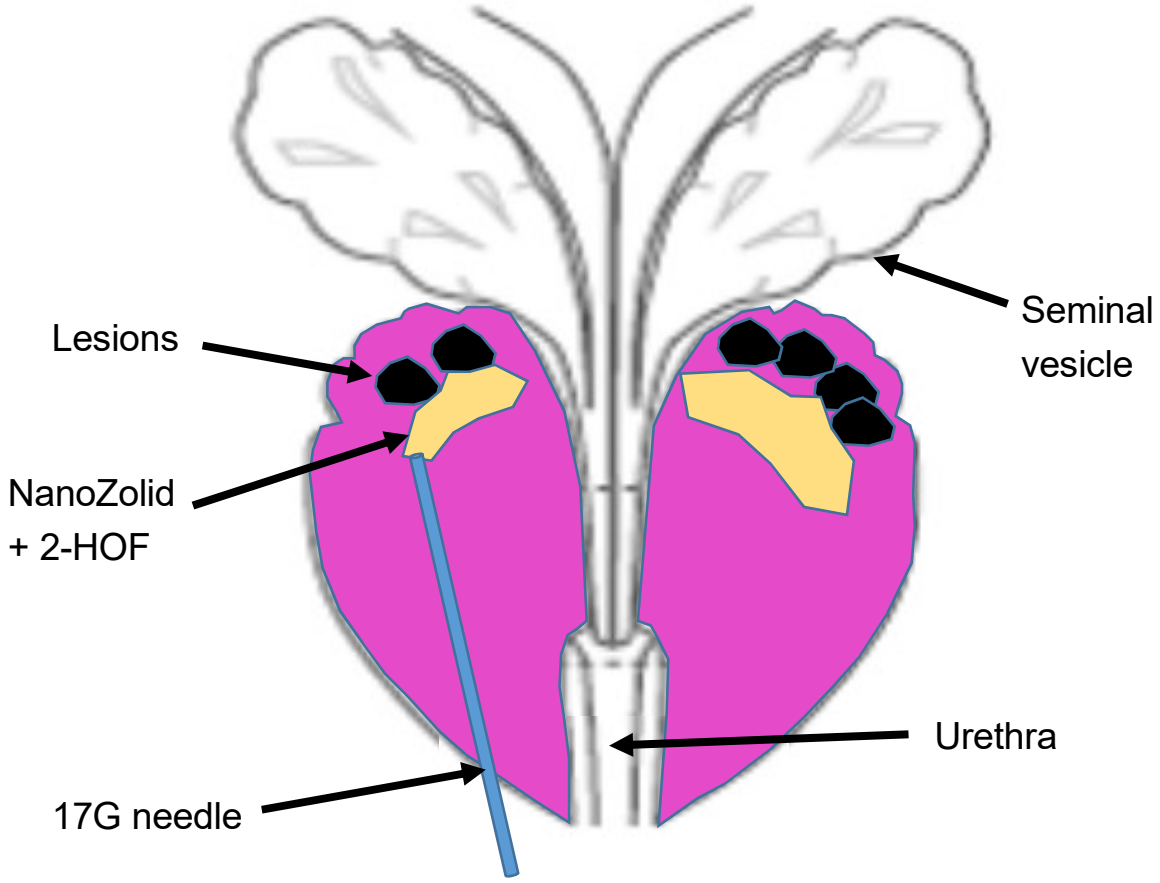

Figure 11. Schematic view of NanoZolid + 2-HOF (Liproca® Depot) treatment of localized prostate cancer.

3.5 STATISTICS

Survival (endpoint) was plotted using the Kaplan-Meier method and compared by the log-rank test (**paper II**).

For the LLC cancer model (**paper II**), groups were compared by one-way analysis of variance (ANOVA) and differences between groups were determined by Holm-Sidak's multiple comparisons test. Data was unevenly distributed and transformed using the natural logarithm. Data were presented as geometric mean ± standard error of the mean or ± 95% confidence interval as stated in figures.

For the A549 lung cancer model (**paper III**), groups were compared by two-way repeated measures analysis of variance (ANOVA) and differences between groups were determined using Bonferroni adjustment, i.e. multiplying each of the significance levels from the least significant difference test by the number of tests performed. Data were presented in figures as arithmetic mean ± standard deviation.

For the human study (**paper IV**), the primary efficacy endpoint, PSA reduction from baseline at month 5, was analyzed using a one-sided paired t-test or a non-parametric one-sided

Wilcoxon matched paired sign rank test. Statistical testing was performed at the one-sided 0.05 significance level. The corresponding secondary efficacy endpoint, PSA percent change from baseline over time, was analyzed using a two-sided paired t-test or a non-parametric two-sided Wilcoxon matched paired sign rank test. Statistical testing was performed at the two-sided 0.05 significance level. Other secondary endpoints were summarized and presented descriptively.

Statistical analysis was done using GraphPad Prism. A $p<0.05$ was considered statistically significant.

4 RESULTS

4.1 TWO NEW PROCESSES TO THE PHARMA INDUSTRY

In the present investigations, we introduced new applications to two equipment from the materials industry and have been adapted to the pharmaceutical industry: The Cold Isostatic Press (CIP) and the Jaw crusher. The CIP presented in these studies was obtained from Quintus Technologies LLC (USA, CIP42260) and the Jaw crusher was purchased from Retsch GmbH (Germany, BB-250-XL). Both instruments were adjusted to be used in pharmaceutical Good Manufacturing Practice (GMP). The equipment was installed at the contract pharma manufacturer Recipharm AB, Solna, Sweden.

The CIP (Figure 12) is used to create solid and dense powder bodies, and the Jaw crusher (Figure 13) is used for the crushing/rough milling of these bodies, as described in section 3.1.1.

Figure 12. GMP designed Cold Isostatic Press.
CIP42260 from Quintus Technologies LLC.

The CIP was modified to GMP use according to the following: 1) an improved safety level was achieved by adding a transparent cover and safety locking system, 2) accurate pressure monitor in accordance with pharma guidelines, and 3) a stainless steel cover enabling appropriate

cleaning to minimize contamination and dust collection (Figure 12). The pressure chamber was manufactured from stainless steel, for use of pure water without noncorrosive additives as pressure medium. All the adjustments were performed without affecting the accuracy of the manufacturing procedure, including the dry pre-compression step and the wet main-compression step (section 3.1 and **paper I**).

The modifications of the Jaw crusher were similar to that of the CIP: 1) a safer and more robust feeder mechanism – including a revised safety locking system, 2) all parts in contact with product material including the powder collector system were replaced with stainless steel devices, to fulfil pharma guidelines (Figure 13).

Figure 13. GMP designed Jaw crusher.
Jaw Crusher BB-250-XL from Retsch GmbH.

4.2 NANOZOLID FORMULATIONS WITH 2-HOF (LIPROCA DEPOT)

4.2.1 Drug distribution in the powder fractions

The solidification time after reconstitution depends on the amount of densified and hydrated granules (dihydrate) in the powder, as these granules act as seeding points for the solidification. Furthermore, the ratio between dihydrate and hemihydrate calcium sulfate is important in the

formulation design to achieve a suitable depot with desired physical and pharmaceutical features. Also, the distribution of drug in the solidified depots is important for the drug release.

Images of cross-sections of solidified depots with densified granules illustrate the distribution of the densified granules in the porous matrix as well as the distribution of the drug (2-HOF) in the porous matrix and in the granules as shown in Figure 14. The densified granules are evenly distributed in the non-densified matrix, and 2-HOF is present as precipitations both within the densified granules and in the porous matrix.

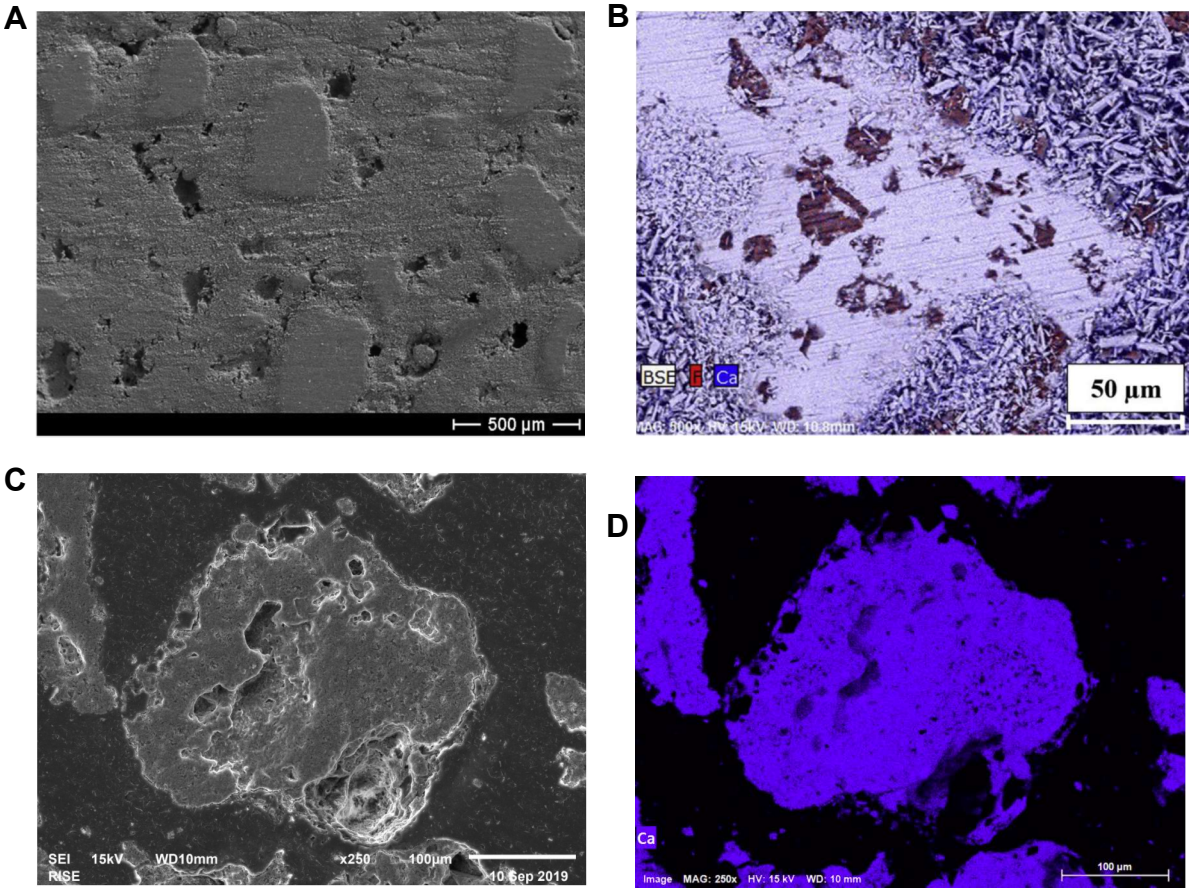

Figure 14. SEM images of cross-sections of depots and densified granules.
A) 25% 2-HOF depot, secondary electron mode, B) 25% 2-HOF depot EDS for elemental mapping, C) 33% 2-HOF dense milled calcium sulfate dihydrate granules in epoxy, showing the microstructure in secondary electron mode, and D) 33% 2-HOF dense milled calcium sulfate dihydrate granules in epoxy, showing the microstructure and calcium ("Ca", blue/purple) in EDS mode.
Note the differences in magnification (scale bars).

4.2.2 NanoZolid formulation of 2-HOF

To maximize the drug load of 2-HOF in the NanoZolid formulation (Liproca Depot) , the following adjustments were made in preparation: 1) the drug load in the porous material was increased from 43% to 50% (w/w), 2) the drug load in the dense granules was increased from 36% to 42% (w/w), 3) the ratio between loaded and unloaded material was increased from 67% to 72% (w/w), 4) the milling process for the granules was optimized to produce higher yield after the sieving procedure.

By optimizing all these parameters, we managed to increase the drug load in the composite powder from 25% to 33% (w/w), with a maintained drug release profile. Furthermore, flowability tests confirmed that the calcium sulfate-drug powders were suitable for a high yield and a homogeneous filling in the syringe. The static angle of repose was 31-35°.

With the properly balanced formulation, the *in vitro* drug release profile was kept unchanged, with approximately 40% released after 14 days (Figure 15).

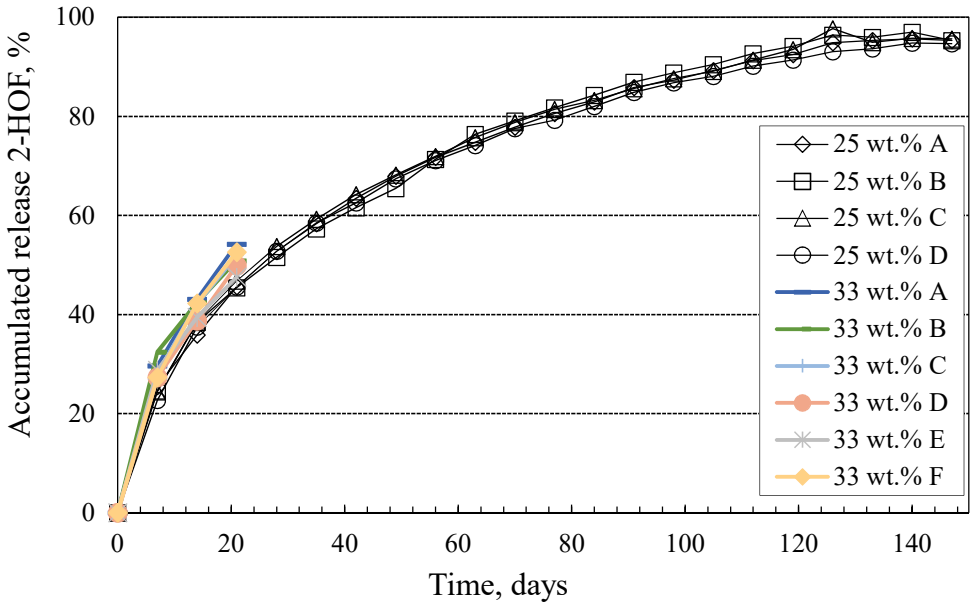

Figure 15. Release profiles from 0.3 g depots with 2-HOF, 25% vs. 33%.

The similarity factor (f_2) of 66% was observed, during the first 3 weeks, when the two formulations: 25% vs. 33%, were compared (**paper I**).

4.3 NANOZOLID FORMULATIONS WITH DOCETAXEL

4.3.1 *In vitro* release of docetaxel

Two NanoZolid formulations containing docetaxel were produced and shown to generate slow release profile as described in **paper II**. The formulations were evaluated *in vitro* and *in vivo*, the NZ-DTX Low with 6.25% (w/w) docetaxel in the powder and the NZ-DTX High with 12.5% (w/w) of docetaxel (section 3.2.6).

The low and the high formulations displayed similar release patterns despite a two-fold difference in drug load. The results indicate that docetaxel release mechanism is likely to be independent on the studied drug load. The measured *in vitro* drug release over 13 days was approximately 5.0% (rel.) for the low dose and 2.5% (rel.) for the high dose formulation (Figure 16).

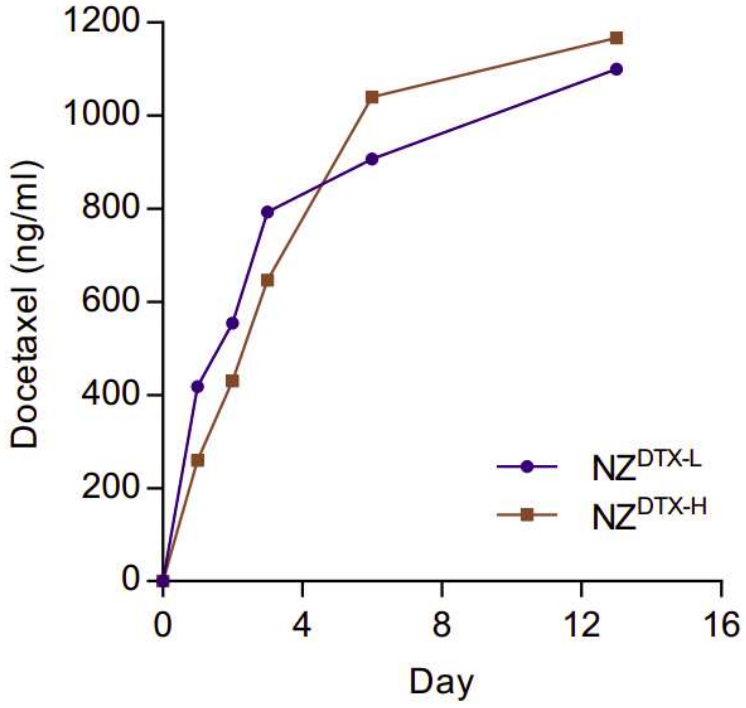

Figure 16. *In vitro* release profiles of docetaxel from NanoZolid formulations.
NanoZolid low dose (NZ^{DTX-L}, n = 2) and high dose (NZ^{DTX-H}, n = 2).

4.3.2 Intratumoral administration of NanoZolid-docetaxel

To evaluate the therapeutic effect of intratumorally administrated NanoZolid, a preclinical study was performed in mice inoculated with s.c. Lewis Lung Carcinoma (LLC). 50 µl NanoZolid formulations were injected into each tumor and solidified.

All the groups that received docetaxel – either intratumorally or intraperitoneally – showed a pronounced antitumor effect already after two days of treatment, when compared to placebo (Figure 17). Furthermore, all the docetaxel treated groups displayed a significant improved survival compared to placebo (Figure 18). There was no significant difference in tumor volume or survival between the docetaxel high and low groups. The NanoZolid formulations showed similar antitumoral effect as docetaxel administrated i.p. However, the adverse effect from docetaxel, including decreased levels of white blood cells and weight loss, were only observed in the group treated with i.p. docetaxel, Figure 19 (**paper II**).

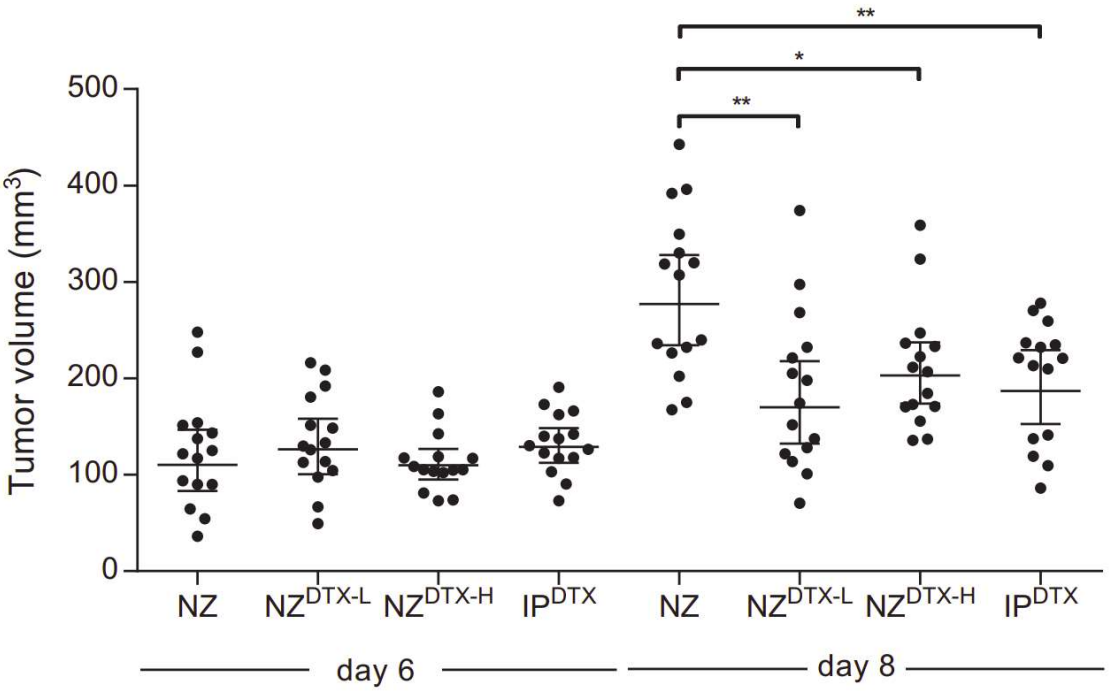

Figure 17. *In vivo* LLC tumor measurements at day 6 (treatment start) and day 8.
NanoZolid placebo (NZ), low dose (NZ^{DTX-L}) and high dose (NZ^{DTX-H}). Intraperitoneal docetaxel (IP^{DTX}).

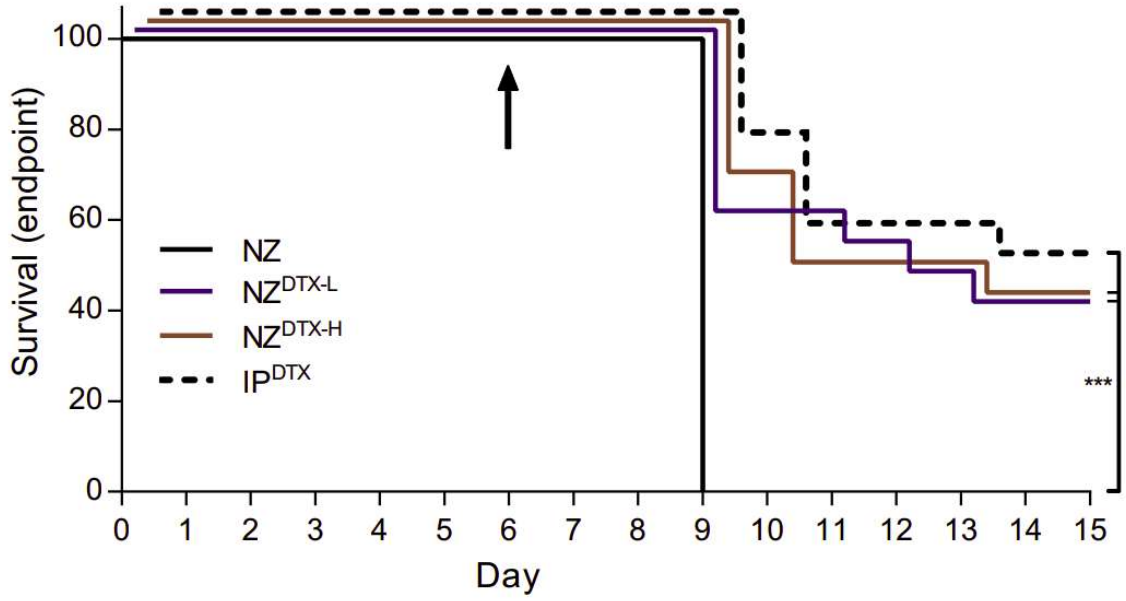

Figure 18. Survival (endpoint) curves for tumor bearing mice depending on treatment.
NanoZolid placebo (NZ), low dose (NZ^{DTX-L}) and high dose (NZ^{DTX-H}). Intraperitoneal docetaxel (IP^{DTX}). Arrow indicates start of treatment.

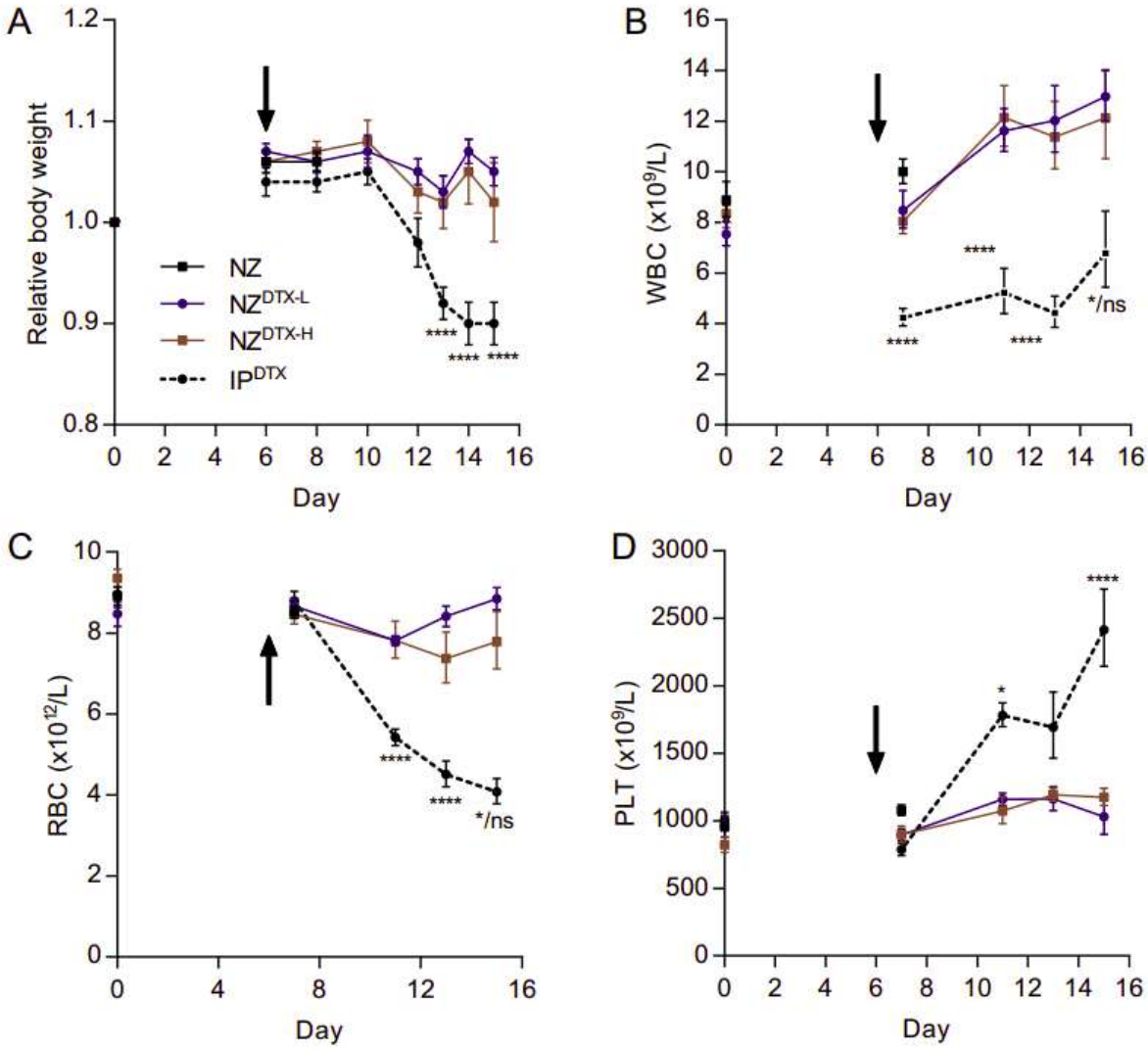

Figure 19. Systemic side effects in tumor bearing mice depending on treatment.
Body weight, white blood cell (WBC), red blood cell (RBC), and platelet (PLT) count.

4.4 NANOZOLID FORMULATIONS WITH BIOMOLECULE

The fluorescence labelled epidermal growth factor protein (EGF) was encapsulated in NanoZolid formulations. Two formulations of varied drug load (see section 3.2.6) were used in a preclinical study in mice. Using fluorescence imaging, EGF was shown to be distributed from the subcutaneous depot in the neck to the EGF receptor positive tumor implanted in the hind leg (Figure 20).

By measuring the fluorescence signal in the neck throughout the study duration, it was shown that the depots slowly released EGF (Figure 21). In addition, the results showed that EGF, at least partly, maintained its receptor binding capacity (Figure 22). This indicates that EGF can endure the chemical (ionic exposures) and mechanical stresses from the manufacturing as well as the *in vivo* solidification by hydration. This was confirmed by *ex vivo* examination showing the presence of fluorescent EGF in the EGF receptor expressing tumor, see Figure 23 (**paper III**).

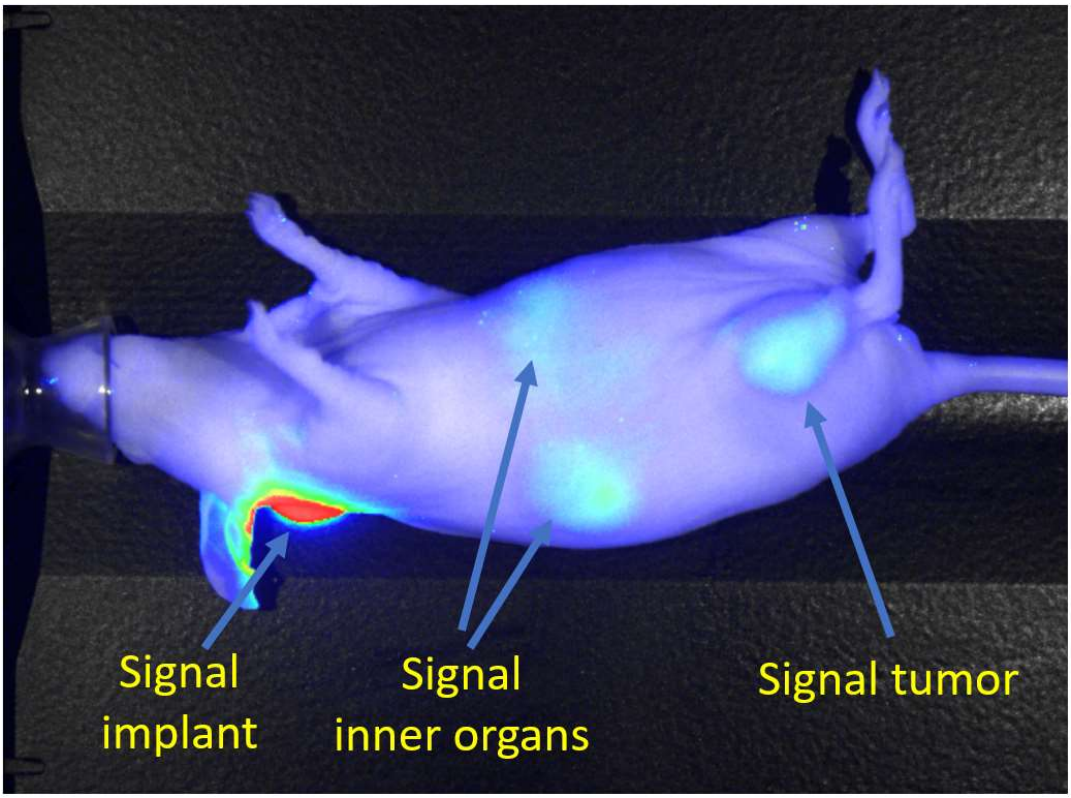

Figure 20. EGF biodistribution at 96 hours post injection, NZ-EGF-NIR-high.

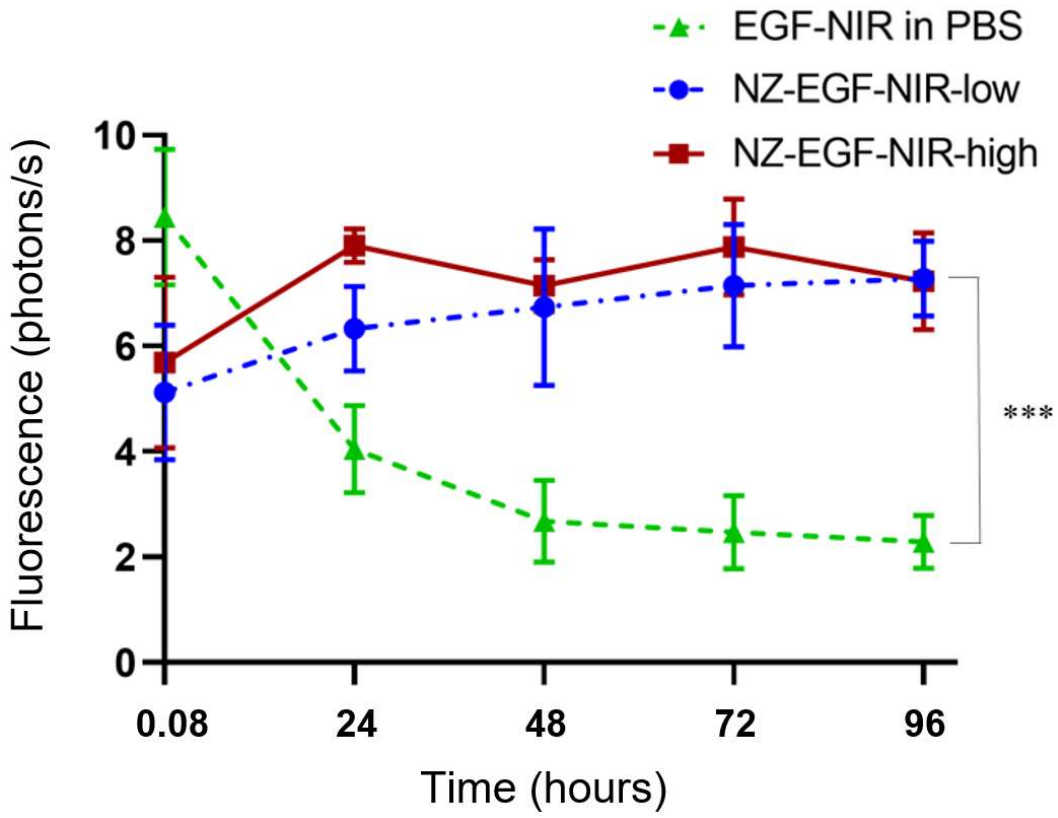

Figure 21. Average longitudinal fluorescence intensities at the neck injection sites.

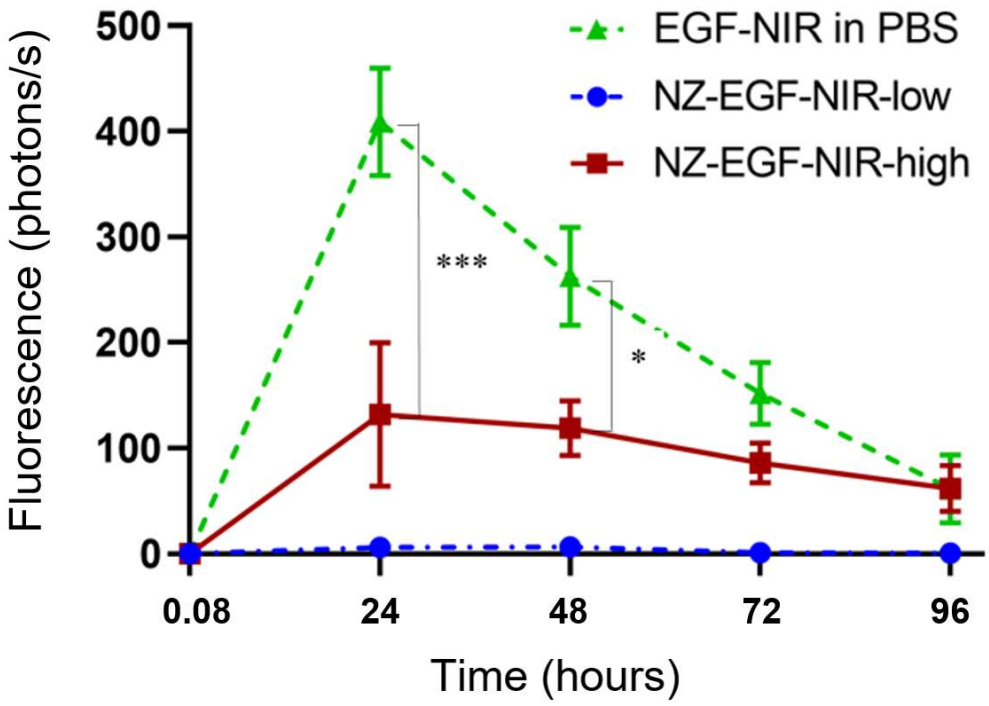

Figure 22. Average longitudinal fluorescence intensities from the tumors.

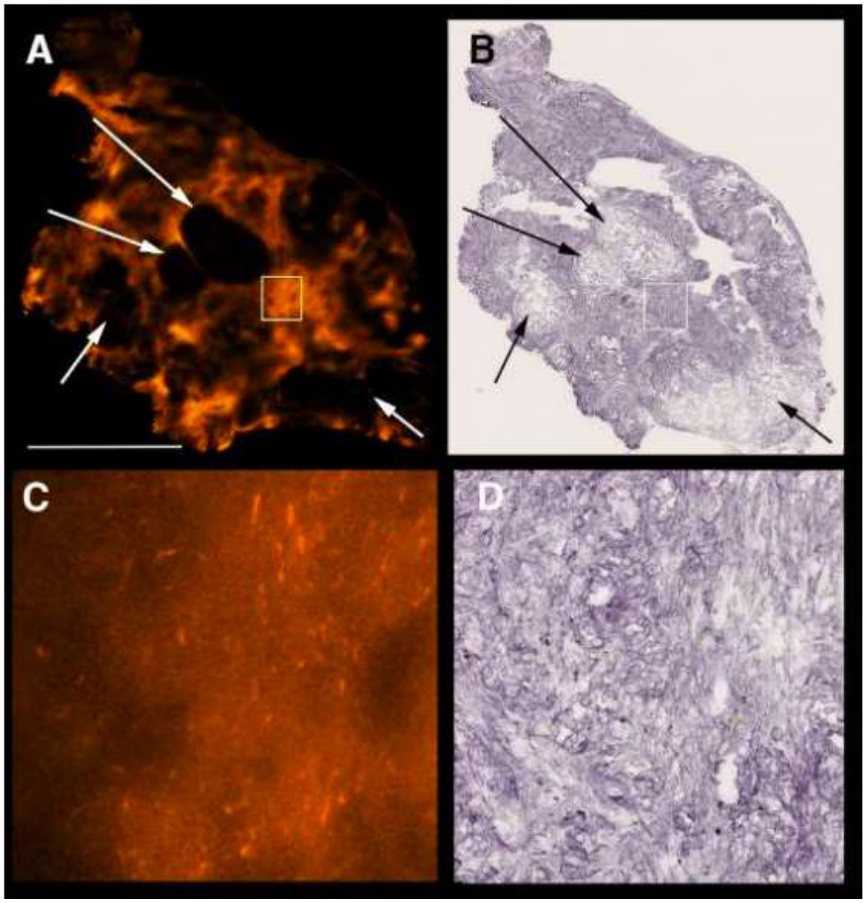

Figure 23. Tumor *ex vivo* NIR fluorescence (orange) and EGFR immunohistochemistry staining (blue-black) from a NZ-EGF-NIR-high treated mouse.
Arrows indicate necrotic cells, indicating an EGF distribution mainly in regions comprising viable cells expressing EGFR. Image C and D are detailed images of A and B at higher magnification.

4.5 NANOZOLID-2-HOF FOR PROSTATE CANCER TREATMENT

NanoZolid containing 2-HOF (Liproca® Depot) was evaluated clinically in patients with localized prostate cancer (**paper IV**). The manufacturing and the design of the formulation is described in **paper I**.

The depot was shown to be safe and tolerable with injection volumes up to 24 ml. 2-HOF levels in plasma were low throughout the evaluation period (6 months), suggesting slow release profile in patients.

A decrease in prostate specific antigen (PSA) level in blood after 5 months (primary endpoint) was observed (Figure 24). At the same time, a decrease in prostate volume (PV) was observed in most of the patients (Figure 25). Similar results were achieved with intraprostatic Liproca® doses of 16 and 20 ml. Therefore a dose of 16 ml would be reasonable in future studies, as the increased dose of 20 ml did not show an improvement in treatment outcome.

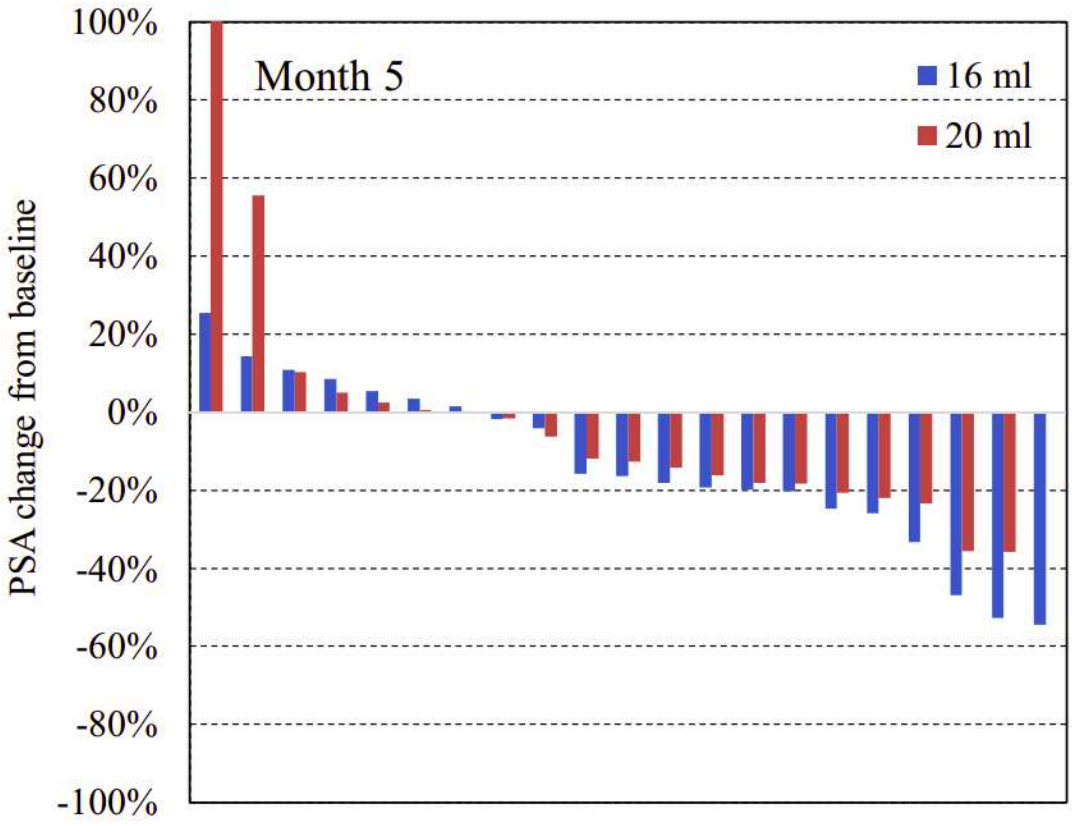

Figure 24. Individual PSA change from baseline at month 5.

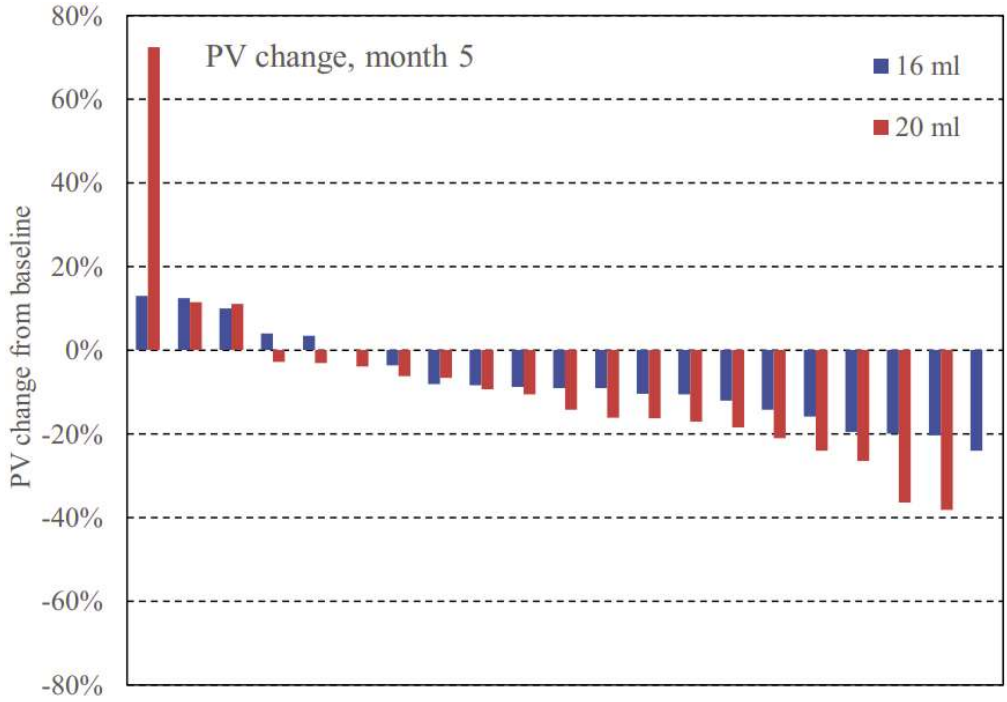

Figure 25. Individual prostate volume (PV) change from baseline at month 5.

Magnetic resonance imaging (MRI) showed no or negative tumor progression, thereby indicating a potential anti-cancer effect as a result of the Liproca Depot injections. An example of negative tumor progression, i.e. decrease in PI-RADS score, is illustrated in Figure 26.

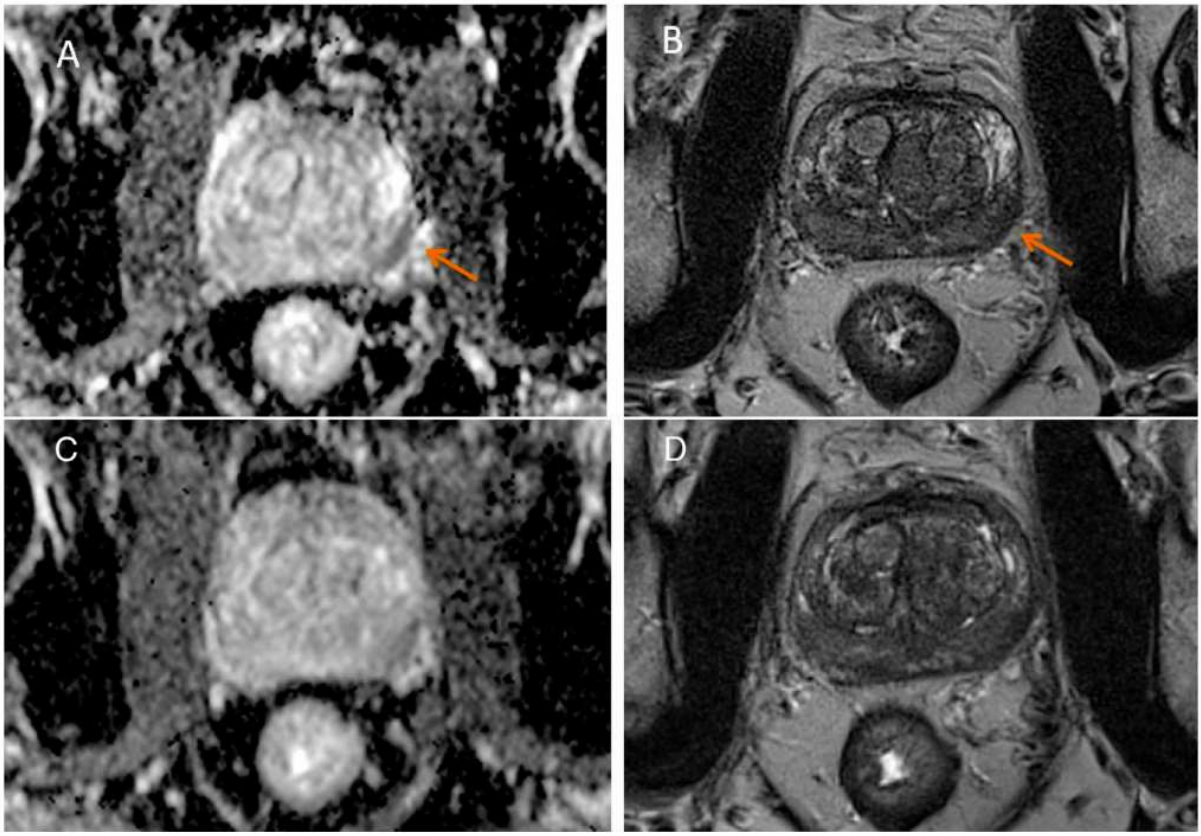

Figure 26. Magnetic resonance Imaging for a patient with a Gleason 3 + 4 tumor in the left peripheral zone. (A,B) Magnetic resonance imaging at screening and (C,D) at a follow-up visit 5 months after local treatment with 16 ml of Liproca Depot. (A) Transaxial apparent diffusion coefficient (ADC) map and (B) transaxial T2- weighted image (T2WI) in the same mid-zone level shows a 1.9-cm tumor in the left peripheral zone (Prostate Imaging-Reporting and Data System [PI-RADS] score 5, orange arrow). (C) ADC map and (D) T2WI showing a decrease in tumor size to 1.1 cm and less demarcation on the ADC map.

The reconstitution process for a NanoZolid powder and an aqueous diluent, as well as the injection of the reconstituted viscous suspension through needles of 17 gauge and 200 mm length, was feasible and convenient for use in a clinical setting.

5 DISCUSSION

Cancer is the second leading cause of death in the developed countries. However, still surgery, chemotherapy, radiotherapy, are the corner stones in cancer treatment. Recently targeted therapy including cell therapy, immune- and hormone-therapy have been introduced.

Patients treated with chemotherapy experience severe side effects due to non-specific toxicity, including tiredness, vomiting, hair loss, infections, anemia, skin bruising and loss of appetite as the chemotherapy also effects normal dividing cells such as epithelial cells, hair follicle cells, neurons, and vascular endothelial cells. Toxicity of the heart, liver, and kidney can be long term and life-threatening. Targeted therapy and local cancer treatment may provide the possibility to overcome some of the adverse effects associated with systemic administration and hence enhance the treatment efficacy and provide a better quality of life for the patient.

In the present thesis, we investigated local cancer treatment utilizing NanoZolid depot implants, developed for the intraprostatic treatment of prostate cancer and intratumor treatment of lung cancer.

Cold isostatic pressing (CIP), and hot isostatic pressing (HIP), are techniques used in material-industry for metal and ceramic component manufacturing from powders. In the present investigation, we examined the densification of calcium sulfate, for the first time, as a carrier for slow-release drug delivery system. By utilizing CIP technology to produce non-porous depots, the addition of pore-filling additives is avoided. The recrystallization originating from the hydration of hemihydrate to dihydrate provide the atomic mobility necessary for the high densification achieved by hydration under an isostatic pressure. Moreover, the NanoZolid product will contain only calcium sulfate and the active substance, which will simplify quality control and registration procedure.

A previous study by Sjögren *et al*. described formulations produced using the CIP technique with similar prototype laboratory equipment. However, their equipment was not adapted for clean room manufacturing.[57] In **paper I**, we developed CIP by substituting oil with water as compression medium to become more environmentally friendly. In addition, the newly developed equipment has been adapted for GMP production, including additional safety modifications and the exchange of several painted parts of plastic or iron etc. to stainless steel. At the present, CIP, a newly introduced powder compression technique in the pharmaceutical field, is used to produce dense granules of calcium sulfate.

The pharmaceutical aspects of NanoZolid loaded with the antiandrogen 2-hydroxyflutamide (2-HOF) was evaluated *in vitro* (**paper I**) and *in vivo* (**paper IV**).

With CIP, extremely dense hydratable calcium sulfate could be produced without heating, which is important as heat can cause chemical degradation of several compounds including drugs. The CIP compression technique may be used as a basis for future development of solid formulations for parenteral administration. One application for highly densified calcium sulfate is drug encapsulated products that can be surgically inserted as pre-solidified implants for slow drug release over long time. Furthermore, metal implants inserted prior to surgery can be coated

with densified calcium sulfate loaded with antibiotics or anti-inflammatory drugs. Such coatings could be applied to dental or orthopedic implants as well as to vascular products, such as stents.

To determine the distribution of the active substances in the powder fractions of the solidified depot, scanning electron microscopy (SEM) and energy dispersive X-ray spectroscopy (EDS) were used for imaging and elemental mapping, respectively. The active substance (2-HOF) was found in both the porous and dense regions of cross-sections of the depots and granules. However, the use of EDS in combination with the sample preparation was not sufficient to differentiate between the elements originating from the active substance in the carrier. Further investigations are warranted to gain more knowledge of the characterization and distribution of the active substance in the calcium sulfate microstructure.

We were able to develop a NanoZolid formulation containing 33% active substance (2-HOF), after the optimization of key parameters during NanoZolid preparation, including the ratio between the drug and the porous material, the ratio between the drug and the dense granules, the ratio between loaded and unloaded material, the milling process and sieving procedure. The modified-release *in vitro* profile was maintained after the optimization. To date, 33% is the highest drug load reported with NanoZolid technology. A high drug load in combination with a slow-release formulation are compulsory requirements for achieving high local tissue concentrations of the drug for an extended period. The drug load defines the injected volume required to maintain an effective concentration of active substance in the tumor/tissue. In addition, the NanoZolid formulations developed have shown a slow-release profile that enables the active substance to release over time while the calcium sulfate is resorbing.

The microstructure of the solidified depot includes both porous components providing fast drug release, and dense components providing slow release. The balance of fast and slow drug release was optimized by adjusting the ratio between the porous and dense calcium sulfate components, as well as the ratio of drug to the different components. The proportion of densified (large) granules cannot be increased indefinitely. The dense granules, which contain dihydrate crystals, act as seeding points in the solidification process and increase the solidification rate. The injectability of NanoZolid formulations through a needle is also affected by the amount and size of the densified granules.

Intratumor injection of NanoZolid formulation containing docetaxel, in different concentrations, was evaluated in a lung cancer animal model (**paper II**). This was the first time that the new drug delivery system had been investigated intratumorally. Today, docetaxel is primarily used as systemic second line treatment for several cancers. Utilizing the NanoZolid technology, it may be possible to administer depots for local drug release into the tumors in lung tissue. A reduced tumor size may enhance the quality of life of the patient in the later stages of the disease, and hopefully a longer survival time can be achieved. The intratumor injections in **paper II** resulted in significantly lower side effects.

The application of NanoZolid can be extended to other types of compound than cytostatic drugs, e.g. to inject immune-triggering agents locally at the tumor site in order to reactivate the patient immune system. In addition, the slow drug release from the NanoZolid depots will

allow less frequent administration, where today injections are needed several times a week, e.g. for TLR9 agonist.

The NanoZolid technology was used to investigate the slow release of a biomolecule, EGF, with preserved functionality (**paper III**). EGF has been well characterized and was therefore chosen as a model molecule to carry out a proof-of-concept study (**paper III**).[154] A lung cancer (A549) xenograft mouse model expressing EGF receptors was utilized. Biodistribution pattern *in vivo* indicated a preserved receptor binding capacity of EGF. These preliminary results may have a high clinical impact for cancer treatment. Further comprehensive investigations with better quantification of biomolecule concentrations and functionality are warranted to fully understand the factors that affected this outcome.

The clinical investigation described in **paper IV** showed that the formulation is safe and well tolerated in low- to intermediate risk prostate cancer patients that otherwise would be on active surveillance without treatment. The administration of NanoZolid loaded with 2-HOF produced a long-term decrease of PSA throughout the study for most patients.

Flutamide is the first generation antiandrogen drug for oral administration in prostate cancer treatment. Currently, bicalutamide and enzalutamide are frequently used in prostate cancer protocols due to fewer systemic side effects. However, as the intraprostatic treatment avoids the systemic side effects, flutamide (2-HOF) still can be used. This is most probably due to the shorter half-life (6 h) of flutamide which can be an advantage compared to bicalutamide and enzalutamide (7 days and 6 days), as it may reduce the risk for side effects from accumulated drug concentrations in the blood system.

From the MRI results a decrease in prostate-volume was observed, as well as signs of improvement in the cancer disease, according to the PI-RADS score. These results indicate a possibility of achieving some control over cancer progression, although further studies with more patients and a longer follow-up period are needed to confirm the present results.

6 CONCLUSIONS

The use of calcium sulfate as a carrier for slow release depot formulations to be used for local drug administration was investigated. Based on the present results, we conclude:

1. Essential drug formulation characteristics such as viscosity, injectability, *in vivo* solidification, drug-release and depot dissolution are controllable by optimizing microstructural properties such as granule size, drug micro-distribution, depot density and drug load. The formulation, based only on calcium sulfate and the constituent drug, can be adapted to several applications.

2. Formulations with up to 33% of the constituent drug in the powder formulation were achieved and only 40% of the drug was released *in vitro* from the formulation within two weeks. The depot was able to retain the drug already at the start, despite the relatively high drug load.

3. The manufacturing procedure for NanoZolid formulations has been developed to fulfil GMP quality requirements and has been used for the production of drugs used clinically.

4. The investigated calcium sulfate-based drug depots were tolerated *in vivo*, as demonstrated with injections of a cytotoxic formulation in subcutaneous tumors in mice, and with an anti-androgen formulation in humans.

5. Initial evaluations in a mouse model with a fluorescent bioactive protein (EGF) in calcium sulfate depots, indicate that biomolecules are compatible with the NanoZolid technology and are released from *in vivo* solidified depots with preserved bioactivity.

In conclusion, our findings show that the calcium sulfate-based drug delivery technology NanoZolid is a promising approach for local cancer treatment.

7 FUTURE PERSPECTIVES

The investigation of the intratumoral distribution of active substances released from NanoZolid depots over time would benefit from more detailed studies. Such studies may be performed by *ex vivo* assay analyses of different parts of the tumor and its surrounding tissue. The results can increase the understanding of the outcome of the local tumor treatments and may contribute to optimal design of the drug depot.

Direct injection into the tumor could not only reduce systemic exposure, off-target toxicities and the amount of drug used, but also induce anti-tumor activity in distant non-injected tumor lesions (i.e. abscopal effect). This could be evaluated by analyzing biomarkers of e.g. tissue reactions and immunological responses resulting from the intratumoral treatment.

A clinical setting for treatment of lung cancer would be a natural continuation of the docetaxel investigation. The depots could be administered intratumorally either through a bronchoscope or directly through the pleura. To facilitate breathing for these patients and at least temporarily postpone cancer progression which can be a great achievement.

Furthermore, new clinical indications for the technology could be explored – such as post-operative chemotherapy for residual cancer cells after surgical removal of brain tumor. Local administration of NanoZolid formulation directly into the brain is a strategy to bypass the blood-brain-barrier (BBB). BBB is the main obstacle when treating brain tumor systemically. Preclinical studies using animal models carrying GL261glioma cells xenograft and treated with cytostatic NanoZolid formulations have been initiated. By utilizing GL261 cells that express luciferase reporter, (GL261.luc) it is possible to monitor the tumor growth and the treatment efficacy over time by bioluminescence imaging. In addition, the treatment outcome can be further improved by combining a systemic anti-PD1 checkpoint inhibitor.

Another interesting approach is to continue the evaluations of NanoZolid formulations with biomolecules. Such formulations can find application in immuno-oncology, where the treatment efficacy can be evaluated in an appropriate animal model. As a continuation, a TLR9 agonist, similar in size to EGF, probably in combination with a systemic anti-PD1 checkpoint inhibitor can be included in the clinical study. Furthermore, large antibodies, such as CD40 agonist antibodies, would be stimulating to formulate with the NanoZolid technology.

8 ACKNOWLEDGEMENTS

This doctoral project has not been a standard one, as I have been an industrially funded doctoral student working actively both in Huddinge and in Uppsala. The way to the completion of this thesis has therefore not followed a standard road, but that has in my opinion also been challenging in a positive way. I would like to acknowledge all persons/sources that have supported, encouraged and accompanied me throughout this journey, especially those below:

Thank you **Karolinska Institutet** and the **Clinical Research Center** for being a great place for doctoral studying and research. Special thanks to **LIDDS AB** for financing this project.

To my main supervisor **Moustapha Hassan,** I would like to express my deepest appreciation for your support, sharp mind and belief in me. I will especially remember the scientific planning discussions in your office – full of opportunities, clever ideas, some loose papers on the table and often a very good sense of humor.

My profound gratitude goes to my mentor and co-supervisor **Niklas Axén** for encouraging me in the downs, for inspiring me in the ups and for coaching me in the landscape of science and research collaborations. Many thanks to my co-supervisor **Martin Sandelin**, who introduced me to the clinical cancer research world and for great scientific discussions. Lots of thanks to my co-supervisor **Manuchehr Abedi-Valugerdi** (co-supervisor 2017-2020) for introducing me to the ECM group, for support and kindness – especially regarding the cell experiments and scientific approach to problems. Thank you **Mikael Hedeland** for scientific discussions, blood analysis expertise and for being my wise mentor and safety net.

Many thanks to the current and previous ECM lab and room members: **Ying Zhao** (co-supervisor 2021) also as co-author and collaborator in cell- and animal experiments, **Rui He**, **Wenyi Zheng**, **Fadwa Benkessou**, **Ibrahim El-Serafi**, **Risul Amin**, **Qiang Wang**, and **Sandra Oerther**. You have been fantastic colleagues and always helping me out with a smile when I have needed guidance. In addition, thanks also to **Kathrin Reiser** and **Emelie Blomberg** for joyful discussions and assistance in cytostatics handling and administration.

Thank you **Uppsala University**, the **Department of Pharmacy** and **Göran Alderborn** for allowing me to be a guest scientist in your group. Special thanks to **Ann-Sofie Persson** and **Samaneh Pazesh** for numerous enjoying discussions about science and doctoral student life when kindly hosting me in your room. Thank you **Josefina Nordström** and **Göran Frenning** for letting me lecture for the Master's students. Thank you all members in the Journal Club for exciting and vivid discussions: especially **Lucia Lazorova**, **Johan Gråsjö**, **Erik Björk**, **Jonas Rudén**, **Sohan Sarangi**, **Henrik Jonsson**, **Dariush Nikjoo**, **Sara Andersson**, **Maryam Tofiq**, **Junxue An**, **Irès van der Zwaan**, **Anna Simonsson** and **Marilena Marinaki**.

Many thanks and deepest appreciations to **Monica Wallter** for supporting the project and for seeing opportunities. Thanks also to the rest of the LIDDS team, Uppsala: **Charlotta Gauffin**, **Erwin Brenndörfer**, **Martin Johansson**, **Carl-Gustav Gölander** and **Anders Bjartell** for scientific discussions and valuable support.

Thank you **Marie Jeansson** at Uppsala University and the Department of Immunology, Genetics and Pathology, IGP, for your valuable preclinical lung cancer work. Thanks to **Patrick Micke**, **Veera Räsänen**, **Pia Petersson**, **Jana Chmielniakova**, **Veronica Sundell** and **Martina Orebrand** from IGP for histological analyses and technical assistance.

Thanks to **Charlott Brunmark** and **Jian Liu** from Truly Labs, Lund, and **Bo Holmqvist** and **Nataliya Lutay** from ImaGene-iT, Lund, for preclinical imaging, histological analyses, and joyful scientific collaboration.

Thank you **Richard Casey**, Oakville, Canada, and **Laurence Klotz** at Sunnybrook Research Institute, Toronto, Canada, for kindly sharing insight into clinical prostate cancer issues and treatment opportunities. Thank you **Ricardo Rendon**, Halifax, Canada, **Jonathan Giddens**, Brampton, Canada, **Mindaugas Jievaltas**, Kaunas, Lithuania, **Albertas Ulys**, Vilnius, Lithuania, **Teuvo Tammela**, Tampere, Finland, **Patrick Richard**, Sherbrooke, Canada, **Peter Incze**, Oakville, Canada, and **Kenneth Jansz**, Burlington, Canada, for scientific support regarding prostate cancer and local antiandrogen treatment.

Thank you **Cecilia Wassberg** at the Radiology Department, Karolinska University Hospital, Stockholm, for teaching me in magnetic resonance imaging and image evaluation.

Thanks to **Erik Adolfsson** and **Melina da Silva** at Research Institutes of Sweden (RISE)/Swerea, Mölndal, for scientific support regarding biomaterials, isostatic pressing and electron microscopy.

Thanks to **Niklas Eriksson**, **Mikael Söderberg**, **Niklas Nilsson** with team from Recipharm, Solna, for scientific participation in the development and design of the Liproca manufacturing.

Thank you **Jeffrey Yachnin** at Karolinska University Hospital, Solna, for scientific discussions regarding clinical applications for NanoZolid in human solid tumors.

Thanks to **Urban Höglund**, **Olivia Larsson** and **Ulrika Randén** from Adlego, Solna, for scientific support regarding preclinical NanoZolid tumor injections and animal care.

Thank you **Fei Ye** at KTH Royal Institute of Technology, Stockholm, for scientific support regarding possibilities and limits with electron microscopy.

Many thanks and appreciation to **Hans Lennernäs** for introducing me to LIDDS and also to Empros Pharma and for being a very good friend in research and science, with expertise in target drug delivery and pharmacokinetics, and also a great teammate in the football team Athletico ("Korpen").

Thank you **Empros Pharma**, Solna, and **Arvid Söderhäll** with team – including **Ulf Holmbäck** and **Anders Forslund** – for scientific discussions and for pushing me to be on the creative edge of formulation design and product development.

Thanks to **Nils-Olof Lindberg**, **Henri Hansson** and **Arne Kristensen** for being the best mentors and support when training me in the art of dosage form design.

Thanks to all wonderful persons of the male choir **Orphei Drängar**, the magician communities **Swedish Magic Circle** and **UMB**, the Korpen football team **Athletico**, the leaders and players of **IF VP F-08** football club, and the **Monday floorball group** in Uppsala Mission Church for adding extra energy and happiness in my life.

Thanks to our cute and affectionate family cats **Nemo** and **Juli**, for giving comfort and joy.

I am also extremely grateful to have wonderful and supporting **friends** and **relatives** – which I all regard as my "extended family" that make my life joyful. Some of you are also sometimes called "**Storfamiljen**". You all know who you are. From the deepest of my heart, I thank you all for being the best friends that one could ever wish for.

Thank you my very finest big brother **Tomas**, including family members, for always being the best brother in the world.

I would like to sincerely acknowledge my parents **Lars** and **Eva** for warm-hearted and respectfully raising me up to a person full of empathy, proudness and curiosity.

Thank you my fantastic and beloved children **Tyra**, **Emrik** and **Hedvig** – so full of wisdom, goodness and joy – making my life worth living.

My endless thanks to **Lotta** for taking care of our family and for all your love and support which have made this thesis possible, my beloved wife, my love, my inspiration, my life coach – my everything.

9 REFERENCES

1 Vandiver, P.B., Soffer, O., Klima, B., Svoboda, J. The origins of ceramic technology at Dolni Věstonice, Czechoslovakia. *Science* **246**, 1002-1008 (1989).

2 Roux, V., de Miroschedji, P. Revisiting the history of the potter's wheel in the Southern Levant. *Levant* **41**, 155-173 (2009).

3 Shockley, W. Electrons and holes in semiconductors: with applications to transistor electronics. *D. Van Nostrand Company, Inc. (New York, N.J.)* (1950).

4 Hench, L.L., Wilson, J. Surface-active biomaterials. *Science* **226**, 630–636 (1984).

5 Hench, L.L. Bioactive materials: The potential for tissue regeneration. *Journal of Biomedical Materials Research* **41,** 511–518 (1998).

6 Dreesmann, H. Ueber Knochenplombierung bei Hohlenforigen Defekten des Knochens. *Beitr. Klin. Chir.* **9**, 804-810 (1892).

7 Sheskey, P.J., Cook, W.G., Cable, C.G. Handbook of Pharmaceutical Excipients. *Pharmaceutical Press* **Eighth Edition**, Monograph for Calcium Sulfate, 160-162 (2017).

8 Agarwal, S., Healey, B. The use of antibiotic impregnated absorbable calcium sulphate beads in the management of infected joint replacement prostheses. *Journal of Arthroscopy and Joint Surgery* **1**, 72–75 (2014).

9 Freyer, D., Voigt, W. Crystallization and phase stability of $CaSO_4$ and $CaSO_4$ - based salts. *Monatshefte für Chemie* **134**, 693-719 (2003).

10 Nilsson, M., Zheng, M.H., Tägil, M. The composite of hydroxyapatite and calcium sulphate: a review of preclinical evaluation and clinical applications. *Expert review of medical devices* **10**, 675-684 (2013).

11 Hewes, C.A., Sullins, K.M. Use of cisplatin containing biodegradable beads for treatment of cutaneous neoplasia in Equidae: 59 cases (2000-2004). *Journal of the American Veterinary Medical Association* **229**, 1617-1622 (2006).

12 Hewes, C.A. How to Use Bioabsorbable Cisplatin Beads to Treat Cutaneous Neoplasia. *American Association of Equine Practioners Proceedings*, **53**, 399-402 (2007).

13 Kim, J.H., Oh, J.H., Han, I., Kim, H.S., Chung, S.W. Grafting using injectable calcium sulfate in bone tumor surgery: comparison with demineralized bone matrix-based grafting. *Clinics in Orthopedic Surgery* **3**, 191-201 (2011).

14 Tammela, T.L., Häggman, M., Ladjevardi, S., Taari, K., Isotalo, T., Lennernäs, H., Weis, J., von Below, C., Wassberg, C., Lennernäs, B., Tolf, A., Axén, N., Gölander, C.-G., Ahlström, H. An Intraprostatic Modified Release Formulation of Antiandrogen 2-Hydroxyflutamide for Localized Prostate Cancer. *Journal of Urology* **198**, 1333-1339 (2017).

15 Bardos, D.I. High strength Co-Cr-Mo alloy by hot isostatic pressing of powder. *Biomaterials, Medical Devices and Artificial Organs* **7,** 73-80 (1979).

16 Blümer, C., Mäder, K. Isostatic ultra-high-pressure effects on supercooled melts in colloidal triglyceride dispersions. *Pharmaceutical Research* **22,** 1708–1715 (2005).

17 Szepes, A., Makai, Z., Blümer, C., Mäder, K., Kása Jr., P., Szabó-Révész, P. Characterization and drug delivery behaviour of starch-based hydrogels prepared via isostatic ultrahigh pressure. *Carbohydrate Polymers* **72**, 571–578 (2007).

18 Rahaman, M.N. Sintering of Ceramics. *CRC Press, Tylor & Francis Group* **First Edition**, Chapter 1, 1-44 (2007).

19 Guo, H., Guo J., Baker, A., Randall C.A. Hydrothermal-assisted cold sintering process: A new guide for low-temperature ceramic sintering. *ACS Applied Materials & Interfaces* **8**, 20909-20915 (2016).

20 Kuo, S.T., Wu, H.W., Tuan, W.H., Tsai, Y.Y., Wang, S.F., Yoshio, S. Porous calcium sulfate ceramics with tunable degradation rate. *Journal of Materials Science. Materials in Medicine* **23,** 2437–2443 (2012).

21 Goldberg, M., Obolkina, T., Smirnov, S., Protsenko, P., Titov, D., Antonova, O., Konovalov, A., Kudryavtsev, E., Sviridova, I., Kirsanova, V., Sergeeva, N., Komlev, V., Barinov, S. The influence of Co additive on the sintering, mechanical properties, cytocompatibility, and digital light processing based stereolithography of 3Y-TZP-5Al_2O_3 ceramics. *Materials* **13**, 2789 *(*2020).

22 Vallet-Regí, M. Bioceramics with Clinical Applications. Edited by María Vallet-Regí. *John Wiley & Sons, Ltd*. **First Edition**, Chapter 1, 3-22 (2014).

23 Itoh, H., Wakisaka, Y., Ohnuma, Y., Kuboki, Y. A new porous hydroxyapatite ceramic prepared by cold isostatic pressing and sintering synthesized flaky powder. *Dental Materials Journal* **13**, 25–35 (1994).

24 Mangal, S., Meiser, F., Morton, D., Larson, I. Particle Engineering of Excipients for Direct Compression: Understanding the Role of Material Properties. *Current Pharmaceutical Design* **21**, 5877-5889 (2015).

25 Harper, E., Dang, W., Lapidus, R.G., Garver Jr, R.I. Enhanced efficacy of a novel controlled release paclitaxel formulation (PACLIMER delivery system) for local-regional therapy of lung cancer tumor nodules in mice. *Clinical Cancer Research* **5**, 4242-4248 (1999).

26 Anderson, J.M., Shive, M.S. Biodegradation and biocompatibility of PLA and PLGA microspheres. *Advanced Drug Delivery Reviews* **28**, 5-24 (1997).

27 Gefvert, O., Eriksson, B., Persson, P., Helldin, L., Björner, A., Mannaert, E., Remmerie, B., Eerdekens, M., Nyberg, S. Pharmacokinetics and D2 receptor occupancy of long-acting injectable risperidone (Risperdal Consta) in patients with schizophrenia. *The International Journal of Neuropsychopharmacology* **8**, 27-36 (2005).

28 Colao, A., Bronstein, M.D., Freda, P., Gu, F., Shen, C.C., Gadelha, M., Fleseriu, M., van der Lely, A.J., Farrall, A.J., Hermosillo Reséndiz, K., Ruffin, M., Chen, Y., Sheppard, M. Pasireotide versus octreotide in acromegaly: a head-to-head superiority study. *The Journal of Clinical Endocrinology and Metabolism* **99**, 791-799 (2014).

29 Guo, Y., Yang, Y., He, L., Sun, R., Pu, C., Xie, B., He, H., Zhang, Y., Yin, T., Wang, Y., Tang, X. Injectable sustained-release depots of PGLA microspheres for insoluble drugs prepared by hot-melt-extrusion. *Pharmaceutical Research* **34**, 2211-2222 (2017).

30 Guzman, L.A., Labhasetwar, V., Song, C., Jang, Y., Lincoff, A.M., Levy, R., Topol, E.J. Local intraluminal infusion of biodegradable polymeric nanoparticles. A novel approach for prolonged drug delivery after balloon angioplasty. *Circulation* **94**, 1441-1448 (1996).

31 Molpeceres, J., Aberturas, M.R., Guzman, M. Biodegradable nanoparticles as a delivery system for cyclosporine: preparation and characterization. *Journal of Microencapsulation* **17**, 599-614 (2000).

32 Simeonova, M., Ilarionova, M., Ivanova, T., Konstantinov, C., Todorov, D. Nanoparticles as drug carriers for vinblastine. Acute toxicity of vinblastine in a free form and associated to polybutylcyanoacrylate nanoparticles. *Acta Physiologica et Pharmacologica Bulgarica* **17**, 43-49 (1991).

33 Fattal, E., Vauthier, C., Aynie, I., Nakada, Y., Lambert, G., Malvy, C., Couvreur, P. Biodegradable polyalkylcyanoacrylate nanoparticles for the delivery of oligonucleotides. *Journal of Controlled Release* **53**, 137-143 (1998).

34 Zimmer, A., Mutschler, E., Lambrecht, G., Mayer, D., Kreuter, J. Pharmacokinetic and pharmacodynamic aspects of an ophtalmic pilocarpine nano-particle-delivery-system. *Pharmaceutical Research* **11**, 1435-1442 (1994).

35 Li, J.K, Wang, N., Wu, X.S. A novel biodegradable system based on gelatin nanoparticles and poly(lactic-co-glycolic acid) microspheres for protein and peptide drug delivery. *Journal of Pharmaceutical Science* **86**, 891-895 (1997).

36 Rajaonarivony, M., Vauthier, C., Couarraze, G., Puisieux, F., Couvreur, P. Development of a new drug carrier made from alginate. *Journal of Pharmaceutical Sciences* **82**, 912-917 (1993).

37 Wilson, B., Samanta, M.K., Santhi, K., Kumar, K.P.S., Ramasamy, M., Suresh, B. Chitosan nanoparticles as a new delivery system for the anti-Alzheimer drug tacrine. *Nanomedicine: Nanotechnology, Biology and Medicine* **6**, 144-152 (2010).

38 Gradishar, W.J. Albumin-bound paclitaxel: a next generation taxane. *Expert Opinion on Pharmacotherapy* **7**, 1041-1053 (2006).

39 Oerlemans, C., Bult, W., Bos, M., Storm, G., Nijsen, J.F., Hennink, W.E. Polymeric micelles in anticancer therapy: Targeting, imaging and triggered release. *Pharmaceutical Research* **27**, 2569-2589 (2010).

40 Gulati, K., Ramakrishnan, S., Aw, M.S., Atkins, G.J., Findlay, D.M., Losic, D. Biocompatible polymer coating of titania nanotube arrays for improved drug elution and osteoblast adhesion. *Acta Biomaterialia* **8**, 449-456 (2012).

41 Wang, T., Weng, Z., Liu, X., Yeung, K.W.K., Pan, H., Wu, S. Controlled release and biocompatibility of polymer/titania nanotube array system on titanium implants. *Bioactive Materials* **2**, 44-50 (2017).

42 Dimatteo, R., Darling, N.J., Segura, T. In situ forming injectable hydrogels for drug delivery and wound repair. *Advanced Drug Delivery Reviews* **127**, 167-184 (2018).

43 Jeong, B., Bae, Y.H., Kim, S.W. Drug release from biodegradable injectable thermosensitive hydrogel of PEG-PLGA-PEG triblock copolymers. *Journal of Controlled Release* **63**, 155-163 (2000).

44 Silverman, L.A., Neely, E.K., Kletter, G.B., Lewis, K., Chitra, S., Terleckyj, O., Eugster, E.A. Long-Term Continuous Suppression With Once-Yearly Histrelin Subcutaneous Implants for the Treatment of Central Precocious Puberty: A Final Report of a Phase 3 Multicenter Trial. *The Journal of Clinical Endocrinology and Metabolism* **100**, 2354-2363 (2015).

45 Cocarta, A.-I., Hobzova, R., Sirc, J., Cerna, T., Hrabeta, J., Svojgr, K., Pochop, P., Kodetova, M., Jedelska, J., Bakowsky, U., Uhlik, J. Hydrogel implants for transscleral drug delivery for retinoblastoma treatment. *Materials Science & Engineering C* **103**, 109799 (2019).

46 Li, D., Zhao, L., Cong, M., Liu, L., Yan, G., Li, Z., Li, B., Yu, W., Sun, H., Yang, B. Injectable thermosensitive chitosan/gelatin-based hydrogel carried erythropoetin to effectively enhance maxillary sinus floor augmentation in vivo. *Dental Materials* **36**, e229-e240 (2020).

47 Parent, M., Clarot, I., Gibot, S., Derive, M., Maincent, P., Leroy, P., Boudier, A. One-week in vivo sustained release of a peptide formulated into in situ forming implants. *International Journal of Pharmaceutics* **521**, 357-360 (2017).

48 Gomez, C., Blanco, M.D., Bernardo, M.V., Sastre, R.L., Teijón, J.M. Poly(acrylamide-co-monoethyl itaconate) hydrogels as devices for cytarabine release in rats. *Journal of Pharmaceutical Pharmacology* **50**, 703-712 (1998).

49 Dyondi, D., Webster, T.J., Banerjee, R. A nanoparticulate injectable hydrogel as a tissue engineering scaffold for multiple growth factor delivery for bone regeneration. *International Journal of Nanomedicine* **8**, 47-59 (2013).

50 Hennings, E., Schmidt, H., Voigt, W. Crystal structures of hydrates of simple inorganic salts. II. Water-rich calcium bromide and iodide hydrates: CaBr2·9H2O, CaI2·8H2O, CaI2·7H2O and CaI2·6.5H2O. *Acta Crystallographica. Section C, Structural Chemistry* **70**, 876-881 (2014).

51 Werner, A.G. Geschichte, Karakteristik, und kurze chemische Untersuchung des Apatits. IV. Kurze Nachricht von den sogennanten arragonischen Apatiten. *Bergmännisches Journal* **1**, 76-96 (1788).

52 Gerhartz, W. (exec. ed.). Ullmann's Encyclopedia of Industrial Chemistry. *VCH Publishers* **5th Ed. Vol A1**, VA19 499 (1985).

53 Xie, C., Lu, H., Li, W., Chen, F.-M., Zhao, Y.-M. The use of calcium phosphate-based biomaterials in implant dentistry. *Journal of Materials Science. Materials in Medicine* **23**, 853-862 (2012).

54 Melville, A.J., Rodríguez-Lorenzo, L.M., Forsythe, J.S. Effects of calcination temperature on the drug delivery behaviour of ibuprofen from hydroxyapatite powders. *Journal of Materials Science. Materials in Medicine* **19**, 1187-1195 (2008).

55 Lide, D.R. (ed.). CRC Handbook of Chemistry and Physics. *CRC Press LLC,* **84th Edition**, 8-111 (2004).

56 Mohr, D., Wolff, M., Kissel, T. Gamma irradiation for terminal sterilization of 17beta-estradiol loaded poly-(D,L-lactide-co-glycolide) microparticles. *Journal of Controlled Release* **61,** 203-217 (1999).

57 Sjögren, E., Tammela, T.L., Lennernäs, B., Taari, K., Isotalo, T., Malmsten, L.-Å., Axén, N., Lennernäs, H. Pharmacokinetics of an injectable modified-release 2-hydroxyflutamide formulation in the human prostate gland using a semiphysiologically based biopharmaceutical model. *Molecular Pharmaceutics* **11,** 3097–3111 (2014).

58 Mönkäre, J., Hakala, R.A., Vlasova, M.A., Huotari, A., Kilpeläinen, M., Kiviniemi, A., Meretoja, V., Herzig, K.H., Korhonen, H., Seppälä, J.V., Järvinen, K. Biocompatible photocrosslinked poly(ester anhydride) based on functionalized poly(epsilon-caprolactone) prepolymer shows surface erosion controlled drug release in vitro and in vivo. *Journal of Controlled Release* **146**, 349–355 (2010).

59 Naim, S., Samuel, B., Chauhan, B., Paradkar, A. Effect of potassium chloride and cationic drug on swelling, erosion, and release from κ-Carrageenan matrices. *AAPS Pharmaceutical Science Technology* **5**, 1-8 (2004).

60 Roy, D.S., Rohera, B.D. Comparative evaluation of rate of hydration and matrix erosion of HEC and HPC and study of drug release from their matrices. *European Journal of Pharmaceutical Sciences* **16**, 193-199 (2002).

61 Bhise, K.S., Dhumai, R.S., Paradkar, A.R., Kadam, S.S. Effect of drying methods on swelling, erosion and drug release from chitosan-naproxen sodium complexes. *AAPS Pharmaceutical Science Technology* **9**, 1-12 (2008).

62 Martinez, M.N., Rathbone, M.J., Burgess, D., Hyunh, M. Breakout session summary from AAPS/CRC joint workshop on critical variables in the in vitro and in vivo performance of parenteral sustained release products. *Journal of Controlled Release* **142**, 2-7 (2010).

63 Iyer, S.S., Barr, W.H., Karnes, H.T. A 'biorelevant' approach to accelerated in vitro drug release testing of a biodegradable, naltrexone implant. *International Journal of Pharmaceutics* **340**, 119-125 (2007).

64 Externbrink, A., Clark, M.R., Friend, D.R., Klein, S. Investigating the feasibility of temperature-controlled accelerated drug release testing for an intravaginal ring. *European Journal of Pharmaceutics and Biopharmaceutics* **85**, 966-973 (2013).

65 Gerber, D.E. Targeted therapies: A new generation of cancer treatments. *American Family Physician* **77**, 311-319 (2008).

66 Bedard, P.L., Hyman, D.M., Davids, M.S., Siu, L.L. Small molecules, big impact: 20 years of targeted therapy in oncology. *The Lancet (British edition)* **395**, 1078-1088 (2020).

67 Nasiri, H., Valedkarimi, Z., Aghebati-Maleki, L., Majidi, J. Antibody-drug conjugates: Promising and efficient tools for targeted cancer therapy. *Journal of Cellular Physiology* **233**, 6441-6457 (2018).

68 Ray, A., Larson, N., Pike, D.B., Grüner, M., Naik, S., Bauer, H., Malugin, A., Greich, K., Ghandehari, H. Comparison of active and passive targeting of docetaxel for prostate cancer therapy by HPMA copolymer-RGDfK conjucates. *Molecular Pharmaceutics* **8**, 1090-1099 (2011).

69 Alavi, M., Hamidi, M. Passive and active targeting in cancer therapy by liposomes and lipid nanoparticles. *Drug Metabolism and Personalized Therapy* **34**, 20180032 (2019).

70 Xu, Z., Guo, D., Jiang, Z., Tong, R., Jiang, P., Bai, L., Chen, L., Zhu, Y., Guo, C., Shi, J., Yu, D. Novel HER2-targeting antibody-drug conjugates of trastuzumab beyond T-DM1 in breast cancer: Trastuzumab Deruxtecan(DS-8201a) and (Vic-)Trastuzumab Duocarmazine (SYD985). *European Journal of Medicinal Chemistry* **183**, 111682 (2019).

71 Qie, Y., Yuan, H., von Roemeling, C.A., Chen, Y., Liu, X., Shih, K.D., Knight, J.A., Tun, H.W., Wharen, R.E., Jiang, W., Kim, B.Y. Surface modification of nanoparticles enables selective evasion of phagocytic clearance by distinct macrophage phenotypes. *Scientific Reports* **6,** 26269-26269 (2016).

72 Maulhardt, H.A., Hylle, L., Frost, M.V., Tornio, A., Dafoe, S., Drummond, L., Quinn, D.I., Kamat, A.M., diZerega, G.S. Local Injection of Submicron Particle Docetaxel is Associated with Tumor Eradication, Reduced Systemic Toxicity and an Immunologic Response in Uro-Oncologic Xenografts. *Cancers (Basel)* **11,** 577 (2019).

73 Bray, F., Ferlay, J., Soerjomataram, I., Siegel R.L., Torre, L.A., Jemal, A. Global cancer statistics 2018: GLOBOCAN estimates of incidence and mortality worldwide for 36 cancers in 185 countries. *CA: A Cancer Journal for Clinicians* **68,** 394–424 (2018).

74 Nguyen, P.L., Chen, M.-H., D'Amico, A.V., Tempany, C.M., Steele, G.S., Albert, M., Cormack, R.A., Carr-Locke, D.L., Bleday, R., Suh, W.W. Magnetic resonance image-guided salvage brachytherapy after radiation in select men who initially presented favourable-risk prostate cancer: A prospective phase 2 study. *Cancer* **110**, 1485-1492 (2007).

75 Lee, H.K., Adams, M.T., Motta, J. Salvage prostate brachytherapy for localized prostate cancer failure after external beam radiation therapy. *Brachytherapy* **7**, 17-21 (2008).

76 Schröder, F.H., Hugosson, J., Roobol, M.J., Tammela, T.L.J, Ciatto, S., Nelen, V., Kwiatkowski, M., Lujan, M., Lilja, H., Zappa, M., Denis, L.J., Recker, F., Páez, A., Määtänen, L., BAngma, C.H., Aus, G., Carlsson, S., Villers, A., Rebillard, X., van der Kwast, T., Kujala, P.M., BLijenberg, B.G., Stenman, U.-H., Huber, A., Taari, K., Hakama, M., Moss, S.M., de Koning, H.J., Auvinen, A. Prostate-cancer mortality at 11 years of follow-up. *The New England Journal of Medicine* **366**, 981-990 (2012).

77 Wang, H., Sun, D., Ji, P., Mohler, J., Zhu, L. An AR-Skp2 pathway for proliferation of androgen-dependent prostate-cancer cells. *Journal of Cell Science* **121**, 2578-2587 (2008).

78 Kaur, P., Khatik, G.L. Advancements in non-steroidal antiandrogens as potential agents for the treatment of prostate cancer. *Mini Reviews in Medicinal Chemistry* **16**, 531-546 (2016).

79 Belikov, S., Öberg, C., Jääskeläinen, T., Rahkama, V., Palvimo, J.J, Wrange, Ö. FoxA1 corrupts the antiandrogenic effect of bicalutamide but only weakly attenuates the effect of MDV3100 (Enzalutamide™). *Molecular and Cellular Endocrinology* **365**, 95-107 (2013).

80 Musunuru, H.B., Yamamoto, T., Klotz, L., Ghanem, G., Mamedov, A., Sethukavalan, P., Jethava, V., Jain, S., Zhang, L., Vesprini, D., Loblaw, A. Active Surveillance for Intermediate Risk Prostate Cancer: Survival Outcomes in the Sunnybrook Experience. *Journal of Urology* **196**, 1651-1658 (2016).

81 Parker, C.C., James, N.D., Brawley, C.D., Clarke, N.W., Hoyle, A.P., Ali, A., Ritchie, A.W.S, Attard, G., Chowdhury, S., Cross, W., Dearnaley, D.P., Gillesen, S., Gilson, C., Jones, R.J., Langley, R.E., Malik, Z.I., Mason, M.D., Matheson, D., Millman, R., Russell, J.M., Thalmann, G.N., Amos, C.L., Alonzi, R., Bahl, A., Birtle, A., Din, O., Douis, H., Eswar, C., Gale, J., Gannon, M.R., Jonnada, S., Khaksar, S., Lester, J.F., O'Sullivan, J.M., Parikh, O.A., Pedley, I.D., Pudney, D.M., Sheehan, D.J., Srihari, N.N., Tran, A.T.H., Parmar, M.K.B., Sydes, M.R. Radiotherapy to the primary tumor for newly diagnosed, metastatic prostate cancer (STAMPEDE): a randomised controlled phase 3 trial. *The Lancet (British edition)* **392**, 2353-2366 (2018).

82 Serra, C., Sandor, N. L., Jang, H., Lee, D., Toraldo, G., Guarneri, T., Wong, S., Zhang, A., Guo, W., Jasuja, R., Bhasin, S. The effects of testosterone deprivation and supplementation on proteasomal and autophagy activity in the skeletal muscle of the male mouse: differential effects on high-androgen responder and low-androgen responder muscle groups. *Endocrinology* **154**, 4594–4606 (2013).

83 Simard, J., Singh, S.M., Labrie, F. Comparison of in vitro effects of the pure antiandrogens OH-flutamide, casodex, and nilutamide on androgen-sensitive parameters. *Urology (Ridgewood, N.J.)* **49**, 580-589 (1997).

84 Shet, M.S., McPhaul, M., Fisher, C.W., Stallings, N.R., Estabrook, R.W. Metabolism of the antiandrogenic drug (Flutamide) by human CYP1A2. *Drug Metabolism and Disposition* **25**, 1298-1303 (1997).

85 Ayub, M., Levell, M.J. The effect of ketoconazole related imidazole drugs and antiandrogens on [3H] R 1881 binding to the prostatic androgen receptor and [3H]5 alpha-dihydrotestosterone and [3H]cortisol binding to plasma proteins. *Journal of Steroid Biochemistry* **33**, 251-255 (1989).

86 Cantin, L., Faucher, F., Couture, J.F., de Jésus-Tran, K.P., Legrand, P., Ciobanu, L.C., Fréchette, Y., Labrecque, R., Singh, S.M., Labrie, F., Breton, R. Structural characterization of the human androgen receptor ligand-binding domain complexed with EM5744, a rationally designed steroidal ligand bearing a bulky chain directed towards helix 12. *Journal of Biological Chemistry* **282**, 30910-30919 (2007).

87 Zhou, J., Liu, B., Geng, G., Wu, J.H. Study of the impact of the T877A mutation on ligand-induced helix-12 postitioning of the androgen receptor resulted in design and synthesis of novel antiandrogens. Proteins, structure, function, and bioinformatics **78**, 623-637 (2010).

88 Yoon, H.-G., Wong, J. The corepressors silencing mediator of retinoid and thyroid hormone receptor and nuclear receptor corepressor are involved in agonist- and antagonist-regulated transcription by androgen receptor. *Molecular Endocrinology* **20**, 1048–1060 (2006).

89 Labrie, C., Susan, L., Plante, M., Lapointe, S., Labrie, F. Analysis of the androgenic activity of synthetic "progestins" currently used for the treatment of prostate cancer. *Journal of Steroid Biochemistry* **28**, 379-384 (1987).

90 Ilagan, R., Zhang, L.J., Pottratz, J., Le, K., Salas, S., Iyer, M., Wu, L., Gambhir, S.S., Carey, M. Imaging androgen receptor function during flutamide treatment in the LAPC9 xenograft model. *Molecular Cancer Therapeutics* **4**, 1662-1669 (2005).

91 Lee, Y.-F., Lin, W.-J., Huang, J., Messing, E.M., Chan, F.L., Wilding, G., Chang, C. Activation of mitogen-activated protein kinase pathway by the antiandrogen hydroxyflutamide in androgen receptor-negative prostate cancer cells. *Cancer Research (Chicago, Ill.)* **62**, 6039–6044 (2002).

92 Górowska-Wójtowicz, E., Hejmej, A., Kamińska, A., Pardyak, L, Kotula-Balak, M., Dulińska-Litewka, J., Laidler, P., Bilińska, B. Anti-androgen 2-hydroxyflutamide modulates cadherin, catenin and androgen receptor phosphorylation in androgen-sensitive LNCaP and androgen-independent PC3 prostate cancer cell lines acting via PI3K/ Akt and MAPK/ERK1/2 pathways. *Toxicology in Vitro* **40**, 324–335 (2017).

93 Koch, D.C., Jang, H.S., O'Donnell, E.F., Punj, S., Kopparapu, P.R., Bisson, W.H., Kerkvilet, N.I., Kolluri, S.K. Anti-androgen flutamide suppresses hepatocellular carcinoma cell proliferation via the aryl hydrocarbon receptor mediated induction of transforming growth factor-β1. *Oncogene* **34**, 6092–6104 (2015).

94 Hejmej, A., Biblinska, B. The effects of flutamide on cell-cell junctions in the testis, epididymis, and prostate. *Reproducive Toxicology* **81**, 1-16 (2018).

95 Shen, P., Sun, J., Xu, G., Zhang, L., Yang, Z., Xia, S., Wang, Y., Liu, Y., Shi, G. KLF9, a transcription factor induced in flutamide-caused cell apoptosis, inhibits AKT activation and suppresses tumor growth of prostate cancer cells. *The Prostate* **74**, 946-958 (2014).

96 Wang, Y., Shao, C., Shi, C-H., Zhang, L., Yue, H.-H., Wang, P.-F., Yang, B., Zhang, Y.-T., Liu, F., Qin, W.-J., Wang, H., Shao, G.-X. Change of the cell cycle after flutamide treatment in prostate cancer cells and its molecular mechanism. *Asian Journal of Andrology* **7**, 375-380 (2005).

97 Mazariego, C.G., Egger, S., King, M.T., Juraskova, I., Woo, H., Berry, M., Armstrong, B.K., Smith, D. Fifteen year quality of life outcomes in men with localised prostate cancer: population based Australian prospective study. *The BMJ* **371**, m3503-m3503 (2020).

98 Howlader, N., Noone, A.M., Krapcho, M., Miller, D., Brest, A., Yu, M., Ruhl, J., Tatalovich, Z., Mariotto, A., Lewis, D.R., Chen, H.S., Feuer, E.J., Cronin, K.A. (eds). SEER Cancer Statistics Review, 1975-2017. *National Cancer Institute* Bethesda, M.D., https://seer.cancer.gov/csr/1975_2017/, based on November 2019 SEER data submission, posted to the SEER web site (2020).

99 Gatzemeier, U., von Pawel, J., Gottfried, M., ten Velde, G.P.M., Mattson, K., DeMarinis, F., Harper, P., Salvati, F., Robinet, G., Lucenti, A., Bogaerts, J., Gallant, G. Phase III comparative study of high-dose cisplatin versus a combination of paclitaxel and cisplatin in patients with advanced non-small-cell lung cancer. *Journal of Clinical Oncology* **18**, 3390-3399 (2000).

100 Belani, C.P., Lee, J.S., Socinski, M.A., Robert, F., Waterhouse, D., Rowland, K., Ansari, R., Lilenbaum, R., Natale, R.B. Randomized phase III trial comparing cisplatin-etoposide to carboplatin-paclitaxel in advanced metastatic non-small cell lung cancer. *Annals of Oncology* **16**, 1069-1075 (2005).

101 Sztankay, M., Giesinger, J.M., Zabernigg, A., Krempler, E., Pall, G., Hilbe, W., Burghuber, O., Hochmair, M., Rumpold, G., Doering, S., Holzner, B. Clinical decision-making and heath-related quality of life during first-line and maintenance therapy in patients with advanced non-small cell lung cancer (NSCLC): findings from a real-world setting. *BMC Cancer* **17**, 565 (2017).

102 Celikoglu, F., Celikoglu S.I. Intratumoral chemotherapy with 5-fluorouracil for palliation of bronchial cancer in patients with severe airway obstruction. *Journal of Pharmacy and Pharmacology* **55**, 1441-1448 (2003).

103 Seto, T., Ushijima, S., Yamamoto, H., Ito, K., Araki, J., Inoue, Y., Semba, H., Ichinose, Y. Intrapleural hypotonic cisplatin treatment for malignant pleural effusion in 80 patients with non-small-cell lung cancer: a multi-institutional phase II trial. *British Journal of Cancer* **95**, 717-721 (2006).

104 Schiff, P.B., Fant, J., Horowitz, S.B. Promotion of microtubule assembly in vitro by taxol. *Nature* **277**, 665-667 (1979).

105 Riou, J.-F., Naudin, A., Lavelle, F. Effects of taxotere on murine and human tumor cell lines. *Biochemical and Biophysical Research Communications* **187**, 164-170 (1992).

106 Mathew, A.E., Mejillano, M.R., Nath, J.P., Himes, R.H., Stella, V.J. Synthesis and evaluation of some water-soluble prodrugs and derivatives of taxol and antitumor activity. *Journal of Medicinal Chemistry* **35**, 145-151 (1992).

107 Du, W., Hong, L., Yao, T., Yang, X., He, Q., Yang, B., Hu, Y. Synthesis and evaluation of water-soluble docetaxel prodrugs-docetaxel esters of malic acid. *Bioorganic & Medicinal Chemistry* **15**, 6323-6330 (2007).

108 Díaz, J.F., Andreu, J.M. Assembly of purified GDP-tubulin into microtubules induced by taxol and taxotere: Reversibility, ligand stoichiometry, and competition. Biochemistry 32, 2747-2755 (1993).

109 Zahedi, P., Stewart, J., De Souza, R., Piquette-Miller, M., Allen, C. An injectable depot system for sustained intraperitoneal chemotherapy of ovarian cancer results in favorable drug distribution at the whole body, peritoneal and intratumoral levels. *Journal of Controlled Release* **158**, 379-385 (2012).

110 Hagisawa, S., Mikami, T., Sato, Y. Docetaxel-induced apoptosis in the mitotic phase: electron microscopic and cytochemical studies of human leukemia cells. *Medical Electron Microscopy* **32**, 167-174 (1999).

111 Haldar, S., Chintapalli, J., Croce, C.M. Taxol induces Bcl-2 phosphorylation and death of prostate cancer cells. *Cancer Research (Chicago Ill.)* **56**, 1253–1255 (1996).

112 Kroon, J., Kooijman, S., Cho, N.-J., Storm, G., van der Pluijm, G. Improving Taxane-Based Chemotherapy in Castration-Resistant Prostate Cancer. *Trends in Pharmacological Sciences* **37**, 451–62 (2016).

113 Jung, J., Park, S.-J., Chung, H.K., Kang, H.-W., Lee, S.-W., Seo, M.H., Park, H.J., Song, S.Y., Jeong, S.-Y., Choi, E.K. Polymeric nanoparticles containing taxanes enhance chemoradiotherapeutic efficacy in non-small cell lung cancer. *International Journal of Radiation Oncology Biology Physics* **84**, e77-e83 (2012).

114 Millrud, C.R., Mehmeti, M., Leandersson, K. Docetaxel promotes the generation of anti-tumorigenic human macrophages. *Experimental Cell Research* **362,** 525–531 (2018).

115 Hodge, J.W., Garnett, C.T., Farsaci, B., Palena, C., Tsang, K.Y., Ferrone, S., Gameiro, S.R. Chemotherapy-induced immunogenic modulation of tumor cells enhances killing by cytotoxic T lymphocytes and is distinct from immunogenic cell death. *International Journal of Cancer* **133,** 624–636 (2013).

116 Chen, J., Yuan, L., Fan, Q., Su, F., Chen, Y., Hu, S. Adjuvant effect of docetaxel on the immune responses to influenza A H1N1 vaccine in mice. *BMC Immunology* **13,** 36 (2012).

117 Kodumudi, K.N., Woan, K., Gilvary, D.L., Sahakian, E., Wei, S., Djeu, J.Y. A novel chemoimmunomodulating property of docetaxel: Suppression of myeloid-derived suppressor cells in tumor bearers. *Clinical Cancer Research* **16,** 4583–4594 (2010).

118 Maulhardt, H.A., Marin, A.M., diZerega, G.S. Intratumoral submicron particle docetaxel inhibits syngeneic Renca renal cancer growth and increases CD4+, CD8+, and Treg levels in peripheral blood. *Investigational New Drugs* **38**, 1618-1626 (2020).

119 Schulmeister, L. Managing vesicant extravasations. *The Oncologist* **13**, 284-288 (2008).

120 Adu-Berchie, K., Mooney, D.J. Biomaterials as local niches for immunomodulation. *Accounts of Chemical Research* **53**, 1749-1760 (2020).

121 Determan, A.S., Wilson, J.H., Kipper, M.J., Wannemuehler, M.J., Narasimhan, B. Protein stability in the presence of polymer degradation products: Consequences for controlled release formulations. *Biomaterials* **27**, 3312-3320 (2006).

122 Kang, J., Lambert, O., Ausborn, M., Schwendeman, S.P. Stability of proteins encapsulated in injectable and biodegradable poly(lactide-co-glycolide)-glucose millicylinders. *International Journal of Pharmaceutics* **357**, 235-243 (2008).

123 Liang, R., Zhang, R., Li, X., Wang, A., Chen, D., Sun, K., Liu, W., Li, Y. Stability of exenatide in poly(D,L-lactide-co-glycolide) solutions: A simplified investigation on the peptide degradation by the polymer. *European Journal of Pharmaceutical Sciences* **50**, 502-510 (2013).

124 Mach, N., Gillessen, S., Wilson, S.B., Sheehan, C., Mihm, M., Dranoff, G. Differences in dendritic cells stimulated in vivo by tumors engineered to secrete granulocyte-macrophage colony-stimulating factor or Flt3-ligand. *Cancer Research (Chicago, Ill.)* **60**, 3239–3246 (2000).

125 Nelson, W.G., Simons, J.W., Mikhak, B., Chang, J.F., DeMarzo, A.M., Carducci, M.A., Kim, M., Weber, C.E., Baccala, A.A., Goeman, M.A., Clift, S.M., Ando, D.G., Levitsky, H.I., Cohen, L.K., Sanda, M.G., Mulligan, R.C., Partin, A.W., Carter, H.B., Piantadosi, S., Marshall, F.F. Cancer cells engineered to secrete granolucyte-macrophage colony-stimulating factor using ex vivo gene transfer as vaccines for the treatment of genitourinary malignancies. *Cancer Chemotherapy Pharmacology* **46**, 67-72 (2000).

126 Dobbs, N.A., Zhou, X., Pulse, M., Hodge, L.M., Schoeb, T.R., Simecka, J.W. Antigen-pulsed bone marrow derived and pulmonary dendritic cells promote Th2 cell responses and immunopathology in lungs during the pathogenesis of murine mycoplasma pneumonia. *The Journal of Immunology (1950)* **193**, 1353–1363 (2014).

127 Kim, I.-K., Koh, C.-H., Jeon, I., Shin, K.-S., Kang, T.-S., Bae, E.-A., Seo, H., Ko, H.-J., Kim, B.-S., Chung, Y., Kang, C.-Y. GM-CSF promotes antitumor immunity by inducing Th9 cell responses. *Cancer Immunology Research* **7**, 498-509 (2019).

128 Baines, J., Celis, E. Immune-mediated tumor regression induced by CpG-containing oligodeoxynucleotides. *Clinical Cancer Research* **9**, 2693–2700 (2003).

129 Lu, R., Groer, C., Kleindl, P.A., Moulder, K.R., Huang, A., Hunt, J.R., Cai, S., Aires, D.J., Berkland, C., Forrest, L. Formulation and preclinical evaluation of a Toll-like receptor 7/8 agonist as an anti-tumoral immunomodulator. *Journal of Controlled Release* **306**, 165-176 (2019).

130 Ronsley, R., Kariminia, A., Ng, B., Mostafavi, S., Reid, G., Subrt, P., Hijiya, N., Schultz, K.R., The TLR9 agonist (GNKG168) induces a unique immune activation pattern in vivo in children with minimal residual disease positive acute leukemia: Results of the TACL T2009-008 phase I study. *Pediatric Hematology and Oncology* **36**, 468-481 (2019).

131 Schmidt, J., Welsch, T., Jäger, D., Mühlradt, P.F., Büchler, M.W., Märten, A. Intratumoral injection of the toll-like receptor-2/6 agonist 'macrophage-activating lipopeptide-2' in patients with pancreatic carcinoma: a phase I/II trial. *British Journal of Cancer* **97**, 598-604 (2007).

132 Sato-Kaneko, F., Yao, S., Ahmadi, A., Zhang, S.S., Hosoya, T., Kaneda, M.M., Varner, J.A., Ou, M., Messer, K.S., Guidicci, C., Coffman, R.L., Kitaura, K., Matsutani, T., Suzuki, R., Carson, D.A., Hayashi, T., Cohen, E.E. Combination immunotherapy with TLR agonists and checkpoint inhibitors suppresses head and neck cancer. *JCI insight* **2**, e93397 (2017).

133 Wang, D., Jiang, W., Zhu, F., Mao, X., Agarwal, S. Modulation of the tumor microenvironment by intratumoral administration of IMO-2125, a novel TLR9 agonist, for cancer immunotherapy. *International Journal of Oncology* **53**, 1193-1203 (2018).

134 Motedayen Aval, L., Pease, J.E., Sharma, R., Pinato, D.J. Challenges and opportunities in the clinical development of STING agonists for cancer immunotherapy. *Journal of Clinical Medicine* **9**, 3323 (2020).

135 Geary, S.M., Lemke, C.D., Lubaroff, D.M., Salem, A.K. Tumor immunotherapy using adenovirus vaccines in combination with intratumoral doses of CpG ODN. *Cancer Immunology, Immunotherapy* **60**, 1309-1317 (2011).

136 Schaedler, E., Remy-Ziller, C., Hortelano, J., Kehrer, N., Claudepierre, M.-C., Gatard, T., Jakobs, C., Préville, X., Carpentier, A.F., Rittner, K. Sequential administration of a MVA-based MUC1 cancer vaccine and the TLR9 ligande Litenimod (Li28) improves local immune defense against tumors. *Vaccine* **35**, 577-585 (2017).

137 Zhao, Y., Shi, L., Ji, M., Wu, J., Wu, C. The combination of systemic chemotherapy and local treatment may improve the survival of patients with unresectable metastatic colorectal cancer. *Molecular and Clinical Oncology* **6**, 856-860 (2017).

138 Tosco, L., Briganti, A., D'amico, A.V., Eastham, J., Eisenberger, M., Gleave, M., Haustermans, K., Logothetis, C.J., Saad, F., Sweeney, C., Taplin, M.-E., Fizazi, K. Systemiatic review of systemic therapies and therapeutic combinations with local treatments for high-risk localized prostate cancer. *European Urology* **75**, 44-60 (2019).

139 Mole, R.H., Whole body irradiation; radiobiology or medicine? *The British Journal of Radiology* **26**, 234-241 (1953).

140 Chicas-Sett, R., Morales-Orue, I., Castilla-Martinez, J., Zafra-Martin, J., Kannemann, A., Blanco, J., Lloret, M., Lara, P.C. Stereotactic ablative radiotherapy combined with immune checkpoint inhibitors reboots the immune response assisted by immunotherapy in metastatic lung cancer: A systematic review. *International Journal of Molecular Sciences* **20**, 2173 (2019).

141 Thomas, S., Kuncheria, L., Roulstone, V., Kyula, J.N., Mansfield, D., Bommareddy, P.K., Smith, H., Kaufman, H.L., Harrington, K.J., Coffin, R.S. Development of a new fusion-enhanced oncolytic immunotherapy platform based on herpes simplex virus type 1. *Journal for ImmunoTherapy of Cancer* **7**, 214-214 (2019).

142 Davoodi, P., Ng, W.C., Yan, W.C., Srinivasan, M.P., Wang, C.-H. Double-walled microparticles-embedded self-cross-linked, injectable, and antibacterial hydrogel for controlled and sustained release of chemotherapeutic agents. *ACS Applied Materials & Interfaces* **8**, 22785-22800 (2016).

143 Hama, Y., Urano, Y., Koyama, Y., Kamiya, M., Bernardo, M., Paik, R.S., Krischna, M.C., Choyke, P.L., Kobayashi, H. In vivo spectral fluorescence imaging of submillimeter peritoneal cancer implants using a lectin-targeted optical agent. *Neoplasia* **8**, 607-612 (2006).

144 Ito, A., Ohta, M., Kato, Y., Inada, S., Kato, T., Nakata, S., Yatabe, Y., Goto, M., Kaneda, N., Kurita, K., Nakanishi, H., Yoshida, K. A real-time near-infrared fluorescence imaging method for the detection of oral cancers in mice using an indocyanine green-labeled podoplanin antibody. *Technology in Cancer Research & Treatment* **17**, 1-11 (2018).

145 Li, L., Du, Y., Chen, X, Tian, J. Fluorescence molecular imaging and tomography of matrix metalloproteinase-activatable near-infrared fluorescence probe and image-guided orthotopic glioma resection. *Molecular Imaging and Biology* **20**, 930-939 (2018).

146 Hildebrand, S.A., Kelly, K.A., Weissleder, R., Tung, C.-H. Monofunctional near-infrared fluorochromes for imaging applications. *Bioconjugate Chemistry* **16**, 1275-1281 (2005).

147 Becker, A., Hessenius, C., Licha, K., Ebert, B., Sukowski, U., Semmler, W., Wiedenmann, B., Grötzinger, C. Receptor-targeted optical imaging of tumors with near-infrared fluorescent ligands. *Nature Biotechnology* **19**, 327-331 (2001).

148 Ntziachristos, V., Ripoll, J, Weissleder, R. Would near-infrared fluorescence signals propagate through large human organs for clinical studies? *Optics Letters* **27**, 333-335 (2002).

149 Biffi, S., Garrovo, C., Macor, P., Tripodo, C., Zorzet, S., Secco, E., Tedesco, F., Lorusso, V. In vivo biodistribution and lifetime analysis of Cy5.5-conjugated rituximab in mice bearing lymphoid tumor xenograft using time-domain near-infrared optical imaging. *Molecular Imaging* **7**, 272-282 (2008).

150 Pan, Z., Lou, Y., Yang, G., Ni, X., Chen, M., Xu, H., Miao, X., Liu, J., Hu, C., Huang, Q. Preparation of calcium sulfate dihydrate and calcium sulfate hemihydrate with controllable crystal morphology by using ethanol additive. *Ceramics International* **39,** 5495–5502 (2013).

151 Carr, R.L. Evaluating flow properties of solids. *Chemical Engineering* **18,** 163–168 (1965).

152 Shah, R.B., Tawakkul, M.A., Kahn, M.A. Comparative evaluation of flow for pharmaceutical powders and granules. *AAPS PharmSciTech* **9,** 250–258 (2008).

153 Moore, J.W., Flanner, H.H. Mathematical comparison of curves with an emphasis on dissolution profiles. *Pharmaceutal Technology* **20,** 64–74 (1996).

154 Mitchell, R.A., Luwor, R.B., Burgess, A.W. Epidermal growth factor receptor: Structure-function informing the design of anticancer therapeutics. *Experimental Cell Research* **371**, 1-19 (2018).